

## Project acronym: TRITON

**Project title:** Development of management tools and directives for immediate protection of biodiversity in coastal areas affected by sea erosion and establishment of appropriate environmental control systems

### Deliverable No. 4.3

**Pilot test and joint tool development with local/operators and player's involvement**

Delivery date:

**30/09/2020**

Lead Partner

Technical support

Project Partners

<b>PROGRAMME</b>	Interreg V-A Greece-Italy Programme 2014-2020
<b>AXIS</b>	Axis 2 (i.e. Integrated Environmental Management)
<b>THEMATIC OBJECTIVES</b>	06 – Preserving and protecting the environment and promoting resource efficiency
<b>PROJECT ACRONYM</b>	TRITON
<b>PROJECT WEBSITE URL</b>	<a href="https://www.interregtriton.eu/">https://www.interregtriton.eu/</a>
<b>DELIVERABLE NUMBER</b>	No. 4.3
<b>TITLE OF DELIVERABLE</b>	Pilot test and joint tool development with local/operators and player’s involvement
<b>WORK PACKAGE/TASK N°</b>	WP4 Pilot Cases on ICZM; Task 4.3
<b>NAME OF ACTIVITY</b>	Pilot test and joint tool development with local/operators and player’s involvement
<b>PARTNER IN CHARGE (AUTHOR)</b>	PB5
<b>PARTNERS INVOLVED</b>	LB1, PB2, PB5
<b>STATUS</b>	Final version
<b>DUE DATE</b>	Second semester 2020
<b>ADDRESSEE OF THE DOCUMENT<sup>1</sup></b>	TRITON PROJECT PARTNERS; INTERREG V-A GREECE-ITALY PROGRAMME
<b>DISTRIBUTION<sup>2</sup></b>	PP

### Document Revision History

<sup>1</sup>WPL (Work Package Leaders); PB (Project Beneficiaries); AP (Associates); Stakeholders; Decision Makers; Other (Specify)  
<sup>2</sup>PU (Public); PP (Restricted to other program participants); CO (Confidential, only for members of the consortium)

Version	Date	Author/Reviewer	Changes
1.0 - Final	30.09.2020	PB5	Final Version
0.9 - Draft	14.06.2020	PB5	Revisions and integrations
0.8 - Draft	01.06.2020	LB and PB2	Revisions and integrations
0.7 - Draft	17.05.2020	PB5-UoP	PB5-Major corrections and Revision
0.6 - Draft	04.04.2020	PB5-UoP	PB5-Contribution and Revision
0.5 - Draft	24.02.2020	PB2 - CMCC	PB2 Revision
0.4 - Draft	04.02.2020	PB2 - CMCC	PB2 Revision
0.3 - Draft	03-02-2020	LB	LB Contribution
0.2 - Draft	20.01.2020	PB5-UoP	1 <sup>st</sup> Draft – PB5
0.1 - Table of contents	15.12.2019	PB5-UoP	Version sent to PB2 and LB1 for their input

#### Abstract

The current deliverable presents tests and studies performed in the selected pilot areas in both regions, Apulia and Western Greece. Climate change impacts across the shoreline, mapping and prioritization of coastal erosion risk in protected areas and influence on coastal morphodynamics are among the tests and studies that were performed in the selected pilot areas. On the Greek side, in the gulf of Patras, Western Greece, a pilot observatory of erosion has been established, operating as a joint tool with local operators for future development in the respective coastal zone. On the other hand, in Apulia region, indicators and a decision support system for coastal erosion have been applied at the pilot study areas of Bari and Ugento, operating as a joint tool with local operators for future development in the respective coastal zone. Furthermore, remote sensing and GIS-based techniques are used as a risk-based joint tool blending for the multi-temporal detection and analysis of shoreline evolution across the TRITON pilot cases. Specifically, the proposed joint tool was applied across the Messolonghi (Greece), the gulf of Patras (Greece) and the Ugento (Italy) shorelines, identifying hotspots risk areas requiring urgent intervention in terms on management and adaptation measures, including nature-based solutions (NBSs). Finally, a new WebGIS system for interactive visualization of the spatial data collected in the Greek pilot cases was designed and is available to the public through the Municipality of Ieras Poleos Messolonghiou official website. Details on the development of this WebGIS tool are presented in WP5.

Lead Partner

Technical support

Project Partners

## Table of Contents

Acronyms .....	7
List of Figures .....	7
List of Tables.....	11
1. Introduction .....	12
2 Pilot tests and studies in the Apulia region .....	14
2.1 The First Ugento Case Study.....	14
2.1.1 <i>Wave climate and height</i> .....	15
2.1.2 <i>Closure depth</i> .....	17
2.1.3 <i>Ugento and the regional master plan for coastal management (PRC)</i> .....	17
2.1.4 <i>Calculation of the longshore sediment transport</i> .....	18
2.1.5 <i>Approved design</i> .....	19
2.1.6 <i>Lesson learnt</i> .....	20
2.2 The Second Ugento Case Study.....	20
2.2.1 <i>Posidonia oceanica seagrass meadows and dunes rehabilitation</i> .....	20
2.2.2 <i>Lesson learnt</i> .....	23
2.3 The Third San Girolamo – Fesca case study .....	23
2.3.1 <i>The wave climate studies</i> .....	25
2.3.2 <i>The bathymetrical and geomorphological charts</i> .....	25
2.3.3 <i>The planned intervention</i> .....	27
2.3.4 <i>The effectiveness of the coastal protection</i> .....	29
2.3.5 <i>The current situation</i> .....	30
2.3.6 <i>Lesson learnt</i> .....	31
3 Pilot tests and studies in the region of Western Greece.....	32
3.1 The establishment of a pilot erosion observatory in the gulf of Patras and the Kotychi lagoon ....	32
3.2 Procurement of the necessary mobile equipment.....	34
3.3 Site Investigation techniques and studies in the areas of intervention .....	35
3.3.1 <i>Satellite, UAV, aerial photo imaging and USV for shoreline evolution</i> .....	35
3.3.1.1 <i>Medium resolution remote sensing data and processing</i> .....	35
3.3.1.2 <i>Very high-resolution remote sensing data and processing</i> .....	36
3.3.1.3 <i>Analogue air photos processing</i> .....	38

3.3.1.4	<i>UAV processing</i>	38
3.3.1.5	<i>USV data processing</i>	39
3.3.1.6	<i>Medium resolution remote sensing data accuracy assessment</i>	40
3.3.1.7	<i>Shoreline retreat and accretion</i>	42
3.3.2	<i>Marine surveys and digital bathymetric plans</i>	43
3.3.2.1	<i>Research equipment and data acquisition methods</i>	43
3.3.2.2	<i>Survey planning</i>	48
3.3.2.3	<i>Data processing and analysis</i>	48
3.3.2.4	<i>Bathymetric plan of the gulf of Patras</i>	49
3.3.3	<i>Geotechnical survey in the gulf of Patras</i>	50
3.3.3.1	<i>Borehole drilling, soil core sampling, in situ (SPT) and laboratory tests</i>	52
3.3.3.2	<i>Cone Penetration Tests (CPT)</i>	56
3.3.3.3	<i>Development of a geotechnical map for specific coastal applications</i>	58
3.3.4	<i>Environmental monitoring and management in the protected areas</i>	60
3.3.4.1	<i>The Kotychi lagoon</i>	61
3.3.4.2	<i>Anthropogenic interventions, impacts and erosional state</i>	62
3.3.4.3	<i>Environmental monitoring</i>	64
3.3.5	<i>Numerical study of waves, currents, and sediment transport in the Gulf of Patras</i>	66
3.3.5.1	<i>Input data</i>	66
3.3.5.2	<i>Wave Development in the Gulf of Patras</i>	68
3.3.5.3	<i>Coastal Erosion Vulnerability Assessment</i>	70
3.3.5.4	<i>Conclusions</i>	72
4	<b>Development and application of the risk-based joint tool across the TRITON pilot cases</b>	73
4.1	<b>Methodological approach of shoreline extraction from satellite images</b>	74
4.2	<b>Results from the pilot study area of the Ugento shoreline - Apulia region</b>	75
4.2.1	<i>Regional park of Ugento</i>	78
4.2.2	<i>Fontanelle</i>	79
4.2.3	<i>Marina of Torre Mozza</i>	80
4.2.4	<i>Lido Marini</i>	82
4.3	<b>Results on Coastal Erosion Analysis from the pilot study area of the Messolonghi shoreline in the northern part of the gulf of Patras– Region of Western Greece</b>	83
4.3.1	<i>Louros Study site</i>	85

<b>4.3.2</b>	<b><i>Louronisides Study site</i></b> .....	86
<b>4.3.3</b>	<b><i>Alikes and Tourlida Beach Study site</i></b> .....	87
<b>4.3.4</b>	<b><i>Evinos Estuary Study site</i></b> .....	88
<b>4.4</b>	<b>Results on Coastal Erosion Analysis from the pilot study area of the southern part of the gulf of Patras - Region of Western Greece</b> .....	89
<b>4.4.1</b>	<b><i>Carnario study area</i></b> .....	91
<b>4.4.2</b>	<b><i>Gialos study area</i></b> .....	93
<b>4.4.3</b>	<b><i>Patras New Port</i></b> .....	93
<b>5</b>	<b>Discussion</b> .....	95
	<b>Bibliography</b> .....	97
	<b>APPENDIX A: Borehole logs</b>	
	<b>APPENDIX B: CPT results</b>	

Lead Partner



Technical support



Project Partners



## Acronyms

<b>CPT</b>	<i>Cone Penetrometer Test</i>
<b>DSAS</b>	<i>Digital Shoreline Analysis System tool (DSAS)</i>
<b>ICZM</b>	<i>Integrated Coastal Zone Management</i>
<b>HES</b>	<i>Hydrographic Echo Sounder</i>
<b>HSV</b>	<i>Hydrographic Survey Vehicle</i>
<b>NSM</b>	<i>Net Shoreline Movement</i>
<b>SPT</b>	<i>Standard Penetration Test</i>
<b>UAV</b>	<i>Unmanned Aerial Vehicle</i>
<b>USV</b>	<i>Unmanned Surface Vehicle</i>

## List of Figures

- Figure 2.1:** *Location of Ugento (a); stretch of coast (b)*
- Figure 2.2:** *The as built groyne, picture taken in 2003*
- Figure 2.3:** *Wave rose offshore Ugento*
- Figure 2.4:** *Description of the physical system*
- Figure 2.5:** *Coastal erosion vulnerability and Value for the Landscape*
- Figure 2.6:** *Comparison of historical shorelines (2005-2010)*
- Figure 2.7:** *Location of the areas to be dredged and to be nourished*
- Figure 2.8:** *The Posidonia Oceanica around the Salento peninsula*
- Figure 2.9:** *The map of Posidonia Oceanica along the Ugento coastline*
- Figure 2.10:** *Mouth of the drainage channel at San Giovanni, Ugento*
- Figure 2.11:** *Mouth of the drainage channel at Torre Mozza, Ugento*
- Figure 2.12:** *Torre Mozza deployment area and view of the dune at the end of the intervention*
- Figure 2.13:** *Photos before the intervention*
- Figure 2.14:** *The stretch of coast between the two channel mouths*
- Figure 2.15:** *Wave rose offshore Bari*
- Figure 2.16:** *The bathymetry in front of San Girolamo - Fesca*
- Figure 2.17:** *Geomorphological chart*
- Figure 2.18:** *Plan view of the intervention a few months before the end of construction (May 2019)*
- Figure 2.19:** *From the right to the left: a pedestrian path, the bicycle path, the trees, another pedestrian path, an artificial dune, seats made at the retaining wall, the beach*
- Figure 2.20:** *Beach nourishing and the artificial dune with the long seating wall*
- Figure 2.21:** *Values of Hs and wave direction, ante e post operam*

**Figure 2.22:** Wave induced circulation ante e post operam

**Figure 2.23:** Present situation. Photo taken from the East side

**Figure 3.1:** Installed equipment (environmental) stations in the areas of intervention (Gulf of Patras and Kotychi lagoon)

**Figure 3.2** (a) Hydrographic Echo Sounder (HES), (b) Hydrographic Survey Vehicle (HSV), (c) Unmanned Aerial Vehicle (UAV)

**Figure 3.3:** Part of the Landsat 8 NDWI (left image) and NDVI (right image) classified in two classes (Sea and Land). The port of Patras is in the middle of the image

**Figure 3.4:** Part of the Sentinel 8 NDVI image classified in two classes (Sea and Land). The port of Patras is in the middle of the image

**Figure 3.5:** Processing of Worldview-2 data in Leica Photogrammetry Suite.

**Figure 3.6:** Final orthomosaic of Worldview-2 data covering the whole coastline from Rio at the East to Kotychi lagoon at the West

**Figure 3.7:** An example from the 1945 air photo (left image) and 1996 air phot (right image) orthomosaic covering the broader coastline of Rio northeast of Patras (in red color is the 1945 shoreline). The shoreline retreat is evident

**Figure 3.8:** UAV data processing in Agisoft Photoscan Professional software.

**Figure 3.9:** UAV data orthomosaic from Alikes fishery port

**Figure 3.10:** (a) The bottom of the USV where the SONAR, the Side Scan Sonar and the cameras are placed and (b) USV operation in the Alikes fishery port

**Figure 3.11:** A comparison of the shorelines derived from satellite data in the Alikes fishery port

**Figure 3.12:** Statistics of the Sentinel shoreline displacement compared to the worldview-2 shoreline

**Figure 3.13:** Statistics of the Landsat shoreline displacement compared to the worldview-2 shoreline

**Figure 3.14:** Map of the shoreline displacement from 1945 to 2018 in the area of study. Red color represents areas where the erosion is higher than 30m, yellow color represents areas where the accretion is higher that 30m and green color represents areas where the shoreline displacement is lower than 30m.

**Figure 3.15:** The vessel 'Milady Millord III' used for the bathymetric survey

**Figure 3.16:** Leica GS08 RTK GNSS System (left image) and Hemisphere VS101 GPS (right image)

**Figure 3.17:** Hypack 2014 navigation software display

**Figure 3.18:** (a) SMC IMU-108 motion sensor, (b) Hemisphere Vector VS101 GPS Compass & IMU-108 motion sensor

**Figure 3.19:** ELAC transducers array LSE 307 mounted over the side of the vessel (left image) and ELAC Transmit/Receive Unit SEE 30 and the MBES operating workstation (right image)

**Figure 3.20:** The Hydrolite TM echosounder associated with an RTK GPS installed on top of it

**Figure 3.21:** Map of the gulf of Patras presenting the vessel's bathymetric survey track lines

**Figure 3.22:** Bathymetric map of the coastal area of the Southern part of the gulf of Patras

**Figure 3.23:** Google-Earth map representing the geotechnical operations performed along the shoreline of the gulf of Patras (borehole drilling: ΓN, CPT tests and sampling points for sediment analysis: S)

**Figure 3.24:** BOYLES rotary drilling used for the drilling of boreholes

**Figure 3.25:** Log box with soil core samples from borehole ΓN-06 at a depth 0-4m

**Figure 3.26:** The static penetrometer 20tn by Gouda/GeomilB.V, on a 6x6 Volvo / Terberg wheeled truck used in the CPT survey

**Figure 3.27:** Google-Earth map representing the penetration tests performed along the shoreline of the gulf of Patras, in the areas of Kato Achaia and Alykes fishery port

**Figure 3.28:** Geotechnical map of the coastal zone of the gulf of Patras (borehole drilling: ΓN, CPT tests and sampling points for sediment analysis: S)

**Figure 3.29:** Map of Kotychi lagoon including: (a) its catchment's main rivers and torrents, (b) its bathymetry, (c) the topography of the surrounding area, (d) the extents of its flooding plane, (e) the location and extent of the barrier spit and tidal channel (inlet). An air photo of the jetty constructed at the inlet is given in the upper left part of the figure.

**Figure 3.30:** After 2011, the barrier spit has been severely eroded several times and temporary solutions are often been carried out to restrain fish losses. In the satellite images of this figure, the locations of the two main washovers that respectively jeopardizes Kotychi's are indicated with red ellipses and red arrows while the temporary fences to restrict the washover are indicated with black arrows.

**Figure 3.31:** Satellite image (Google Earth) of the pilot area of the Gulf of Patras showing the 8 coastal independent subregions

**Figure 3.32:** The bathymetric computational mesh of the Ionian Sea west of the Gulf of Patras, which was used the numerical in simulations of wind-induced wave generation, growth and propagation.

**Figure 3.33:** Wave height, velocity and direction distribution in the area of the Ionian Sea west of the Gulf of Patras due to the action of northeastern winds (Table 3.8).

**Figure 3.34:** Significant wave height and velocity (vectors) distribution due to northeastern waves (Table 3.8) in the coastal zone of subregion 1.

**Figure 3.35:** Wave-generated currents (vectors) and wave setup due to northeastern waves (Table 3.8) in the coastal zone of subregion 1.

**Figure 3.36:** Bed level change due to northeastern waves (Table 3.8) in the coastal zone of subregion 1.

**Figure 4.1:** Coastline extraction methodology in steps

**Figure 4.2:** Shoreline evolution in the coastal area of the Municipality of Ugento (Apulia region) under the 2009-2018 timeframe

**Figure 4.3:** Net Shoreline Movement (NSM) in coastal zone of the Municipality of Ugento (Apulia region) for the 2009-2018 timeframe

**Figure 4.4:** a) Shoreline changes oacross the Ugento case study as evaluated through the DSAS tool (high accretion – blue; high erosion – red); b) shoreline changes within the Regional park of Ugento (moderate

accretion – light blue; moderate erosion – orange); c) Temporal variability of shoreline movement within the Regional park of Ugento over the 2009-2018 timeframe; d) erosion/accretion rate along the coastal zone of Regional park of Ugento

**Figure 4.5:** a) Shoreline changes across the Ugento case study as evaluated through the DSAS tool (high accretion –blue; high erosion – red); b) shoreline changes within the Fontanelle area (moderate accretion – light blue; high accretion – blue); c) Temporal variability of shoreline movement within the Fontanelle area over the 2009-2018 timeframe ; d) erosion/accretion rate along the coastal zone of Fontanelle

**Figure 4.6:** a) Shoreline changes across the Ugento case study as evaluated through the DSAS tool (high accretion –blue; high erosion – red); b) Shoreline changes within te marina of Torre Mozza (moderate erosion – light red; high erosion – red); c) Temporal variability of shoreline movement of the Torre Mozza area over the 2009-2018 timeframe; d) erosion/accretion rate along the coastal zone of Torre Mozza

**Figure 4.7:** a) Shoreline changes across the Ugento case study as evaluated through the DSAS tool (high accretion –blue; high erosion – red); b) Shoreline changes within Lido Marini (moderate accretion – light blue; moderate erosion – orange); c) Temporal variability of shoreline movement of the Lido Marini area over the 2009-2018 timeframe; d) erosion/accretion rate along the coastal zone of Lido Marini

**Figure 4.8:** Shoreline movement results in coastal zone of the Municipality of Ieras Poleos Messolonghiou; a) for the time period 1985 to 2009 and b) for the time period 2009 to 2019

**Figure 4.9:** a) Temporal variability of shoreline movement over the period 2009-2019, b) illustration of erosion and accretion on coastal zone of Louros beach (moderate accretion- purple and moderate erosion- orange) and c) erosion/accretion rate along coastal zone of Louros beach

**Figure 4.10:** a) Temporal variability of shoreline movement over the period 1009-2019, b) illustration of erosion and accretion on coastal zone of Louronisides (high erosion-red and high accretion- blue) and c) erosion/accretion rate along coastal zone of Louronisides

**Figure 4.11:** a) Temporal variability of shoreline movement over the period 1009-2019, b) illustration of erosion and accretion on coastal zone of Alikes and Tournida study site and c) erosion/accretion rate along coastal zone of Alikes and Tournida study site

**Figure 4.12:** a) Temporal variability of shoreline movement over the period 1009-2019, b) illustration of erosion and accretion on coastal zone of Evinos estuary and c) erosion/accretion rate along coastal zone of Evinos estuary

**Figure 4.13:** Diagram of the mean annual rate of erosion or deposition along the area of study. The circled areas correspond to the areas with an erosion or accretion more than 30m. Transects numbering starts from Kotychi Lagoon (no1) and reaches Rio at Transect (no2150)

**Figure 4.14:** Map of the shoreline displacement from 1945 to 2018 in Karnario area. Red color represents areas with intense erosion while yellow color marks areas where the deposition is high. Areas where the shoreline displacement is lower than 30m during the 1945-2018 period are presented with green color

**Figure 4.15:** Map of the shoreline displacement from 1945 to 2018 in Karnario area. Different colors represent the shoreline position at different dates

**Figure 4.16:** Map of the shoreline displacement from 1945 to 2018 in Gialos area. Red color represents areas with intense erosion

**Figure 4.17:** The area of the new port of Patras. At the left an airphoto of 1945 and at the right a Worldview image of 2018

## List of Tables

**Table 2.1.** Appearance frequency for class of significant wave height,  $H_s$  (m), and direction

**Table 2.2.**  $H_s$  exceedance probability (a) SSW, (b) S, (c) SSE

**Table 2.3.** The 5 years long programme for dredging and nourishing

**Table 3.1.** Information regarding the survey lines conducted

**Table 3.2:** Coordinates of boreholes drilled in the shoreline of the gulf of Patras

**Table 3.3:** Soil classification test results

**Table 3.4:** Unconfined compression test results

**Table 3.5:** Direct shear unconsolidated undrained test results

**Table 3.6:** Coordinates of cone penetration tests performed in the Alykes fishery port

**Table 3.7:** The 8 subregions of the pilot area of the Gulf of Patras from west to east, as presented in Figure 3.31, and the corresponding values of the mean sediment grain diameter,  $D_{50}$ , in the coastal zone of each subregion

**Table 3.8:** Wind and wave data with a return period of 1 year, per wind direction, in deep waters offshore of the coastal zone of the pilot area of the Gulf of Patras.

**Table 3.9:** Characterization of the erosion intensity in the 8 subregions of the pilot area of the Gulf of Patras, for each wind direction, according to the numerical results of the present work.

**Table 4.1.** Metadata of the satellite images used in the frame of the Ugento pilot case

**Table 4.2.** Metadata of the satellite images used in the frame of the Messolonghi pilot case

**Table 4.3.** Metadata of the satellite images used in the frame of the southern part of the gulf of Patras

Lead Partner

Technical support

Project Partners

## 1. Introduction

It is widely recognized among the scientific community that climate change is leading to severe impacts on both terrestrial and marine ecosystems worldwide in a variety of ways (IPCC, 2018). Specifically, rising sea level, changes in the dynamics and energy distribution of waters, as well as variations in the pattern, frequency and intensity of extreme events are expected to increase future coastal flooding and erosion (IPCC, 2018). Against this complex scenario, coastal areas are also suffering relevant pressures resulting from a variety of human-made pressures associated to coastal economic development (e.g. touristic activities and infrastructures along the shoreline) and linked land use changes (e.g. urbanization) (Ramieri et al., 2011).

Resulting impacts of this complex interplay among climate-related and anthropogenic pressures consists in water quality deterioration, biodiversity loss, reduced species survival and species shift which, in turn, will affect ecosystems services flow and generate socio-economic damages, including disruption of coastal urban areas and infrastructures (UNDP, 2011; IPCC, 2014a).

Against this setting, coastal authorities are faced with the challenging task of designing integrated coastal management plans, embracing climate change adaptation and coastal resources development and exploitation, taking into account the high number of environmental and socio-economic factors at stake, as well as the variety and complexity of interactions that may occur among natural and human-induced pressures acting at the land-sea interface. As described in the Deliverable 3.5 “Development of the framework and tool for final users with training”, when focusing on coastal erosion processes, more or less sophisticated tools can be applied to identify, on one side, key drivers contributing to coastal imbalance and to design, on the other, the most appropriate monitoring actions for understanding erosion trends and select required structural or nature-based measures, following the order of priority resulting from the level of risk. These tools and methods range from indicators and index-based methods (e.g. Coastal Vulnerability Index – CVI) to more complex Decision Support Systems (DSS; e.g. DESYCO, DIVA, Theseus) and machine-learning based approaches, including remote sensing techniques widely applied for the multi-temporal detection and analysis of shoreline evolution.

In the current deliverable several pilot cases from both countries have been investigated and presented in order to develop a joint tool for efficient detection and analysis of shoreline evolution.

In Chapter 2 are presented two interventions along the coastline of Puglia region in Italy. The two interventions were selected because they can be assumed as good practices for:

- rehabilitation of an eroded stretch of coast;
- improvement of the social, economic, infrastructural conditions for a degraded coastal urban area.

Coastal works along the Ugento coastline represent the first type (in section 2.1); the second type is represented by the construction of a new sea side promenade in Bari, in the Fesca - San Girolamo neighbourhood (in section 2.3).

In Chapter 3 is presented the establishment of a pilot erosion observatory in the gulf of Patras in Greece. The gulf of Patras suffers significant erosion problems and the pilot erosion observatory aims to collect real-time data, with the monitoring of several parameters that negatively affect shorelines. The collected data can be later used, with the appropriate interpretation, in the long-term protection of the suffered shorelines. Furthermore, another pilot area is examined, that is the Kotychi lagoon, because of its biodiversity and its high protection regime (RAMSAR convention and European Natura network).

The final Chapter 4, presents the Geographic Information System (GIS) framework as well as the remote sensing techniques that were applied as a joint risk-based tool across the TRITON IT-GR pilot cases, in order to analyze the shoreline evolution trend against time from satellite images. Specifically, Chapter 4 describes the designed TRITON risk-based joint tool, providing details on the applied methodological approach and discussing the resulting outputs from its application across the Ugento (Italy), Messolonghi and the Gulf of Patras (Greece) shorelines.

Lead Partner



Technical support

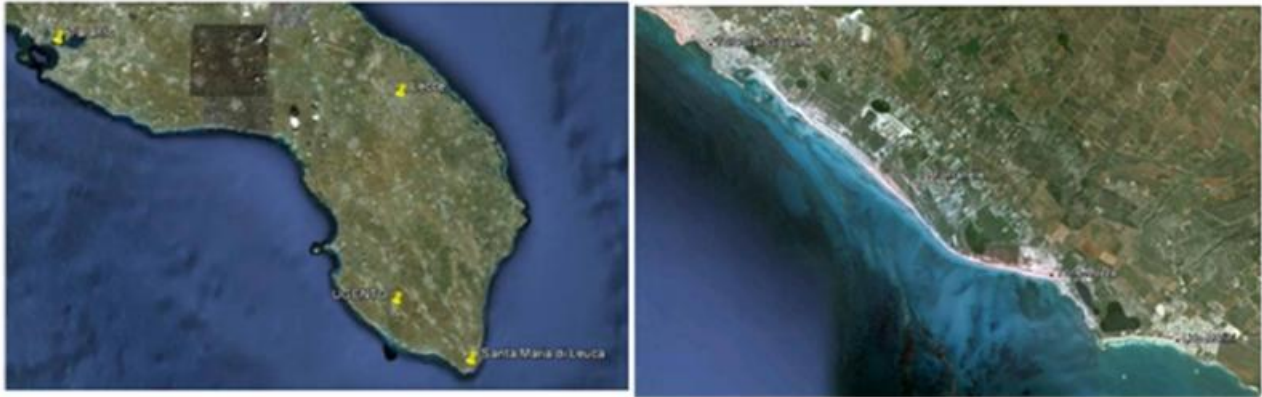


Project Partners



## 2 Pilot tests and studies in the Apulia region

### 2.1 The First Ugento Case Study



The 6 km long stretch of coast between Torre San Giovanni and Torre Mozza nearby Ugento presents a very high environmental value (Figure 2.1).

**Figure 2.1:** Location of Ugento (a); stretch of coast (b)

It has also a considerable role for the economy of the area because of the presence of several resorts, hotels and camping areas. The said stretch of coast is an independent littoral cell, and since decades is undergoing erosion due to the numerous inland interventions that reduce the sediment volumes at sea.

In 2003, the Regione Puglia, designed and built a coastal intervention composed of 3 groynes and nourishing of sand from dredging activity in the small port of Torre San Giovanni (Figure 2.2).



**Figure 2.2:** The as built groynes, picture taken in 2003

After years, the beaches are again suffering an erosion phenomena with reduced area for recreational activities at the many resorts and hotels in the area.

In 2017, the Ugento Municipality has designed a new coastal intervention for the same area. In order to design it, consulting studies have been conducted with the scope to:

- Determine the wave offshore wave climate;
- Quantify the sediment longshore transport;
- Determine the eroded and nourished volumes;
- Establish a plan for future interventions in the area with a 5 years long span.

### 2.1.1 Wave climate and height

The following Table 2.1 and Figure 2.3 present the mean wave climate; i.e. the frequency of appearance for a given class of significant wave height,  $H_s$ , and wave direction.

**Table 2.1.** Appearance frequency for class of significant wave height,  $H_s$  (m), and direction

Hs (m) Sector	0.0-0.5	0.5-1.0	1.0-1.5	1.5-2.0	2.0-2.5	>2.5	%	TOTAL
N	10	9	4	0	0	0	2.24	23
NNE	3	0	0	0	0	0	0.29	3
NE	0	1	0	0	0	0	0.10	1
ENE	1	0	0	0	0	0	0.10	1
E	2	0	0	0	0	0	0.19	2
ESE	9	0	0	0	0	0	0.88	9
SE	44	19	8	2	0	0	7.11	73
SSE	37	32	17	10	1	0	9.44	97
S	42	41	19	2	3	1	10.52	108
SSW	107	35	9	7	2	0	15.58	160
SW	53	29	2	4	3	0	8.86	91
WSW	130	46	12	2	1	0	18.60	191
W	33	30	11	0	1	0	7.30	75
WNW	20	9	0	0	2	1	3.12	32
NW	24	28	10	0	1	0	6.13	63
NNW	33	48	15	2	0	0	9.54	98
%	53.36	31.84	10.42	2.82	1.36	0.19	100.00	
<b>TOTAL</b>	<b>548</b>	<b>327</b>	<b>107</b>	<b>29</b>	<b>14</b>	<b>2</b>		<b>1027</b>



### 2.1.2 Closure depth

The closure depth has been determined by means of the Hallermeier (1978) formula

$$D_C = 2.28 * H_{12h} - 68.5 * \left( \frac{H_{12h}^2}{gT_{12h}^2} \right)$$

where,

$D_C$  closure depth

$H_{12h}$  offshore significant wave height exceeded 12 hours per year (1/730)

$T_{12h}$  peak wave period exceeded 12 hours per year (1/730)

Closure depth results equal to 6.95 m.

### 2.1.3 Ugento and the regional master plan for coastal management (PRC)

The Piano Regionale delle Coste (PRC) classifies this stretch of coast with a high value for the landscape and mean/high vulnerability for the coastal erosion. In the following Figures the graphs from the PRC showing the physical situation and the classification of the considered coastline.

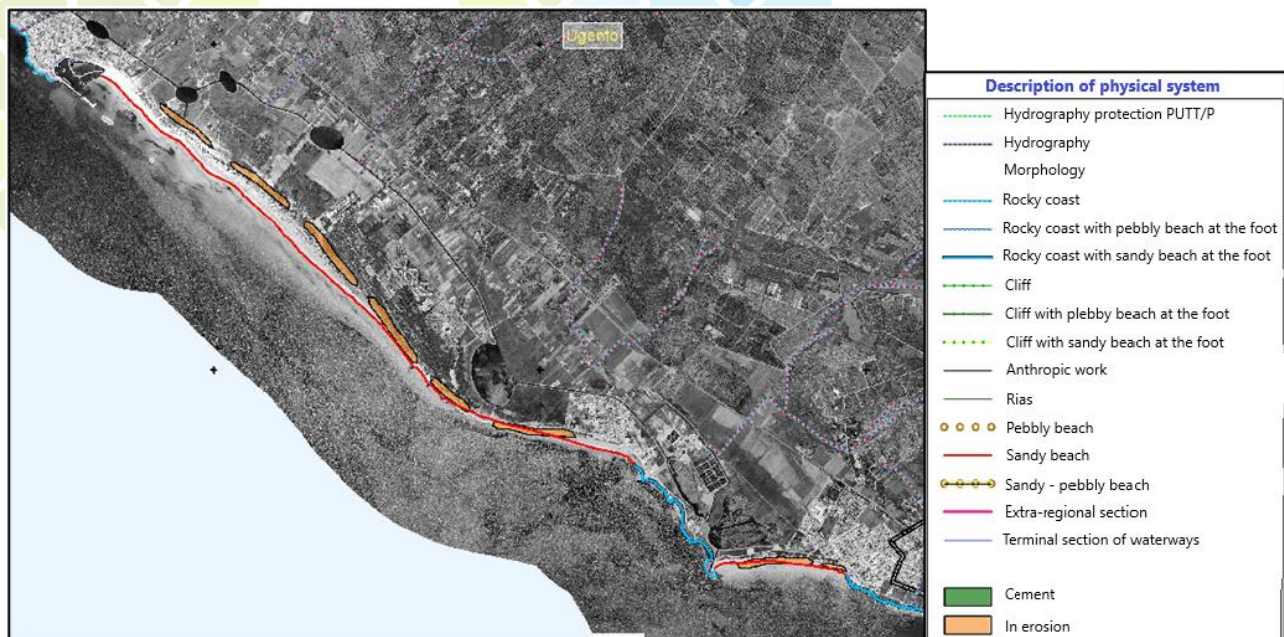
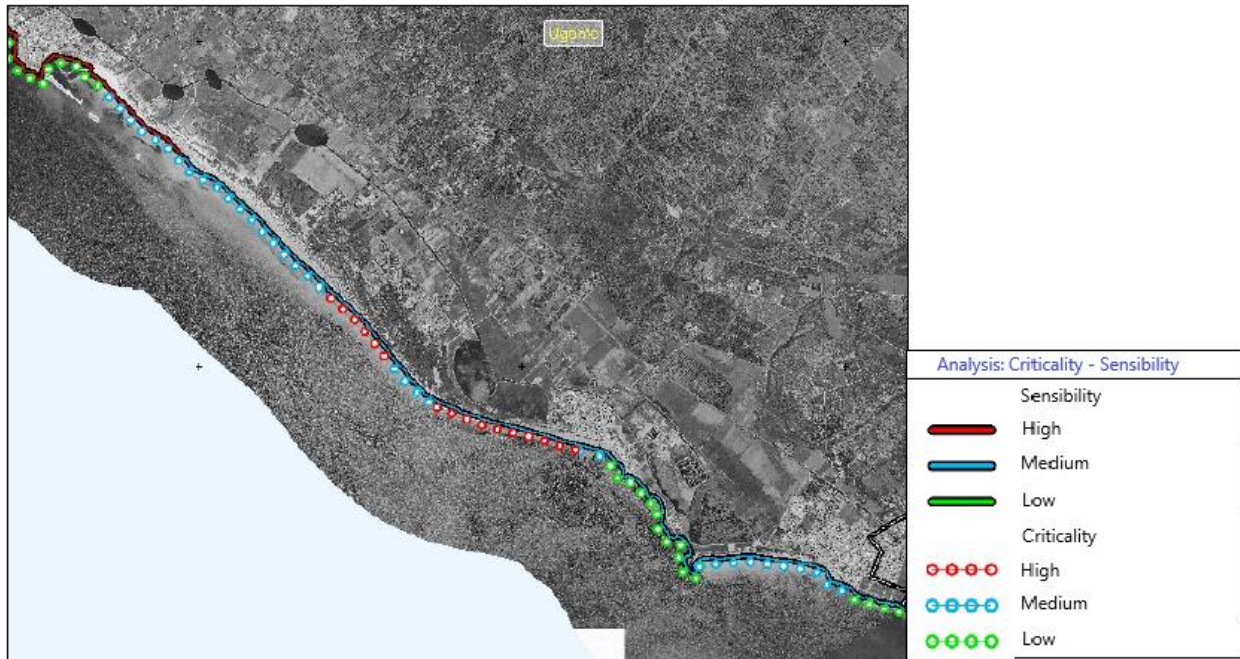


Figure 2.4: Description of the physical system



**Figure 2.5:** Coastal erosion vulnerability and Value for the Landscape

### 2.1.4 Calculation of the longshore sediment transport

Different sources of information have been adopted. Data of sand volumes dredged from the port together with the data obtained from the comparison of historical shorelines since 1978. Figure 2.6 presents a comparison of historical shorelines from 2005 to 2010.



**Figure 2.6:** Comparison of historical shorelines 2005-2010 - 2010 behind the red line

Longshore sediment transport has also been determined by the CERC formula (USACE, 1984). This has allowed to determine the net sediment transport which results ranging between 43.000 and 240.000 m<sup>3</sup> per year and it is directed toward the port.

### 2.1.5 Approved design

Design considers a dredging (dragaggio) campaign of volumes of sand at the port entrance and their use for nourishing of the eroded shorelines to obtain their advancement (avanzamento). The nourishment was carried out in two sites as in the Figure 2.7 below.

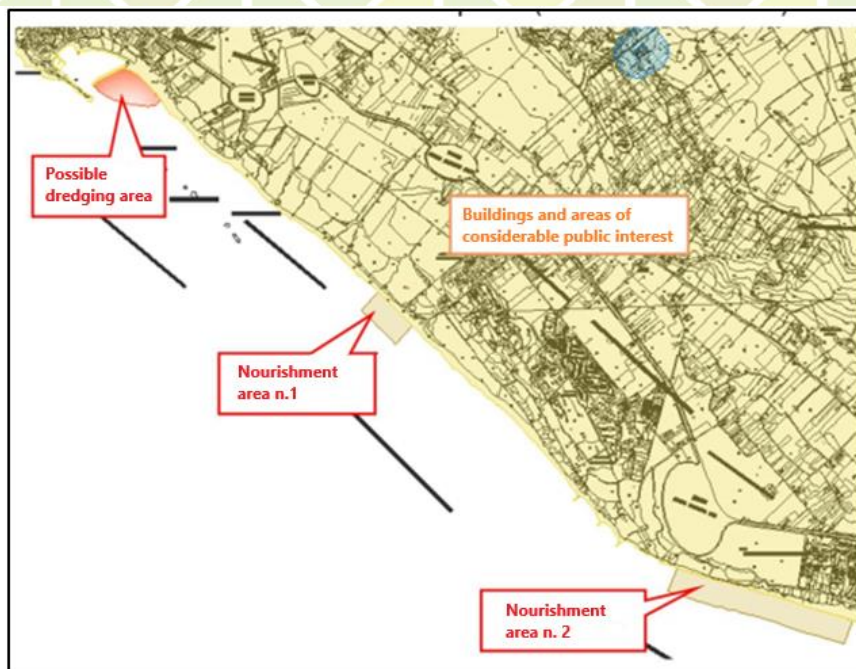


Figure 2.7: Location of the areas to be dredged and to be nourished

The 5 years long programme is given in the following Table; it indicates the volumes to be dredged at the port and their planned reuse at the two selected sites.

Table 2.3. The 5 years long programme for dredging and nourishing

	Ashore panel dredging at Torre San Giovanni m <sup>3</sup>	Shore line advancement m	Fontanelle - Torre Mozza Stretch length m / Surface emerged m <sup>2</sup>	"Victor Village" - "Iberohotel" Stretch length m / Surface emerged m <sup>2</sup>
First year	60.000	6	950 m / 5.700 m <sup>2</sup>	250 m / 1.500 m <sup>2</sup>
Second year	40.000	4	950 m / 3.800 m <sup>2</sup>	250 m / 1.000 m <sup>2</sup>
Third year	20.000	2	950 m / 1.900 m <sup>2</sup>	250 m / 500 m <sup>2</sup>
Fourth year	20.000	2	950 m / 1.900 m <sup>2</sup>	250 m / 500 m <sup>2</sup>
Fifth year	20.000	2	950 m / 1.900 m <sup>2</sup>	250 m / 500 m <sup>2</sup>

### 2.1.6 Lesson learnt

Studies conducted to support the new design demonstrate that the longevity of the intervention made in 2003 presented a 15 years long longevity. The studies and observations also show the effectiveness of the groins built in 2003, particularly when in presence of a headland, where waves are more oblique.

The new design profits of the experience gained with the 2003 interventions and, consequently, the new beach nourishing comprises two different steps: dredging to obtain the sediments and transport and deployment of sediments for nourishing. The intervention will reach two goals: to reobtain water depths for the use of the small marina of San Giovanni and to reobtain emerged beaches for the use of local inhabitants and tourists.

The intervention is made necessary to stabilise the shoreline and, more important, to continue with recreational activities which are fundamental for the local economy.

## 2.2 The Second Ugento Case Study

### 2.2.1 *Posidonia oceanica* seagrass meadows and dunes rehabilitation

*Posidonia oceanica* seagrass meadows are a key ecosystem of the Mediterranean environment. In fact, they protect the coast from erosion and regulate CO<sub>2</sub> absorption in the sea while storing it, mostly below its underground mat. Also well-known is their role as a habitat and food provider for many fishes and invertebrates, including commercial species. Moreover, the development of seagrass habitats around the coastline significantly influences the profile of beaches. In the meadows, the network of rhizomes consolidates the sediment acting as a reef that helps beach stabilization, while the leaf canopy assists in reducing wave energy through the incident friction of the plant leaves with the water.

Furthermore, banquettes act as a natural protector, by minimizing beach erosion through absorption of sea wave energy during storms and strong winds.

Storm waves that form *Posidonia* banquettes on the foreshore and the backshore of the beach can also erode the banquettes and transport part of the wrack material from the beach and dune. Subsequent calm weather with offshore winds will favour the return of the sand and seagrass wrack back to the beach and might transport them further into the sea. Thus, the dunes, the beach, and the nearshore seagrass meadows act as a dynamic, integrated unit, referred to as the *Posidonia* beach–dune system.

Lead Partner

Technical support

Project Partners

Figures 2.8 and 2.9 represent in green colour the mapped sea areas covered by Posidonia Oceanica in the Salento area. It is noticed that the sea area of Ugento is largely covered by Posidonia.

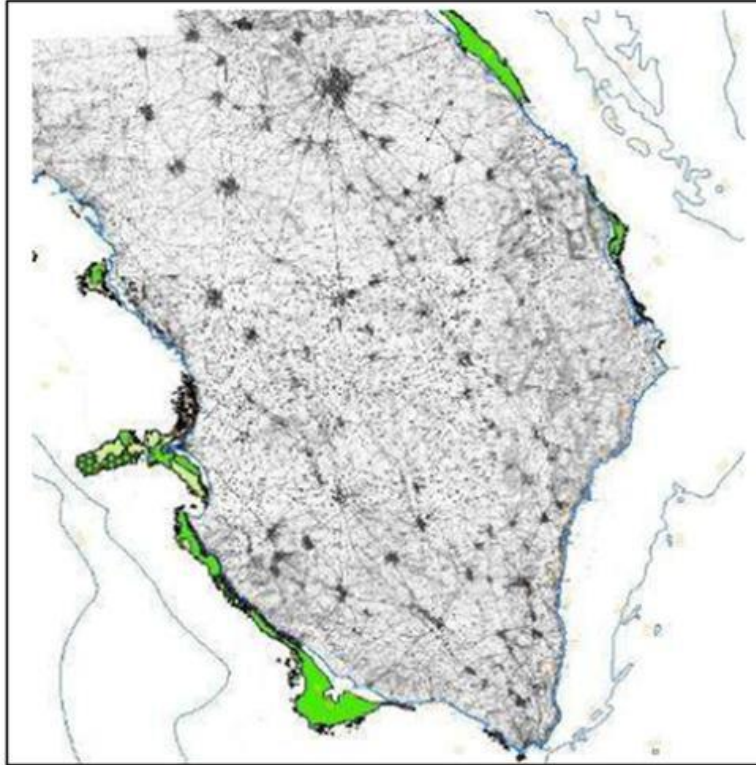


**Figure 2.8:** The Posidonia Oceanica around the Salento peninsula



**Figure 2.9:** The map of Posidonia Oceanica along the Ugento coastline

Lead Partner

Technical support

Project Partners

Due to the large presence of seagrass vegetation, the coastline of Ugento is widely covered by Posidonia banquettes. As the deposits accumulate, the banquettes tend to decrease the transport of sand across the beach and increase sand deposition within the banquette. Consequently, banquettes have an important role in the beach profile configuration and dune formation and stabilization.

But, on the other hand, the deposits generate problems to the mouth of several drainage channels that are in the area. Figures 2.10 and 2.11 show the channels mostly occupied by the Posidonia deposits.



**Figure 2.10:** Mouth of the drainage channel at San Giovanni, Ugento



**Figure 2.11:** Mouth of the drainage channel at Torre Mozza, Ugento

According to the Italian law, the deposits of Posidonia Oceanica represent an urban waste. This determines huge costs for its removal. A different type of approach can be adopted consisting in the reuse of the deposits for the rehabilitation of dunes.

Within this path, an intervention has been designed and actuated consisting in taking the material from the drainage channels at Torre Mozza and San Giovanni and their reuse at the following sites:

1. *South of the port area*
2. *Torre San Giovanni*
3. *Torre Mozza (Figure 2.12)*
4. *Punta del Mocolone*
5. *Lido Marini*



**Figure 2.12:** Torre Mozza deployment area and view of the dune at the end of the intervention

The total volume of reused deposits is about 30.000 m<sup>3</sup>. A monitoring programme is ongoing; each three months morphological, botanical, observations are conducted to detect changes in the dune geometry and the presence of alien botanical species.

### 2.2.2 Lesson learnt

It has been revealed that the accumulation of *Posidonia* beach cast can represent a resource if considered within the integrated unit referred to as the *Posidonia* beach–dune system. In fact, this material, that in the past was considered as a waste, can be now considered a resource for the coastal management, particularly focused on preserving and rehabilitating the dune system.

### 2.3 The Third San Girolamo – Fesca case study

The 1.7 km long stretch of coast north of Bari downtown delimitates an urban area north of Bari called San Girolamo – Fesca. The construction of the San Girolamo – Fesca neighbourhood was started in the first years of the sixties last century. The main connecting road was adjacent the rocky seashore and its retaining wall was subjected to the action of the waves with frequent flooding events for the pathway under intense sea storms. Figure 2.13 refers to the situation before the intervention.



**Figure 2.13:** Photos before the intervention

The 1.7 km stretch of coast is delimited by two channel mouths, with some water flowing only in presence of severe rainstorms (Figure 2.14).



**Figure 2.14:** The stretch of coast between the two channel mouths

In 2009, the Bari Municipality decided to invest more than 15 million euros to create a promenade with some precise objectives:

- To have an area at the sea with restaurants and cafes,
- To create new beaches for recreational purposes,
- To create a small marina,
- To solve the problem of drainage of meteoric waters.

- The project was co-funded by the European Union.

### 2.3.1 The wave climate studies

An offshore wave climate study was conducted based on the wave buoy data collected from 1989 until 2008 in front of Monopoli which is located 45 km south of Bari. Figure 2.15 presents the obtained wave rose; the most intense and frequent sea storms come from the NNW direction.

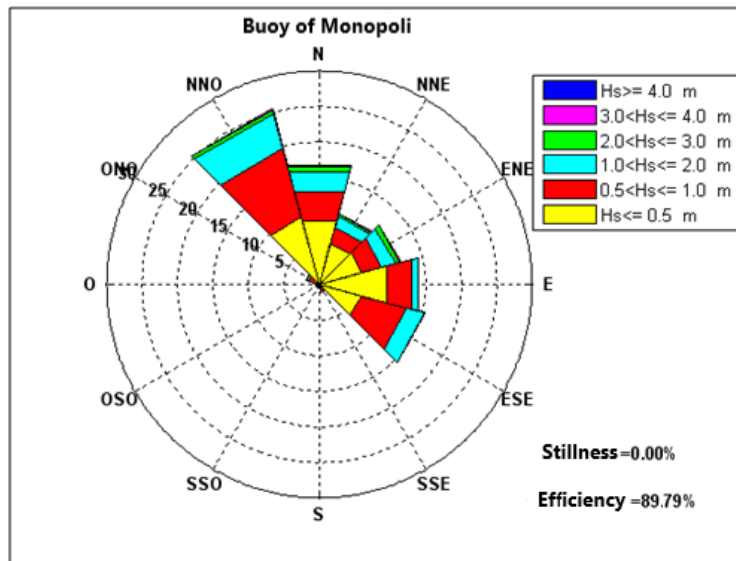
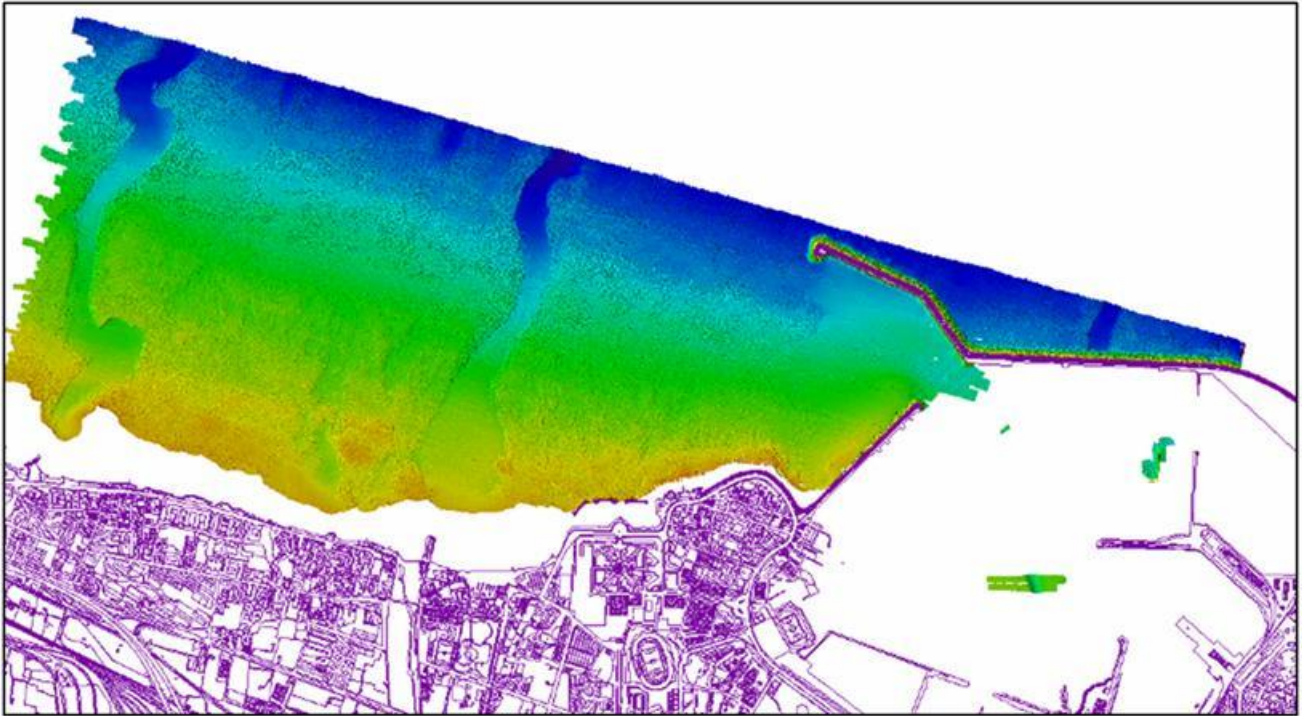


Figure 2.15: Wave rose offshore Bari

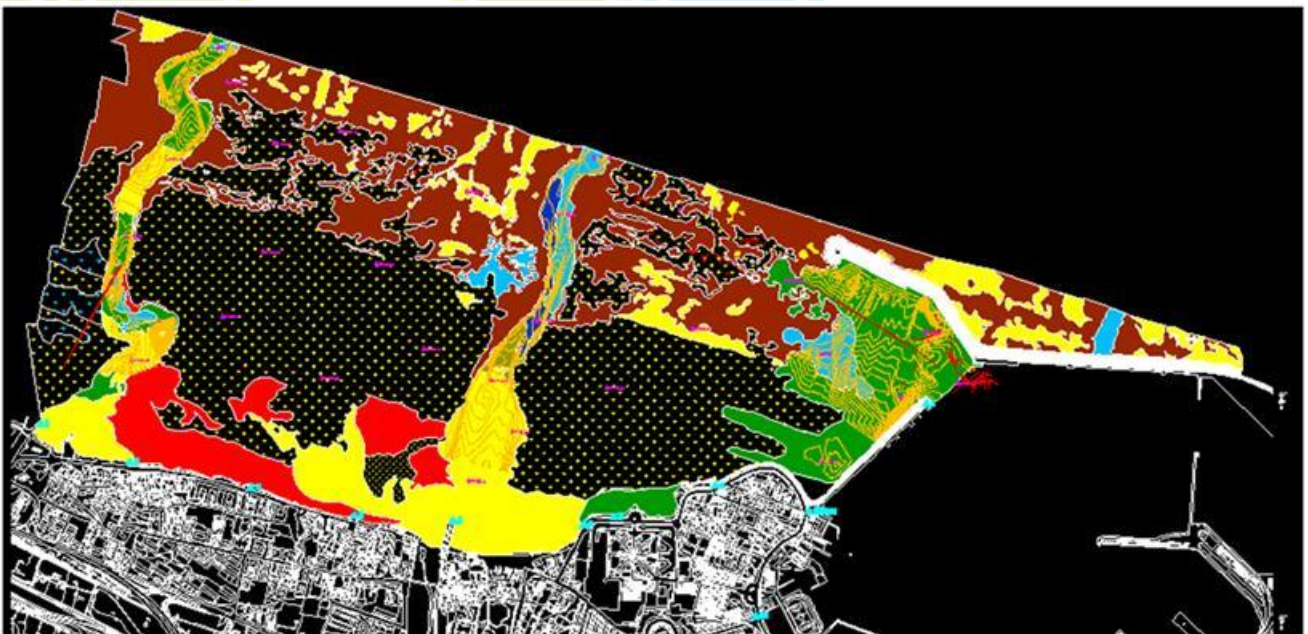
### 2.3.2 The bathymetrical and geomorphological charts

A bathymetric campaign was conducted by means of boats with multi beam acoustic instruments. The result is presented in Figure 2.16 clearly showing the presence of two deepen areas at the sea bottom in front of the two channel mouths.



**Figure 2.16:** The bathymetry in front of San Girolamo - Fesca

A geomorphological investigation was conducted by means of samplings of materials at the sea bottom and video inspections (Figure 2.17).



Lead Partner

Technical support

Project Partners

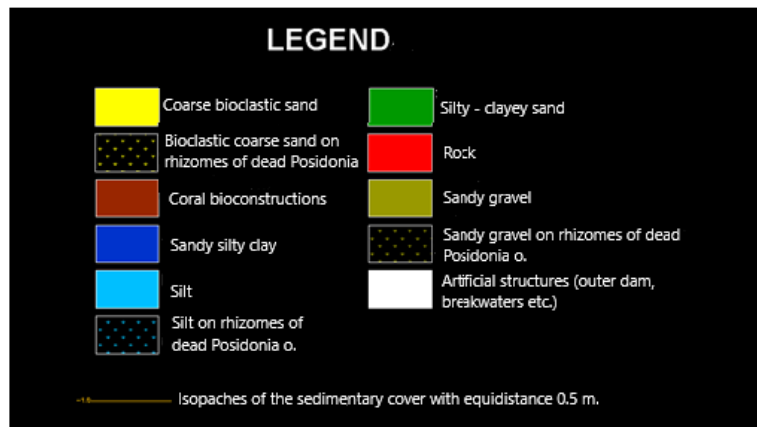


**Figure 2.17: Geomorphological chart**

### 2.3.3 The planned intervention

In order to reach the mentioned goals, the design comprised a number of detached breakwaters (emerged and submerged), a small marina, sand and gravel nourishing to obtain 4 new beaches (2 sandy and 2 gravel beaches), a square with restaurants and cafes facing the sea (Figure 2.18). The design included a 1.7 km long pedestrian and biking paths, planted trees, an artificial dune facing the new beaches and the traffic was reduced to a one-way road limitation. A drainage system was considered to collect the rainstorm waters, to treat them and to reuse for the irrigation of trees and plants.

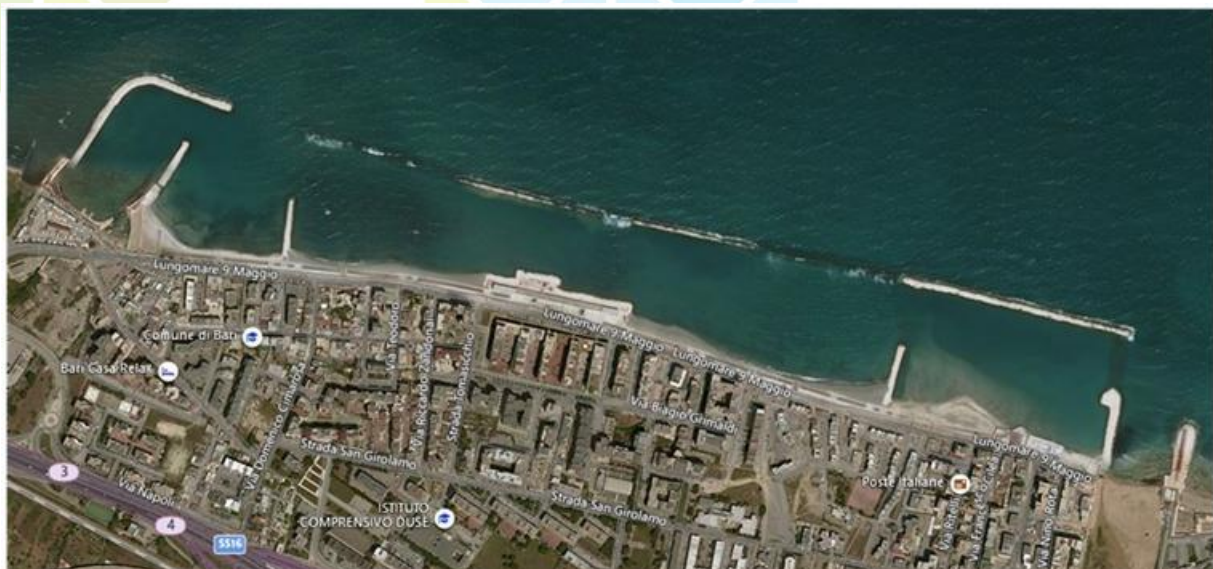


**Figure 2.18: Plan view of the intervention a few months before the end of construction (May 2019)**

In summary, the coastal works include, from West to the East (Figures 2.19, 2.20):

- A main breakwater protecting the new marina;
- A groyne, also acting as secondary breakwater for the marina;
- A sandy beach
- A groyne;
- A continuous detached breakwater reaching the channel mouth to the East, made emerged and submerged;
- A gravel beach;
- A square at the sea with a terrace,
- A gravel beach;
- A groyne;
- A sandy beach;
- The last groyne to the East



**Figure 2.19:** From the right to the left: a pedestrian path, the bicycle path, the trees, another pedestrian path, an artificial dune, seats made at the retaining wall, the beach



**Figure 2.20:** Beach nourishing and the artificial dune with the long seating wall

Lead Partner

Technical support

Project Partners

### 2.3.4 The effectiveness of the coastal protection

The influence of the planned coastal structures was tested by means of numerical models to determine the wave conditions, the wave induced circulation and water quality. The wave propagation modelling was conducted for the present (before works) and design (after works) scenarios. As an example, Figure 2.21 presents, with values in a chromatic scale, the significant wave height,  $H_s$ , and wave direction, before and after works, for waves coming from NNW and with  $H_s=2.0$  m and peak wave period,  $T_p$ , equal to 9 s.

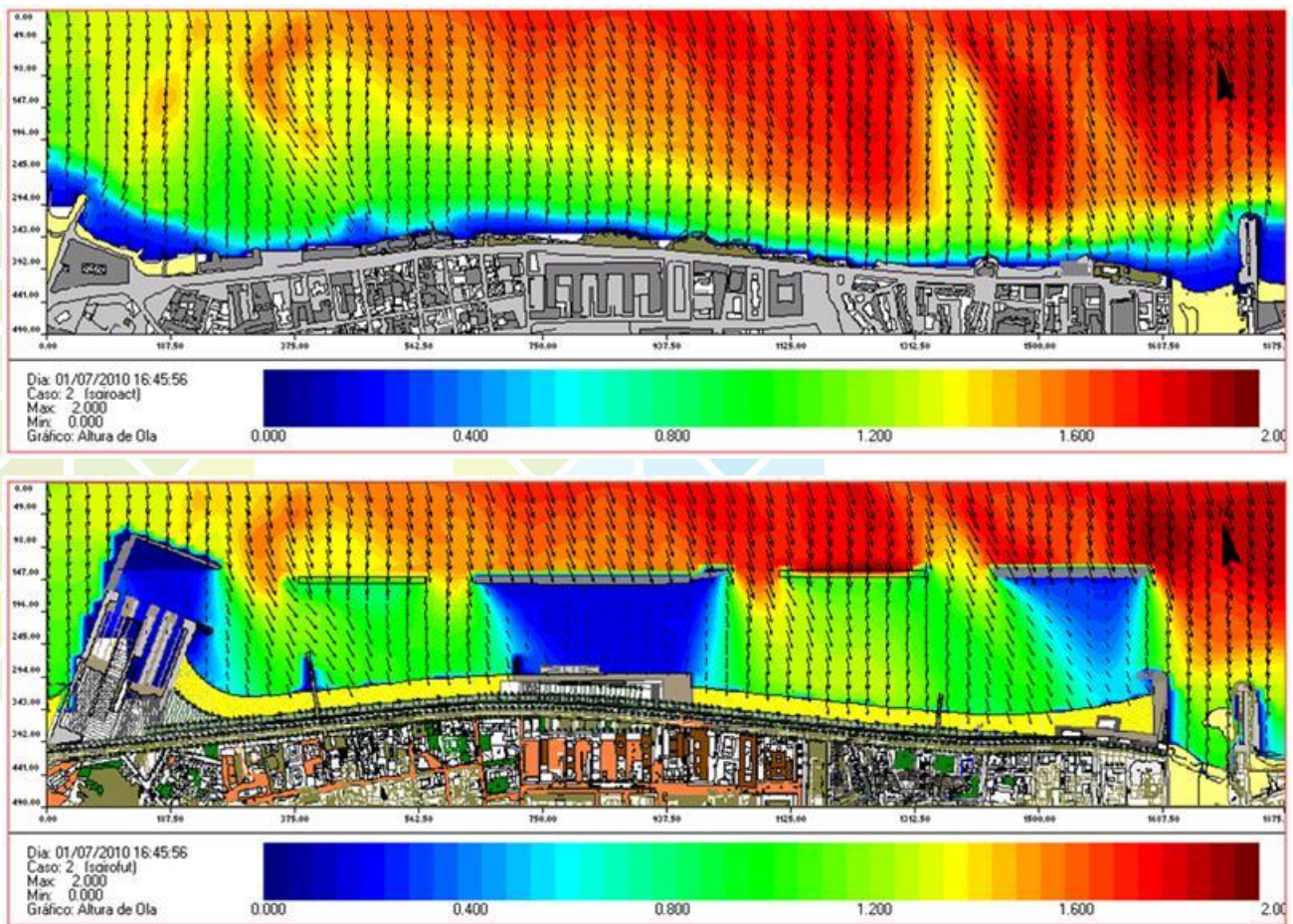
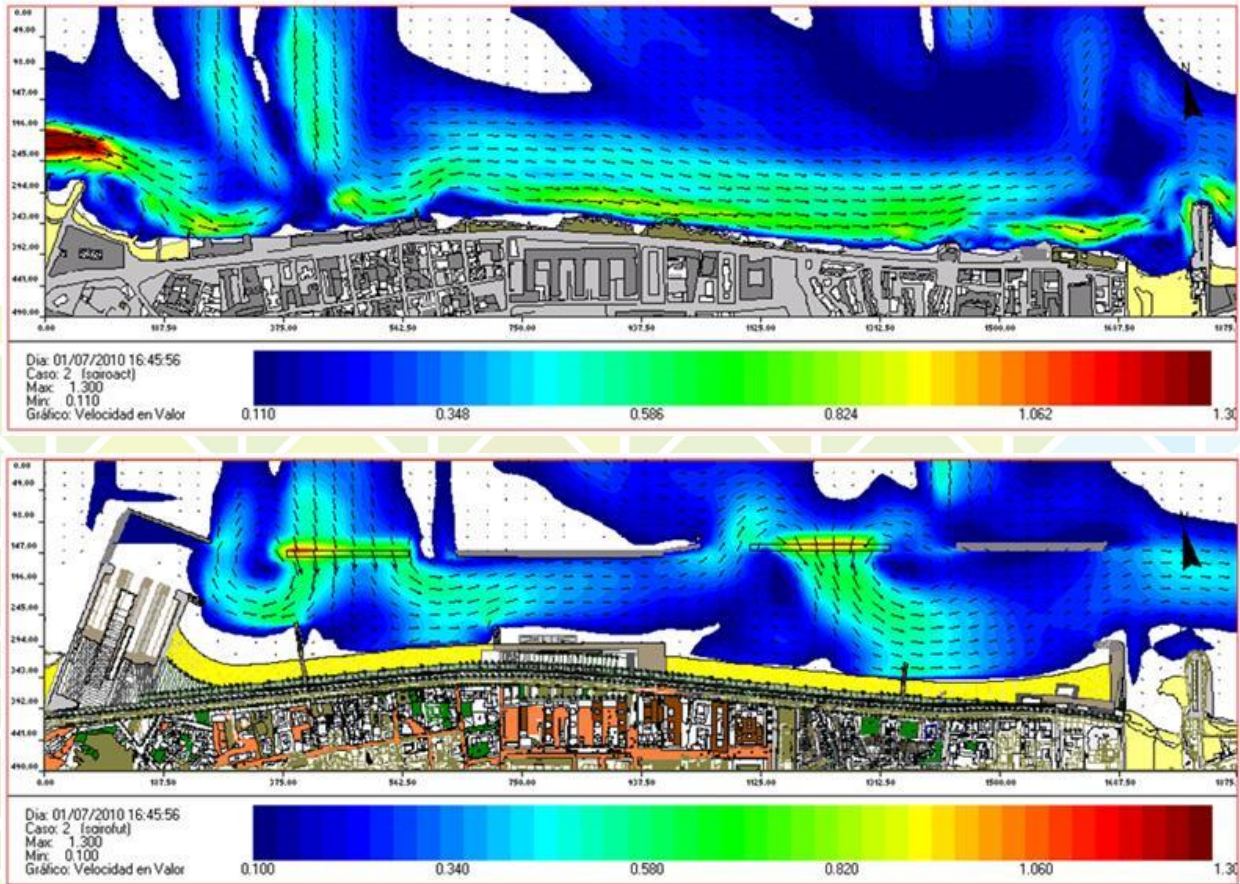


Figure 2.21: Values of  $H_s$  and wave direction, before and after works

Circulation was simulated (before and after works), for the same input conditions, resulting in Figure 2.22.



**Figure 2.22: Wave induced circulation before and after works**

### 2.3.5 The current situation

The works ended in May 2019 and Figure 2.23 represents the current situation.

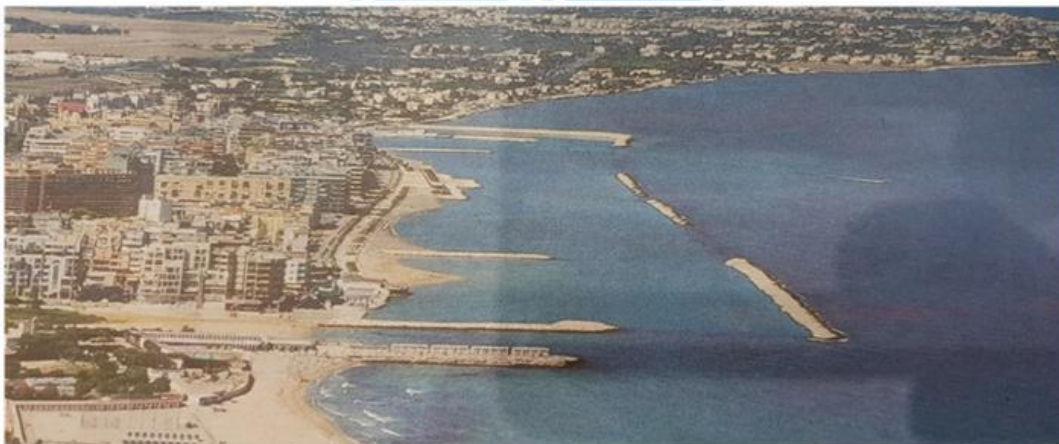


**Figure 2.23: Present situation. Photo taken from the East side**

### 2.3.6 Lesson learnt

There are several things that emerged during the 10 years long process to reach the end of works (2009-2019). The decision of the Municipality to share with the population the design process by means of public forums, helped the design and the works to be accepted from the local inhabitants. Nevertheless, during the construction there were several complains from locals with attempts to stop the construction. Major claim was the partial interruption of the seaside road for some years.

In the end, local people are very happy now, not only because a large recreational area, with 1.7 km long beaches and a marina, is at their places, but also because there are higher values for the real estates. In fact, some seaside apartments have been sold even to foreign people who intend to live in the Santa Claus town and enjoy the beaches and the marina.

Finally, as expected, the intervention resulted in the reach of all the objectives posed by the Bari Municipality and can certainly stimulate further similar works, sure that they will produce good results for the local inhabitants within a social and economic view.

Lead Partner



Technical support



Project Partners



### 3 Pilot tests and studies in the region of Western Greece

#### 3.1 The establishment of a pilot erosion observatory in the gulf of Patras and the Kotychi lagoon

The establishment of a pilot erosion observatory in areas that suffer significant erosion problems aims to collect real-time data, with the monitoring of several parameters that negatively affect shorelines. The collected data can be later used, with the appropriate interpretation, in the long-term protection of the suffered shorelines. In order to achieve this goal, it is necessary to design an accurate geomorphological and coastal plan of the study area as well use the necessary mobile and immobile equipment for the appropriate monitoring.

In the region of Western Greece two study areas were selected for the establishment of a pilot erosion observatory:

- (a) the gulf of Patras, because of its biodiversity and the increased urban and touristic development that is expanding along its shoreline
- (b) the Kotychi lagoon, because of its biodiversity, which is under protection with the RAMSAR convention and the European Natura network.

In order to fulfill the all the prerequisites of a pilot erosion observatory, an accurate geomorphological and coastal design plan as well as a detailed site investigation program was conducted in the gulf of Patras. Moreover, the necessary mobile equipment that was used during the site investigation process consisted of (a) one Unmanned Aerial Vehicle (UAV), (b) one Hydrographic Survey Vehicle (HSV) and (c) one Hydrographic Echo Sounder (HES), all of them purchased with funds from the TRITON project. The additional necessary geotechnical, marine and aerial equipment was provided by the team members of the project (laboratories of Engineering Geology, Marine Geology and Physical Oceanography, Remote sensing and GIS, Department of Geology, University of Patras)

The immobile equipment used for data monitoring consisted of: (a) two weather stations, (b) two marigraphs and (c) one wave buoy system, all of them installed by the region of Western Greece in the frame of the TRITON project (see D4.2 Call for tender for interventions selected in the pilot study areas). Additionally, it consisted of: (a) one weather station and (b) four water quality stations, provided by the Management Body of Kotyhi Strofylia Wetlands & Kyparissia Gulf especially for this project.

All mobile equipment (environmental stations) mentioned above are presented in the following Figure 3.1

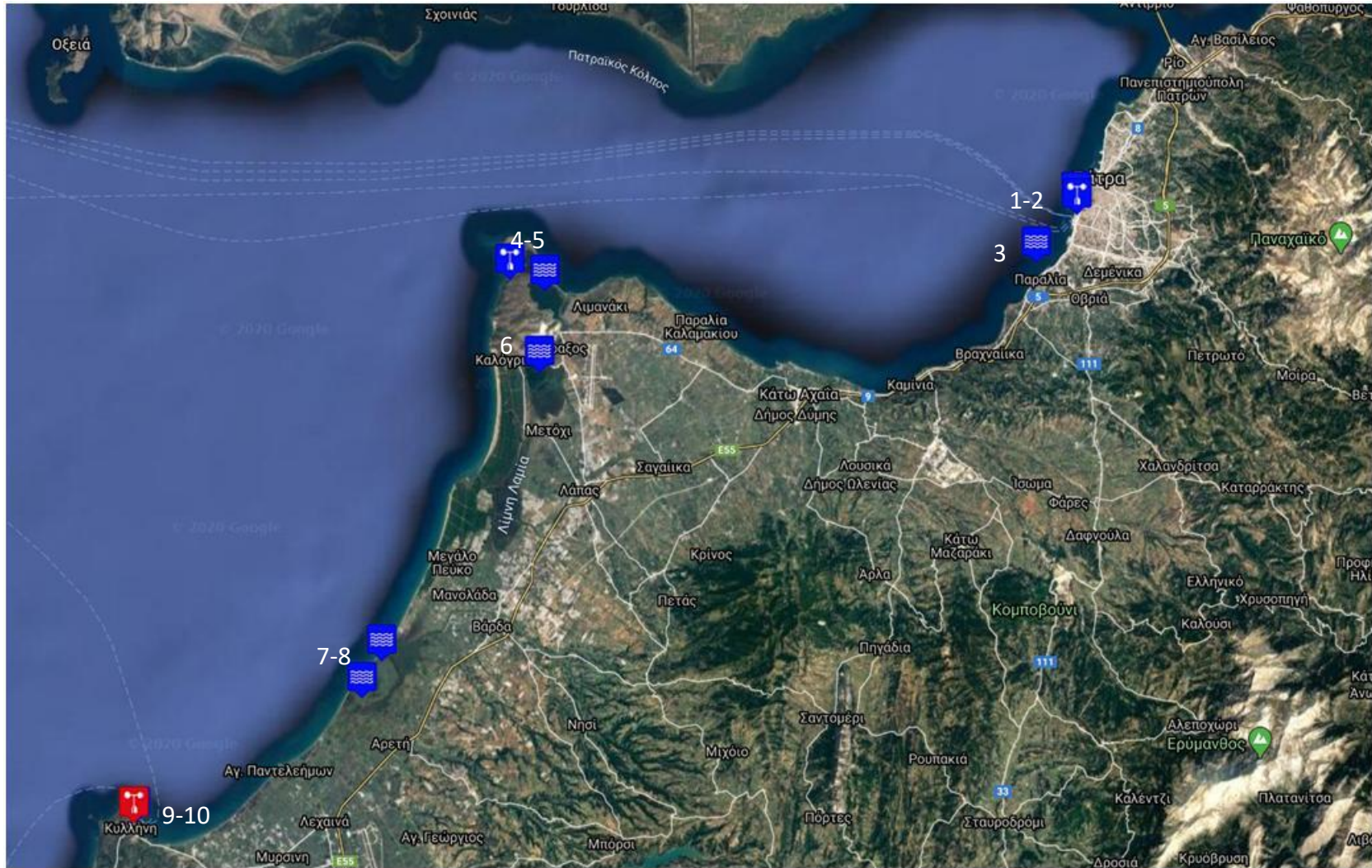


**Figure 3.1:** Installed equipment (environmental) stations in the areas of intervention (Gulf of Patras and Kotychi lagoon)

[1-2: weather station and marigraph in the new port of Patras; 3: wave buoy system in the gulf of Patras; 4-5: weather and water quality stations in the Papas lagoon; 6: water quality station in the Prokopos lagoon; 7-8: water quality stations in the Kotychi lagoon; 9-10: weather station and marigraph in the Killini port]

### 3.2 Procurement of the necessary mobile equipment

On November 02, 2018 a call for tender for the equipment procurement of (a) one Hydrographic Echo Sounder (HES), (b) one Unmanned Aerial Vehicle (UAV) and (c) one Hydrographic Survey Vehicle (HSV) was published on the University of Patras website [link] and the portal for public tenders [www.eprocurement.gov.gr] (online suspension number: ΑΔΑΜ: 18PROQ003944113). The call for tender was repeated on February 25, 2019 for the equipment procurement of the Unmanned Aerial Vehicle (UAV) and was published again on the University of Patras website [link] and the portal for public tenders [www.eprocurement.gov.gr] (online suspension number: ΑΔΑΜ: 19PROQ004513816).

Both calls were publicized according to the National Law 4412/2016 “Public works, supplies and services contracts-Transposition of Directives 2014/14/EU and 2014/25/EU”. The public tender’s documents were available for complete, direct & free online access on the web through a) the University of Patras website and b) the web portal for public tenders. Tenders were completed successfully, and a public contract was signed with the awarded contractors for the procurement of the relevant mobile equipment.



**Figure 3.2** (a) Hydrographic Echo Sounder (HES)  
(b) Hydrographic Survey Vehicle (HSV)  
(c) Unmanned Aerial Vehicle (UAV)

### 3.3 Site Investigation techniques and studies in the areas of intervention

#### 3.3.1 Satellite, UAV, aerial photo imaging and USV for shoreline evolution

In the frame of TRITON project digital processing of diverse remote sensing data had been performed in the gulf of Patras. Medium to Very High Resolution (VHR) satellite data are being processed in order to map the recent coastline while classical analogue air photos covering the period 1945-2008 are used in order to detect the shoreline changes. Additionally, Unmanned Aerial Vehicles and Unmanned Surface vehicles are used for up-to-day data collection in specific areas. In more details the remote sensing monitoring activities that had been used in the frame of TRITON project can be divided in the following approaches.

##### 3.3.1.1 Medium resolution remote sensing data and processing

The first approach focused on the automatic extraction of instantaneous coastline, as identified in the freely available **Sentinel-2 and Landsat-8 OLI imagery** without considering the tide. The shoreline identification was based on grouping all the pixels from the imagery into only two classes: sea and land. The classification results were achieved using two very well-known indices: The Normalized Difference Vegetation Index (NDVI) and the Normalized Difference Water Index (NDWI). The processing has focused on the different spectral reflectance of water compared with that of the land environment and especially the man-made constructions. In the past the specific indexes (NDVI and NDWI) have been used frequently for water body mapping using medium resolution multispectral images. NDWI was introduced about twenty years ago aiming to separate land surface water and vegetation in Landsat TM images. Both NDVI and NDWI were initially designed to map surface water body in Landsat TM images but there are adaptations of them for use with other sensor data. The behaviour of the two above mentioned indexes, although they have a similar algebraic structure, they may not produce similar results when applied to data from different sensors (like OLI or Sentinel-2), was examined in qualitative and in quantitative terms.

NDVI and NDWI images have been produced from the Sentinel 2 and the Landsat 8 images. Then the NDWI and NDVI images were classified in two main classes (sea and Land) and the results are presented below. Figure 3.3 presents the Landsat 8 derived products, NDWI and NDVI classified images, respectively, whereas Figure 3.4 presents the NDWI classified image from the Sentinel data.

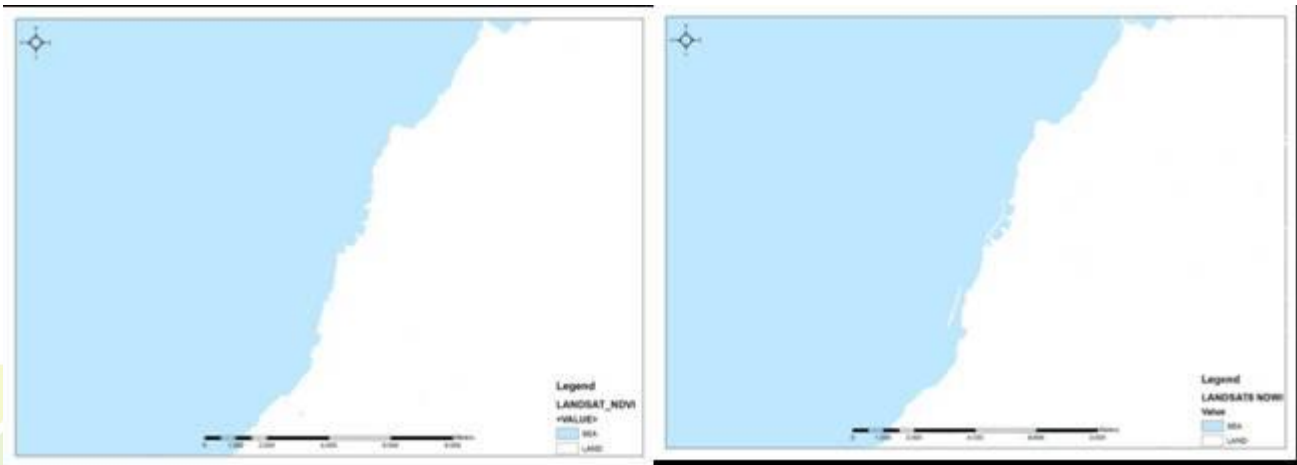


**Figure 3.3:** Part of the Landsat 8 NDWI (left image) and NDVI (right image) classified in two classes (Sea and Land). The port of Patras is in the middle of the image.

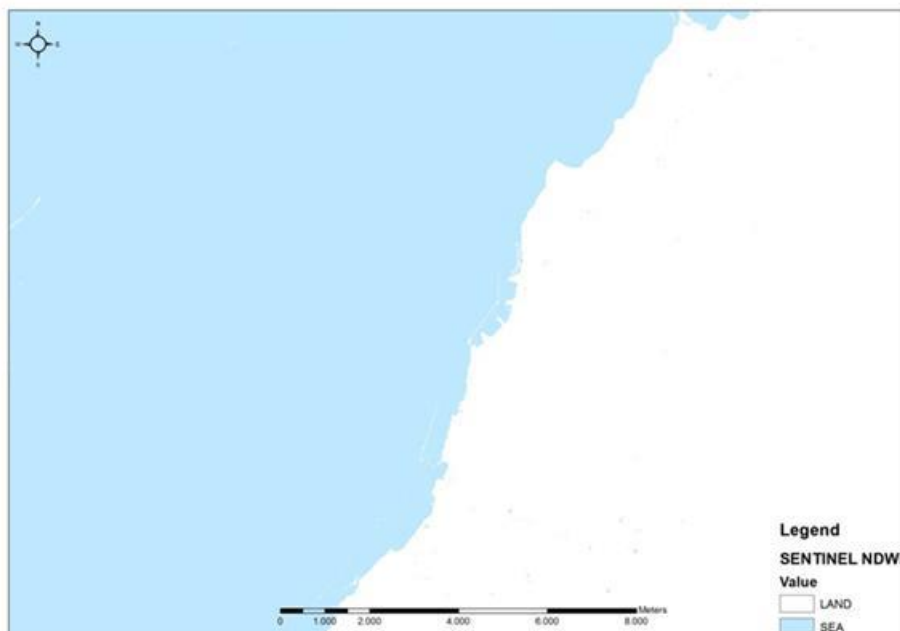


**Figure 3.4:** Part of the Sentinel 8 NDVI image classified in two classes (Sea and Land). The port of Patras is in the middle of the image.

### 3.3.1.2 Very high-resolution remote sensing data and processing

The second approach focused on the processing of Worldview-2 images that were purchased in the frame of TRITON project on September 2018. An orthomosaic covering the whole coastline from Rio area to the East up to the Araxos Cape and the Kotychi lagoon at the West was produced using Leica Photogrammetry Suite (Figure 3.5). The final orthomosaic (Figure 3.6) with a spatial resolution of 0.5m was used in order to map the shoreline in the areas of intervention in September 2018.



Figure 3.5: Processing of Worldview-2 data in Leica Photogrammetry Suite.

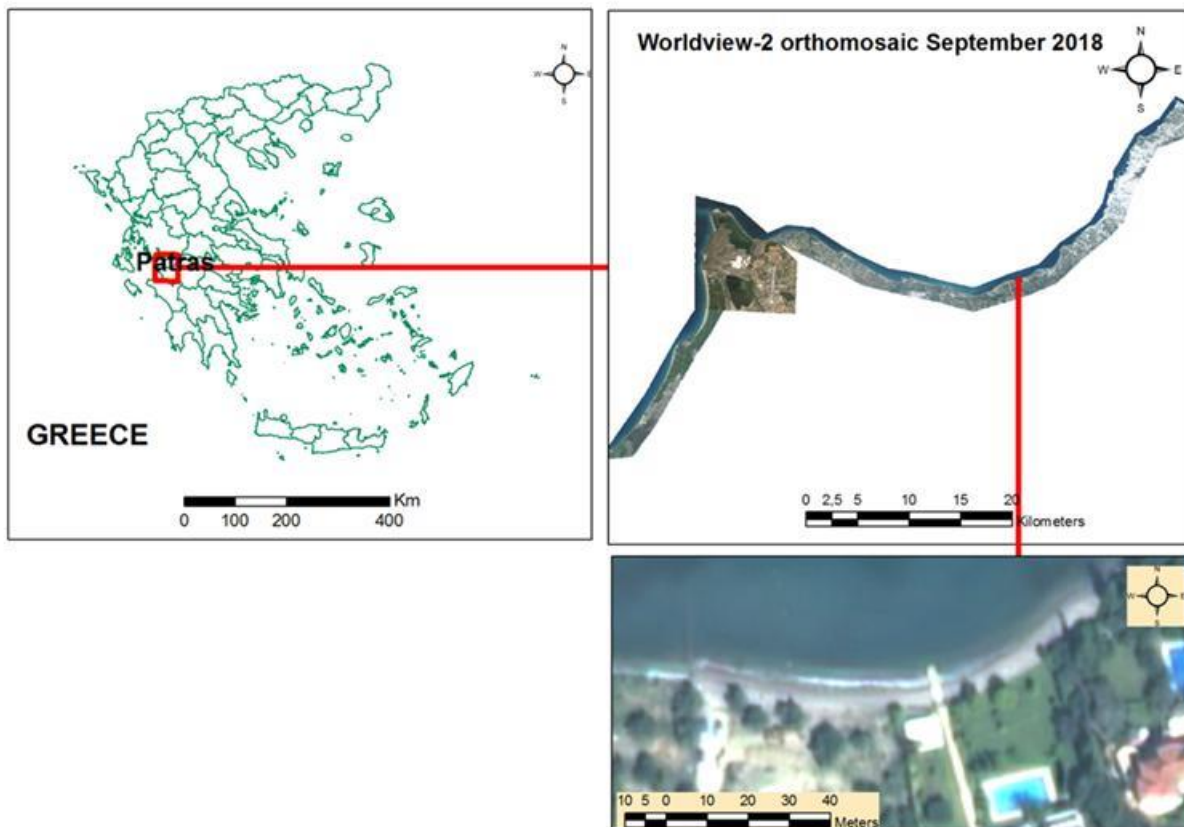


Figure 3.6: Final orthomosaic of Worldview-2 data covering the whole coastline from Rio at the East to Kotychi lagoon at the West

### 3.3.1.3 Analogue air photos processing

The third approach focused on the processing of historical analogue air photos dating from 1945 to 1996 (Figure 3.7) that were purchased in the frame of TRITON project in order to define the diachronic shorelines changes. The data have been processed using aerial photogrammetry in Leica Photogrammetry Suite resulting orthomosaics for the respective periods. Then the shoreline was digitized in GIS environment.



**Figure 3.7:** An example from the 1945 air photo (left image) and 1996 air phot (right image) orthomosaic of the broader coastline northeast of Patras (in red color is the 1945 shoreline). The shoreline retreat is evident

### 3.3.1.4 UAV processing

In specific areas where air photos and satellite data processing detect major changes in the shoreline repeated UAV flights provide very accurate data for the continuous monitoring of the shoreline's retreat or accretion. The UAV used for the monitoring in specific areas of the Triton project had been purchased with funds coming from the project. The UAV data were processed using Agisoft Photoscan Professional software (Figure 3.8) and Digital Surfaces Models and orthophotos were created. In Figure 3.9 is presented an orthophoto created from UAV images acquired in the Alikes fishery port located in the gulf of Patras.

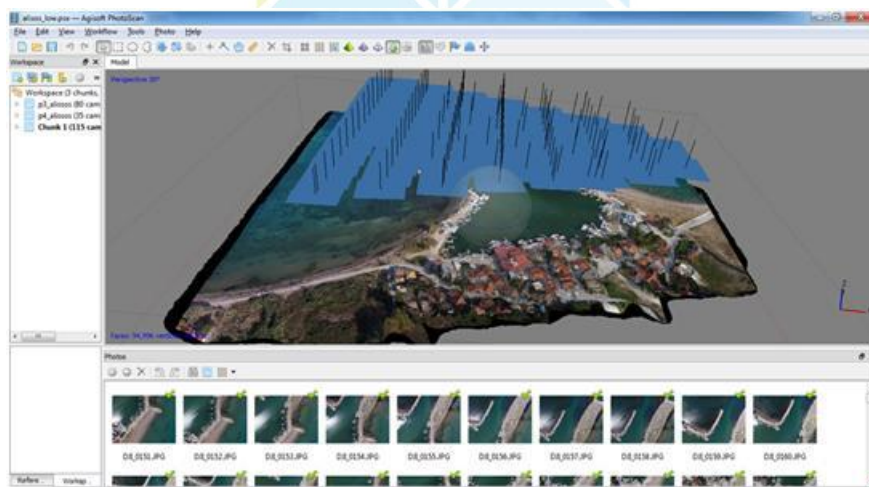


**Figure 3.8:** UAV data processing in Agisoft Photoscan Professional software.



**Figure 3.9:** UAV data orthomosaic from Alikes fishery port

### 3.3.1.5 USV data processing

In areas where air photos and satellite data processing detect major changes in the shoreline, USV surveys provide very accurate data of the sea bottom and therefore can monitor the shoreline retreat or accretion. In the frame of TRITON project an Unmanned Surface Vehicle (USV) and very accurate SONAR had been purchased with funds coming from same project. Except of the SONAR the specific small boat was also equipped with a Side Scan Sonar and cameras (Figure 3.10a). In Figure 3.10b a photo of the USV operation in the Alikes fishery port, located in the gulf of Patras, is presented.



**Figure 3.10:** (a) The bottom of the USV where the SONAR, the Side Scan Sonar and the cameras are placed and (b) USV operation in the Alikes fishery port

### 3.3.1.6 Medium resolution remote sensing data accuracy assessment

The coastlines produced from the medium resolution satellite data (Landsat 8 OLI and Sentinel 2) were compared with the coastline that was digitized from the very high-resolution satellite data Worldview-2. In Figure 3.11 a comparison between the three shorelines is presented. The most accurate shoreline digitized from the Worldview-2 data is presented with black color while the shoreline from the Landsat 8 OLI is presented with green color and the Sentinel-2 shoreline is presented with red color. As is can be observed the shorelines produced from Sentinel or Landsat data differ a lot from the shoreline produced from the Worldview-2 data. There are places where the Sentinel or Landsat shoreline are moved towards the land (negative difference from the Worldview coastline) and other places where the Sentinel or Landsat shorelines are shifted towards the sea (positive difference from the Worldview coastline).

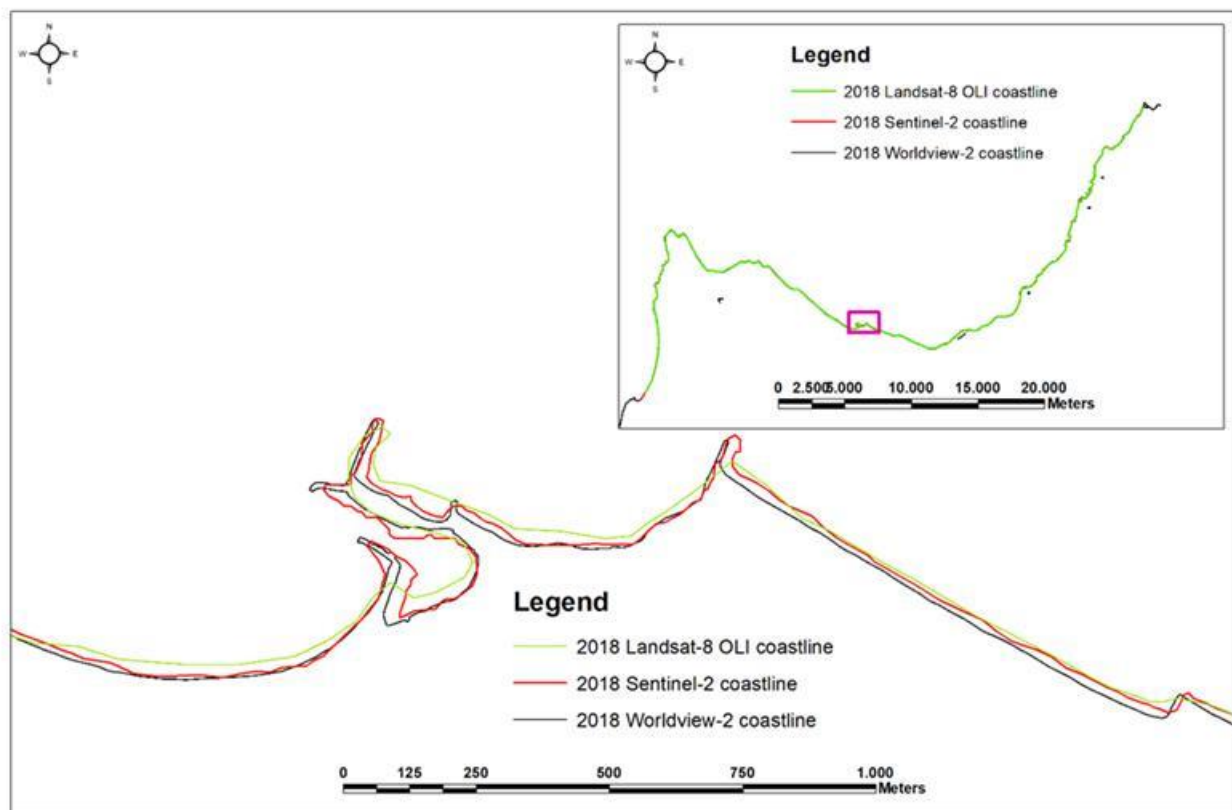


**Figure 3.11:** A comparison of the shorelines derived from satellite data in the Alikes fishery port

The accuracy of the shorelines derived from Landsat-8 OLI and Sentinel-2 MSI has been evaluated in the ARCGIS environment in comparison to the worldview-2 shoreline. The evaluation proved that both datasets present inappropriate accuracies for the coastline monitoring. The metrics of the coastline difference

between Worldview-2 and Sentinel as well as Worldview-2 and Landsat 8 OLI are presented in Figures 3.12 and 3.13, respectively.

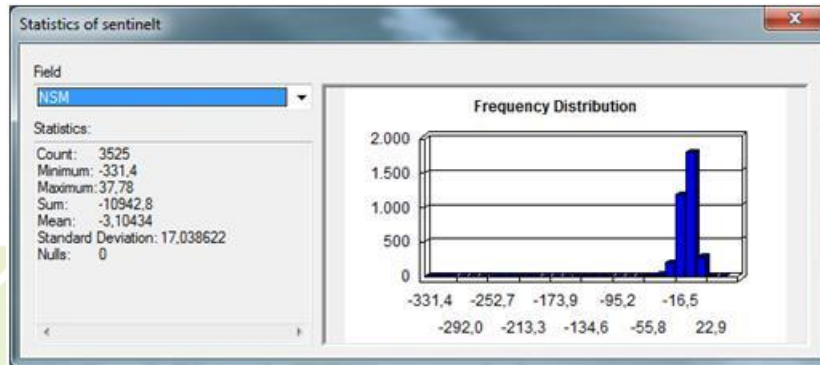


**Figure 3.12:** Statistics of the Sentinel shoreline displacement compared to the worldview-2 shoreline

The coastline derived from the Sentinel-2 data has a mean difference of -3.1 meters compared with the coastline derived from the Worldview-2 orthoimage. While the mean difference is -3.1 meters, the minimum difference is almost one hundred times higher (-331.4m) and the maximum difference is ten times higher (37.78m). The minimum difference of -331.4m means that there is a place along the Gulf of Patras where the shoreline derived from the Sentinel data seems to have been displaced 331.4m towards the land (erosion) compared to the shoreline derived from the Worldview-2 orthoimagery.

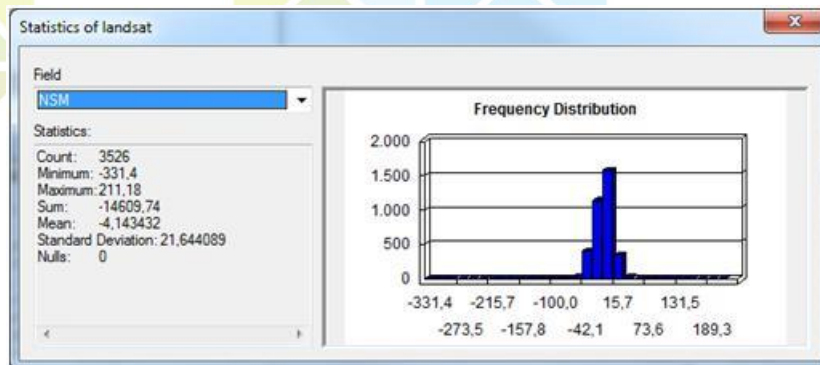


**Figure 3.13:** Statistics of the Landsat shoreline displacement compared to the worldview-2 shoreline

The coastline derived from the Landsat data has a mean difference of -4.14 meters compared with the coastline derived from the Worldview-2 orthoimage. While the mean difference is -4.14 meters, the minimum difference is almost eighty times higher (-331.4m) and the maximum difference is fifty times higher (211.18m). The maximum difference of 211.18m means that there is a place along the Gulf of Patras where the shoreline derived from the Landsat data seems to have been moved 211.8m towards the sea (accretion) compared to the shoreline derived from the Worldview-2 orthoimagery.

### 3.3.1.7 Shoreline retreat and accretion

The digital processing of satellite data and aerial photography led to the calculation of the rate of change of the coastline from 1945 to 2018. Due to the large extent of the study area, the investigation concentrated in the areas where the erosion or accretion had overpassed the 30 meters and as a result the corresponding map presented in Figure 3.14, was finally created.

Figure 3.14 presents the area of study from the East (Rio canal and beginning of the gulf of Patras) to the West (Araxos cape and ending of the gulf of Patras), as well as the southern part, where the Kotychi lagoon exists. The highly eroded areas (more than 30 meters) are presented with a red color, the highly accreted areas (more than 30 meters) are presented with a yellow color, and the mild eroded or accreted areas (less than 30 meters) are presented with a green color.

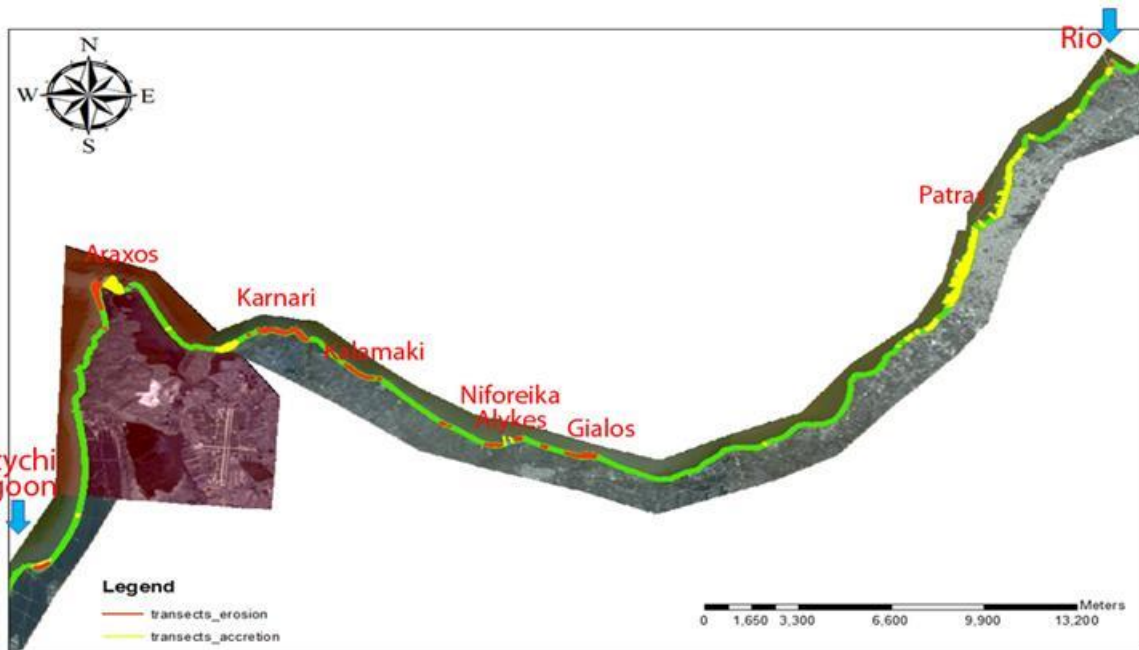


**Figure 3.14:** Map of the shoreline displacement from 1945 to 2018 in the area of study. Red color represents areas where the erosion is higher than 30m, yellow color represents areas where the accretion is higher than 30m and green color represents areas where the shoreline displacement is lower than 30m.

### 3.3.2 Marine surveys and digital bathymetric plans

The current chapter presents: (a) the research equipment and data acquisition methods undertaken for mapping the bathymetry of the southern part of the gulf of Patras, (b) the survey planning conducted, (c) processing and analysis of the collected data, and (d) presentation of the bathymetric plans of the research area. The marine survey was carried out between the 24th and 30th of September 2019.

#### 3.3.2.1 Research equipment and data acquisition methods

The survey was conducted using the vessel “Milady Millord III” modified to meet the survey’s specifications (Fig.3.15).



**Figure 3.15:** The vessel ‘Milady Millord III’ used for the bathymetric survey

A Differential Global Positioning System (DGPS) system was utilized for the positioning of the survey vessel.

The system comprised two components:

- Primary: Leica GS08 GNSS System (Figure 3.16). The system worked in RTK mode with corrections from the HEPOS (Hellenic POsitioning System). The accuracy of this system was  $\pm 8 \text{ mm} + 1 \text{ ppm RMS}$  in horizontal scale and  $\pm 15 \text{ mm} + 1 \text{ ppm RMS}$  in real time and less than 0.5m in dynamic mode in vertical scale.
- Secondary: Hemisphere VS - 101 GNSS System (Figure 3.16). It consists of two multipath-resistant antennas and it is capable of using differential corrections received through an internal SBAS demodulator (Satellite Based Augmentation System). The accuracy of the system was  $\pm 0.6\text{m}$  at the 95% of the time.

The navigation of the vessel was carried out with the software package HYPACK 2014 (Figure 3.17) towards:

- storing and displaying route navigation data of the pre-planned survey lines,
- continuous graphic presentation of the vessel movement (tracks),
- across track error limits
- logging depth data and the corresponding geographical coordinates

The positioning of the equipment, which was utilized during the fieldwork, was linked to the above-described navigation systems therefore the data acquisition was georeferenced throughout the fieldwork. In particular, the GPS systems were situated exactly above the MBES echo sounder in order to minimize the position-offset uncertainty of the system.



**Figure 3.16:** Leica GS08 RTK GNSS System (left image) and Hemisphere VS101 GPS (right image)

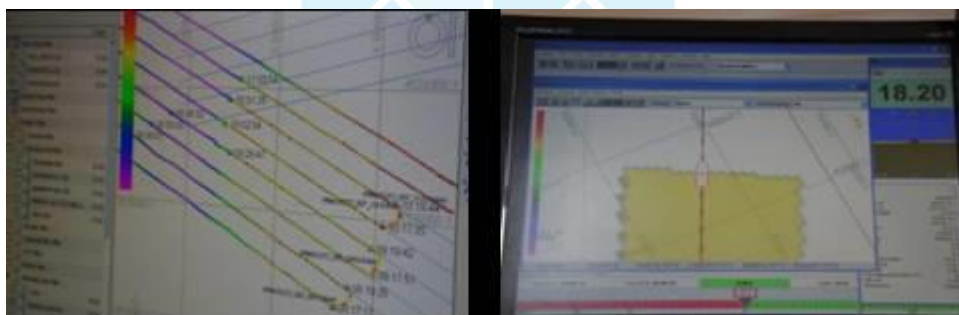


**Figure 3.17:** Hypack 2014 navigation software display

A Motion Sensor (FOG) and a heading sensor were used for the recording of the vessel movements (Figure 3.18). In detail there were used:

- One SMC IMU-108 motion sensor was used for pitch, roll and heave compensation with resolution angle  $0.001^\circ$  (pitch, roll) and resolution Heave 0.01m.
- A hemisphere Vector VS101 GPS Compass with two multipath-resistant antennas, with heading accuracy  $< 0.10^\circ$  RMS was used for yaw compensation.

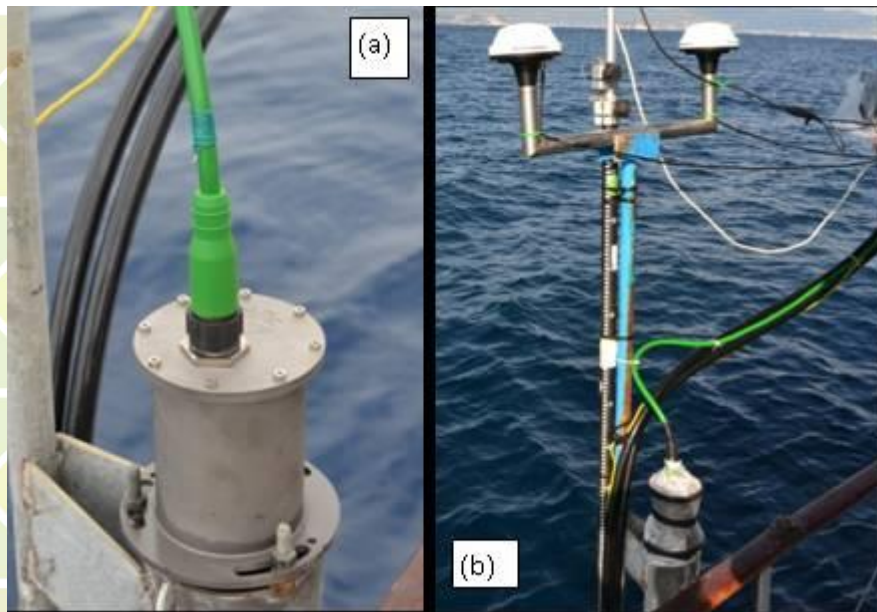


**Figure 3.18:** (a) SMC IMU-108 motion sensor, (b) Hemisphere Vector VS101 GPS Compass & IMU-108 motion sensor

The bathymetric surveying employed a multi-beam interferometric echosounder (MBES) and a single beam echosounder (SBES).

- The multi-beam interferometric echosounder (MBES) used is a BathySwath1, ITER System consisting of: (i) two transducers (Figure 3.19) attached to the mounting pole tided up to the bow of the ship, and (ii) one (1) digital recording unit (Figure 3.19). BathySwath1 uses a wide swath width with operational depth ranging from 0.2 m to 100 m. The capacities of this system are effective in the surveying of shallow depths providing high speed in surveying with resolutions up to 2 cm. For the acquisition of the bathymetric data sets, the Bathyswath Swath Processor and the HYPACK 2014 software were used. Bathymetric data sets acquired from an area of about 30 km<sup>2</sup>.

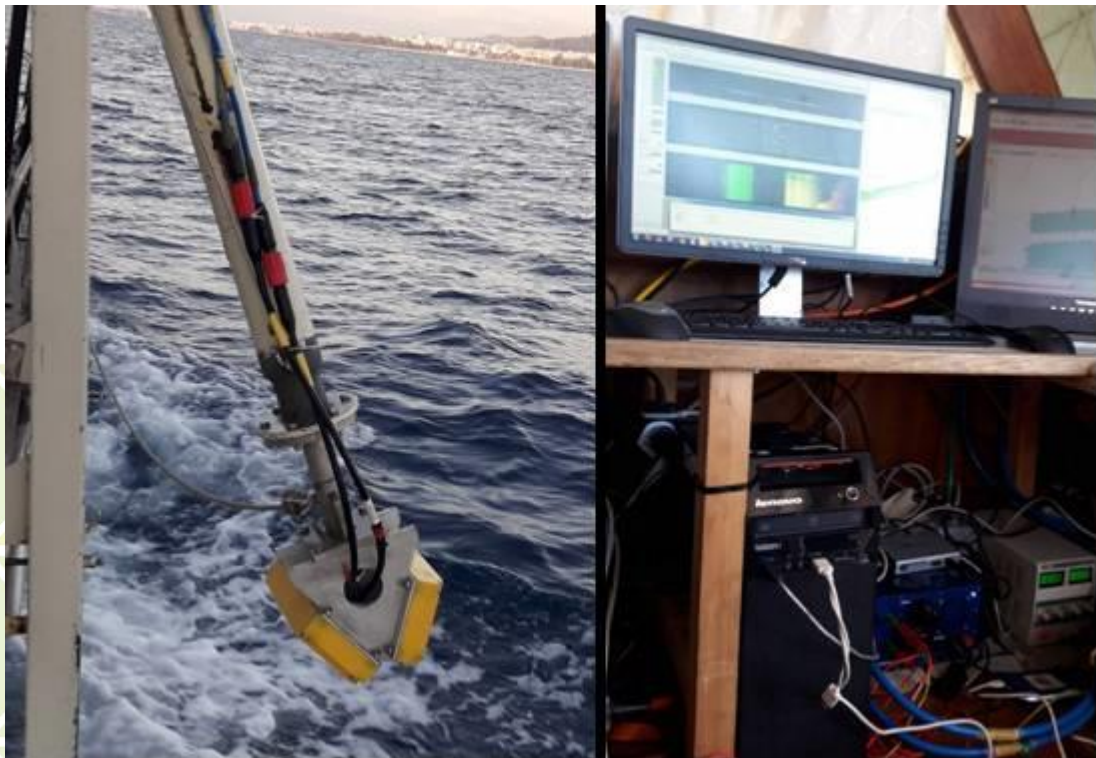


**Figure 3.19:** ELAC transducers array LSE 307 mounted over the side of the vessel (left image) and ELAC Transmit/Receive Unit SEE 30 and the MBES operating workstation (right image)

Acquisition of data and system control is performed on a Windows based high-performance computer. In detail:

- The acquisition speed was about 4knots.
- The depth range was 30 to 50 meters.
- The survey had been planned so that all areas sampled at least once
- A SMC IMU-108 motion sensor used for pitch, roll and heave compensation with resolution angle 0.001° (pitch, roll) and resolution Heave 0.01m.
- A hemisphere Vector VS101 GPS Compass with two multipath-resistant antennas, with heading accuracy < 0.10° rms used for yaw compensation.
- A Leica GNSS GPS system with RTK accuracy used for positioning the sensor.
- Tide data provided from the Patras Harbour tide gauge.
- A Sea & Sun Technology Sound Velocity Profiler with resolution 0.001m/s and accuracy ±0.02m/ used for collecting sound velocity profile

- Bathyswath Swath Processor software used for operation of echosounder and Hypack Hysweep software used for data acquisition. The files stored in HSX format.

The faces of data acquisition are described below:

- Sound Velocity Profile: Sound velocity profile of the seawater added to Hypack for correction of the soundings. A sound velocity profile was obtained once per day.
- System Alignment: Using the 'Patch Test' in HYSWEEP®'s MULTIBEAM EDITOR, determined the exact mounting angles and time delays for multi-beam sonar system.
- Data Collection and Review: HYSWEEP® SURVEY running simultaneous with the HYPACK® SURVEY program performs all data collection, logging and time tagging while providing graphics for data visualization, bottom coverage and quality control.

Finally, a Single beam echosounder (SBS) Hydrolite-TM (Figure 3.20) was used as duplicate checking system on the swathe system. The Hydrolite-TM is a single beam echosounder designed for shallow water hydrographic surveys. The system is configured at 200kHz frequency and its depth accuracy is 1cm/0.1% the water depth. The depth from the single beam echosounder logged on Hypack Survey with MBES data.



*Figure 3.20: The Hydrolite TM echosounder associated with an RTK GPS installed on top of it*

Lead Partner

Technical support

Project Partners

### 3.3.2.2 Survey planning

The survey had been planned in order to achieve full coverage mappings of the seabed through bathymetric (MBES) data. Fifty-two (52) survey lines conducted in a way so that all points on the seafloor were sampled at least once, through a grid of parallel swaths, with the adjacent ones having more than 10% overlap, e.g. 100m distance to each other (see Table 3.1 and Figure 3.21)

**Table 3.1.** Information regarding the survey lines conducted

Instrumentation used	No. of survey-lines	Total length (km)	Line Order/Orientation	Line spacing (m)	Research area
MBES, SBES	52	276	Parallel to the coastline	100	Southern part of the gulf of Patras



**Figure 3.21:** Map of the gulf of Patras presenting the vessel's bathymetric survey track lines

### 3.3.2.3 Data processing and analysis

The processing of multi-beam and single beam echosounder data performed with the use of Hypack and Hysweep software. The data processing included the following stages:

**Stage 1- Data Review:** The first stage included the review of the navigation track lines, heave-pitch-roll, tide-and-draft and sound velocity profile information. The sound velocity profile added to the data. The tides retrieved from the tide gauge which installed in the framework of the TRITON project in the area and the true Heave from the MRU data applied to correct multi-beam data

**Stage 2 - Swath-by-swath editing:** Precise examination of bottom detail, clear spikes and errors. Each swath examined for errors and cleared. Finally, automated geometric filters applied to eliminate outliers.

Stage 3 - Area-based editing: Points are grouped into ‘cells’ and statistical filters applied based on the distribution of z-values in each cell.

Stage 4 - Cube: CUBE that has been developed by B. Calder of UNH-CCOM provides for near-automated editing of multibeam data, allowing for rapid turn-around data. CUBE generates a gridded pattern of XYZ depth estimates that accurately represents actual survey data.

Stage 5 - Contouring: XYZ data added to the ArcGIS software where depth contours revealed using Inverse Distance Weighting method (IDW) is a quick deterministic interpolator that is exact.

### 3.3.2.4 Bathymetric plan of the gulf of Patras

The processing of the multibeam datasets led to a detailed bathymetric map of the coastal area of the Southern part of the gulf of Patras (Figure 3.22)

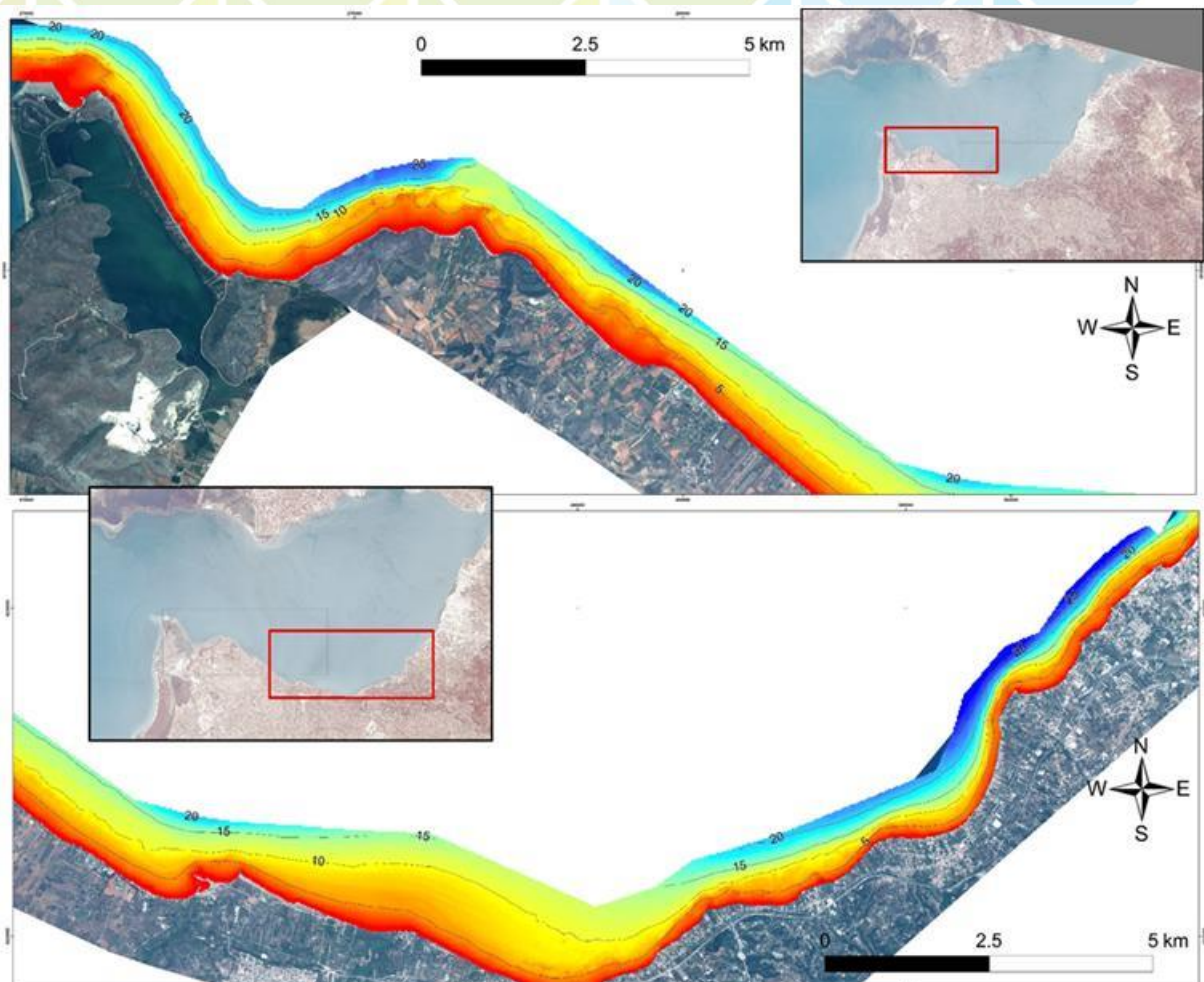


**Figure 3.22:** Bathymetric map of the coastal area of the Southern part of the gulf of Patras

### 3.3.3 Geotechnical survey in the gulf of Patras

In the frame of the TRITON project an extensive geotechnical investigation program was performed along the shoreline of the gulf of Patras, comprising of: (a) Borehole drilling and core sampling, (b) in-situ tests, (c) lab tests, and (d) sediment analysis. The purpose of this program was to identify the soil's stratigraphy and its geotechnical properties for specific coastal applications.

Figure 3.23 presents the locations and the kind of the geotechnical operations performed.



Lead Partner



Technical support



Project Partners





**Figure 3.23:** Google-Earth map representing the geotechnical operations performed along the shoreline of the gulf of Patras (borehole drilling: ΓN, CPT tests and sampling points for sediment analysis: S)

### 3.3.3.1 Borehole drilling, soil core sampling, in situ (SPT) and laboratory tests

Six (6) boreholes were drilled along the shoreline of the gulf of Patras (Figure 3.23), with a total length of 86,53m and the relevant soil core sampling, in-situ (SPT: Standard Penetration Tests) and laboratory tests were performed. The boreholes were labelled from ΓN-01 to ΓN-06 and their coordinates, depth and date of drilling, is given in the following Table 3.2.

**Table 3.2:** Coordinates of boreholes drilled in the shoreline of the gulf of Patras

Borehole	X(EGSA)	Y(EGSA)	φ(WGS84)	λ(WGS84)	Depth (m)	Date
ΓN-01	278252	4229416	38,18803	21,46975	13,50	22/10/2019
ΓN-02	280200	4228133	38,17695	21,49237	15,00	23/10/2019
ΓN-03	284186	4225650	38,15554	21,53865	15,45	19/10/2019
ΓN-04	286632	4225131	38,15145	21,56667	15,45	20/10/2019
ΓN-05	287327	4225013	38,15055	21,57442	15,13	21/10/2019
ΓN-06	293425	4225661	38,15765	21,64408	12,00	24/10/2019

Standard soil penetration (SPT) tests, according to ASTM D 1586–08a standards, were also performed, in the soil penetrated formations. During the test, the number of blows required to penetrate 15 cm per phase is measured in three successive phases using the standard sampler (Terzaghi). The NSPT number is the sum of the last two measurements. If the sampler does not penetrate 45 cm into the ground, the number of blows and the corresponding penetration depth shall be recorded as a Denied (D). The results of the tests are listed in the survey borehole logs at the relevant test depths, in order to directly correlate the soil type with the number of Nspt (see Appendix A).

All soil core samples, after on-site macroscopic examination and recording, were placed in special log boxes, photographed, and transported in the lab for testing. All borehole logs are given in Appendix A.

The laboratory tests were performed according to the ASTM (American Society for Testing and Materials) specifications and their results are summarized in the following Tables.

In the following Figures 3.24 and 3.25 is presented the equipment used for the borehole drilling as well as log box with 4m soil core sample from the borehole ΓN-06, respectively



**Figure 3.24:** BOYLES rotary drilling used for the drilling of boreholes



**Figure 3.25:** Log box with soil core samples from borehole ΓN-06 at a depth 0-4m

**Table 3.3: Soil classification test results**

BOREHOLES	SAMPLE	DEPTH (m)	MOISTURE CONTENT(%)	ATTERBERG LIMITS			GRAIN SIZE ANALYSIS (%)										GRAVEL	SAND	MUD / CLAY	SPECIFIC GRAVITY	CLASSIFICATION AUSCS	
				w (%)	LL (%)	PL (%)	PI (%)	1 1/2" (%)	1" (%)	3/4" (%)	1/2" (%)	3/8" (%)	No4 (%)	No10 (%)	No40 (%)	No200 (%)						< 0.005mm (%)
FN-03	Δ1	1.40-2.00	19	NP	NP	NP	100	96	96	95	94	93	91	79	21		7	72	21		SM	
	T2	4.00-4.45	26.8	NP	NP	NP						100	100	97	57		0	43	57		ML	
	T3	5.55-6.00	26.4	27	19	8							100	100	64		0	36	64		CL	
	Δ2	7.30-7.50	28.8	38	18	20							100	100	99	32	0	1	99	2.71	CL	
	T4	8.30-8.75	28.0	28	20	8								100	93		0	7	93		CL	
	Δ3	9.60-9.80	26.4	28	19	9								100	90	26	0	10	90	2.70	CL	
	T5	10.30-10.75	24.4	NP	NP	NP					100	100	99	78	13		0	87	13		SM	
	Δ4	12.30-12.50	20.1	NP	NP	NP							100	100	45		0	55	45		SM	
	Δ5	14.80-15.00	19.2	NP	NP	NP							100	99	41		0	59	41		SM	
FN-04	Δ1	1.30-2.00	19.0	NP	NP	NP	100	89	82	74	66	52	41	21	7		48	45	7		GW-GM	
	Δ2	3.60-3.80	29.1	24	23	1							100	100	81	26	0	19	81	2.68	ML	
	Δ3	5.30-5.60	34.1	38	20	18							100	100	97	38	0	3	97	2.70	CL	
	Δ4	7.20-7.50	13	NP	NP	NP		100	97	93	90	82	77	69	24		18	58	24		SM	
	T4	8.00-8.45	25.4	23	16	7					100	100	100	99	53		0	47	53		CL	
	T5	10.40-10.85	24.7	25	18	7							100	100	74	20	0	26	74	2.66	CL-ML	
	T6	12.30-12.75	24.9	NP	NP	NP							100	100	47		0	53	47		SM	
	Δ5	14.80-15.00	27.9	23	17	6							100	100	59		0	41	59	2.68	CL-ML	
FN-05	Δ1	1.50-2.00	17	NP	NP	NP		100	99	95	93	83	68	30	10		17	73	10		SW-SM	
	Δ2	3.20-3.60	22.0	28	19	9								100	88	22	0	12	88	2.72	CL	
	Δ3	5.00-5.30	27.1	58	24	34								100	100	88	0	0	100	2.70	CH	
	T3	6.00-6.45	18.1	NP	NP	NP								100	100	53		0	47	53		ML
	Δ4	7.10-7.40	21.6	26	18	8								100	100	74		0	26	74		CL
	Δ5	8.30-8.50	21.7	43	20	23								100	97	59	0	3	97	2.72	CL	
	T5	10.00-10.45	20.8	23	15	8								100	100	56		0	44	56		CL
	Δ6	11.10-11.30	20.2	NP	NP	NP								100	100	52		0	48	52		ML
	Δ7	14.10-14.30	18.7	NP	NP	NP								100	100	40		0	60	40		SM

**Table 3.4: Unconfined compression test results**

BOREHOLES - SAMPLE	DEPTH (m)	MOISTURE CONTENT (%)	LIQUID LIMIT	PLASTICITY INDEX	PASSING No.4	PASSING No.200	DRY UNIT WEIGHT	DEGREE OF SATURATION	FINAL DEFORMATION	UNCONFINED COMPRESSIVE STRENGTH	DESCRIPTION
		w	LL	PI			$\gamma_d$	S	$\epsilon_{fn}$	$q_u$	
		(%)	(%)	(%)	(%)	(%)	( $\text{kN/m}^3$ )	(%)	(%)	(kPa)	
ΓN3-Δ4	12.30-12.50	20.1	NP	NP	100	45	16.52		4.2	56	SM
ΓN3-Δ5	14.80-15.00	19.2	NP	NP	100	41	16.50		3.2	35	SM
ΓN5-Δ4	7.10-7.40	21.6	26	8	100	74	16.41		10.8	65	CL
ΓN5-Δ6	11.10-11.30	20.2	NP	NP	100	52	16.64		3.0	116	ML
ΓN5-Δ7	14.10-14.30	18.7	NP	NP	100	40	16.76		2.8	26	SM

**Table 3.5: Direct shear unconsolidated undrained test results**

BOREHOLES - SAMPLE	DEPTH (m)	MOISTURE CONTENT (%)	LIQUID LIMIT	PLASTICITY INDEX $\Sigma$	PASSING No.200	SPECIFIC GRAVITY	DRY UNIT WEIGHT	VERTICAL STRESS	MAX SHEAR STRESS	FRICTION ANGLE	COHESION
		w	LL	PI		$G_s$	$\gamma_d$	$\sigma$	$\tau_{max}$	$\phi$	c
		(%)	(%)	(%)	(%)		( $\text{kN/m}^3$ )	(kPa)	(kPa)	( $^\circ$ )	(kPa)
ΓN3 - Δ2	7.30-7.50	27.6	38	20	99	2.71	14.76	100	68	24.7	29.9
		28.7					15.25	200	138		
		30.0					14.46	300	160		
ΓN3 - Δ3	9.60-9.80	27.1	28	9	90	2.70	15.30	100	56	26.0	11.1
		26.6					15.60	200	117		
		25.5					15.98	300	153		
ΓN4 - Δ3	5.30-5.60	33.9	38	18	97	2.70	14.19	100	39	8.3	24.7
		33.8					13.33	200	54		
		34.6					13.56	300	68		
ΓN4 - Δ5	14.80-15.00	28.0	23	6	59	2.68	13.52	100	11	5.9	1.8
		27.9					13.78	200	25		
		27.7					13.69	300	31		
ΓN5 - Δ2	3.20-3.60	22.2	28	9	88	2.72	16.27	100	91	37.7	10.0
		22.2					16.38	200	156		
		21.7					16.26	300	246		
ΓN5 - Δ3	5.00-5.30	25.4	58	34	100	2.70	15.90	100	85	9.1	61.2
		26.9					14.84	200	78		
		29.1					14.87	300	117		
ΓN5 - Δ5	8.30-8.50	22.9	43	23	97	2.72	16.06	100	86	21.2	47.4
		20.4					16.50	200	126		
		21.7					16.31	300	164		

### 3.3.3.2 Cone Penetration Tests (CPT)

The Cone Penetration Tests (CPT) are another type of in situ test and were performed with the use of a static penetrometer 20tn by Gouda/GeomilB.V, on a 6x6 Volvo / Terberg wheeled truck, equipped with a fully automated eight (8) channel measuring system (GME 500) and a 15cm<sup>2</sup> S (Subtraction) electric cone (Figure 3.26). These tests detect ground pore pressure distribution, soft sediments which are subjected to liquefaction and/or consolidation and with the appropriate interpretation the potential eroded material may be identified.



**Figure 3.26:** The static penetrometer 20tn by Gouda/GeomilB.V, on a 6x6 Volvo / Terberg wheeled truck used in the CPT survey

Totally, twenty (20) penetration tests were performed along the shoreline of the gulf of Patras, in the areas of Kato Achaia and Alykes fishery port (Figure 3.27). The penetrations were labelled from Π1 to Π20 and their coordinates, depth and date of testing, is given in the following Table 3.6.

**Table 3.6:** Coordinates of cone penetration tests performed in the Alykes fishery port

Number of test	X(EGSA)	Y(EGSA)	φ(WGS84)	λ(WGS84)	Depth (m)	Date
Π1	286223	4225290	38,152799	21,561923	12.88	26/10/19
Π2	2863761	4225235	38,152340	21,563686	13.94	26/10/19
Π3	286496	4225196	38,152020	21,565065	13.82	26/10/19

Π4	286626	4225146	38,151591	21,566551	0.33	26/10/19
Π5	286626	4225146	38,151591	21,566551	13.94	26/10/19
Π6	285972	4225400	38,153733	21,559017	1.65	26/10/19
Π7	285944	4225395	38,153672	21,558700	1.22	26/10/19
Π8	285904	4225421	38,153906	21,558247	16.64	26/10/19
Π9	285754	4225456	38,154185	21,556514	2.35	26/10/19
Π10	285647	4225479	38,154358	21,555299	13.83	26/10/19
Π11	285488	4225558	38,155032	21,553462	13.81	26/10/19
Π12	285051	4225600	38,155306	21,548466	12.89	26/10/19
Π13	284593	4225802	38,157025	21,543182	13.85	26/10/19
Π14	284505	4225791	38,156889	21,542182	13.98	26/10/19
Π15	284409	4225840	38,157314	21,541061	20.70	26/10/19
Π16	284207	4225675	38.155787	21.538818	15.92	27/10/19
Π17	286315	4225258	38.152534	21.562982	20.98	27/10/19
Π18	286419	4225218	38.152198	21.564180	16.02	27/10/19
Π19	286554	4225177	38.151861	21.565731	15.71	27/10/19
Π20	286621	4225052	38.150751	21.566533	14.99	27/10/19



**Figure 3.27:** Google-Earth map representing the penetration tests performed along the shoreline of the gulf of Patras, in the areas of Kato Achaia and Alykes fishery port

The results from the CPT tests (soil classification and stratigraphy), conducted in the areas of Kato Achaia and Alykes fishery port, are given in the Appendix B.

### 3.3.3.3 Development of a geotechnical map for specific coastal applications

From the interpretation of all geotechnical data mentioned before a geotechnical map of the coastal zone of the gulf of Patras was designed providing information for specific coastal applications (Fig. 3.28). The geotechnical units prevailing in the coastal zone of the gulf of Patras are:

- 1) Recent embankments 0.5-2 m thick.
- 2) Sand, silty sand, gravel and gravelly sands of coastal sediments and river deposits with varying grain size  $D_{50} = 0.67-3.97$  mm (SP, SP-SM, SW-SM, GP, GW-GM, GM, GP-GM).
- 3) Lacustrine, lagoon, coastal, river and aeolian deposits consisted of clay, silt, sand and weatherings from older formations.
- 4) Screens of pebbles and gravels of various size consisting of sand and fine-grained materials.
- 5) Recent deposits and torrential deposits consisting of clayey silt, silty clay, sand of varying grain size and gravels.
- 6) Yellowish to grey clayey marls, sands and sandstones of river, lake, and lagoon deposits with thin layers of conglomerates.
- 7) Flysch: Alternations of sandstones, siltstones, clayey marls, and conglomerates.
- 8) Limestones: Thin to thick – bedded, white – light brown limestone with layers of chert.

Lead Partner

Technical support

Project Partners

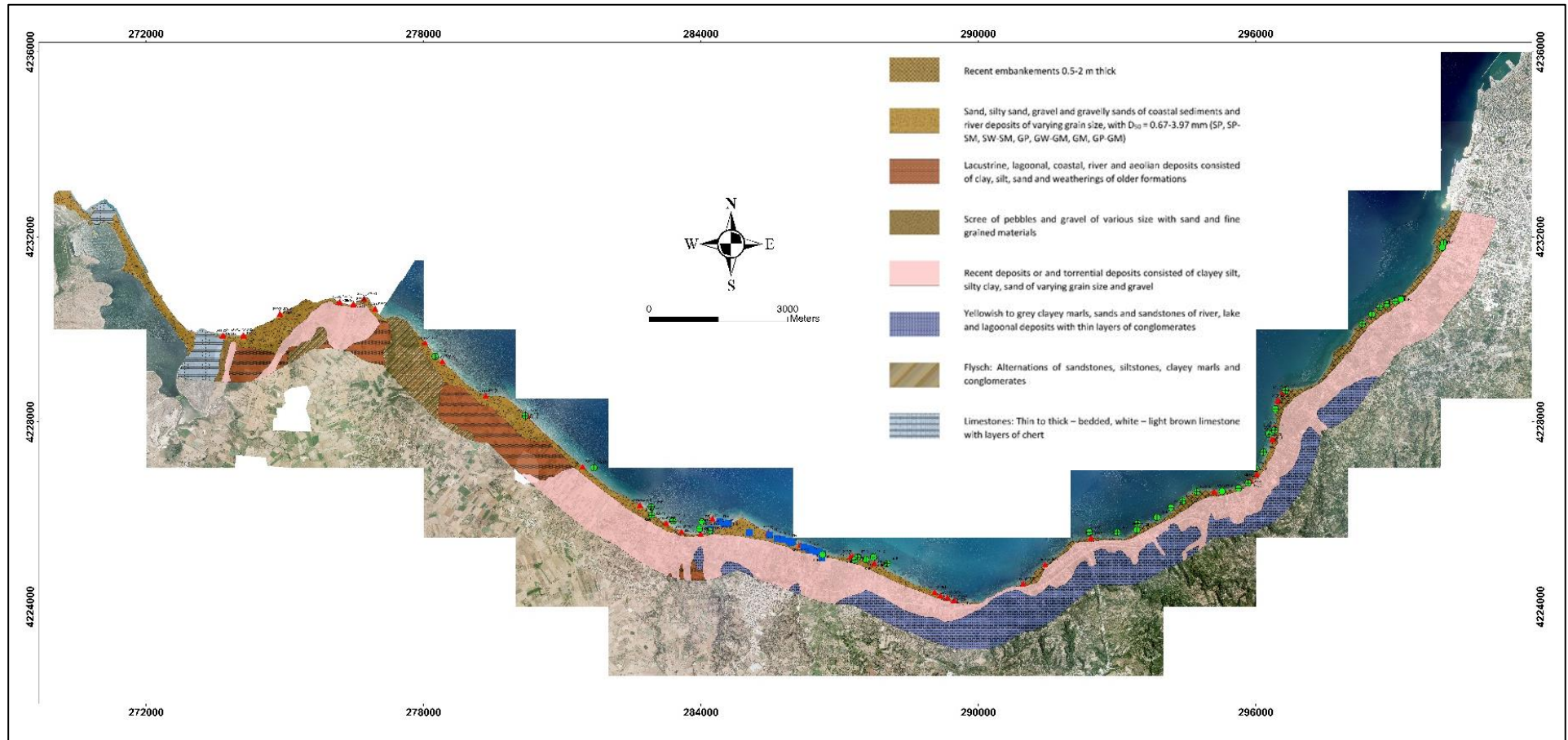


**Figure 3.28:** Geotechnical map of the coastal zone of the gulf of Patras (borehole drilling: FN, CPT tests and sampling points for sediment analysis: S)

### **3.3.4 Environmental monitoring and management in the protected areas**

The National Park Kotychi and Strofyliya Wetlands is considered a site of high biodiversity and rare aesthetic value. Thus, several protection designations have been assigned to the area. Part of it has been recognized as a Wetland of International Importance in 1975, when it was included in the 10 Wetlands of Greece protected under the Ramsar Convention. Later, parts of the area were recognized as Special Protection Areas (SPAs) for Birds, in accordance with the Directive 2009/147/EE, as well as Sites of Community Importance (SCIs) in accordance with the Directive 92/43/EEC, which led to the establishment of the European NATURA 2000 Network of protected areas.

The Protected Area extends over an area of 14300 Ha, with a shoreline of approximately 22 km, spanning across both Achaia and Ilia Regional Units. The area presents a mosaic of different habitats which include wetlands and seasonally flooded expanses, the Umbrella pine forest, sand dunes and calcareous hills with remnant shrub vegetation. The system of wetlands comprises 4 water bodies along with their adjoining floodplains. At the northern border of the National Park, lies the lagoon of Araxos which shows the highest salinity of all the water bodies in the area. To its south, at the foot of the Black Mountains hills, lies Prokopos lagoon, which is characterized by frequent alternations in depth, thus forming a variety of habitat conditions. Of the permanent wetlands of the area, Kotychi is the largest lagoon of the Peloponnese.

Traditional fishing, by means of retractable nets, is practiced in all three lagoons by local fishermen's associations. Large expanses of floodplains surround the wetlands. During winter, they collect the seasonal water and act as feeding ground for waterfowl, whereas during summer, when they dry off, and serve as breeding ground for rare water bird species and they present varied vegetation including rare halophytic species. South of Prokopos lagoon one encounters the marshes of Lamia, an extended shallow marsh seasonally connected to Prokopos lagoon. The Management Body of Kotychi and Strofyliya Wetlands is a nonprofit private legal Entity, supervised by the Ministry of Environment, Energy and Climate Change. It was founded in 2002 by National Law and it is governed by a Board of 11 members that represent central Government, all levels of local Government, Environmental Organisations, local stakeholders, and the scientific community. In 2009 the "Terrestrial, aquatic and marine areas of Kotychi Lagoon, Strofyliya Forest and their adjacent regions" received the designation of "National Park of Kotychi and Strofyliya Wetlands", under National Law. The Administrative office of the Body and the Information Centre are in the village of Lappa, in the Achaia Regional Unit. The Management Body's area of responsibility exhibits a rural character,

Lead Partner

Technical support

Project Partners

with strong elements of prosperity and a trend of ongoing development with 63 % of the region's population being employed in agriculture.

### 3.3.4.1 The Kotychi lagoon

Kotychi Lagoon, Western Peloponnese, Greece, is the largest Lagoon in the Peloponnese with an area of about 500 hectares during summer and about 750 hectares during winter and an average depth of 0.40 and maximum of 1.5m. It is situated to the north of Lehera region and is separated from the Ionian Sea on the west side by a narrow (30-100m) 5 km long sand barrier spit. The tidal channel is in the middle of the barrier spit and has a width of 50m. The location of the inlet is situated where the wave energy has its minimum. The barrier spit consists of recent aeolian sand deposits (dune) and bivalve shells. The prevailing wind directions are S - SW during winter and N - NW during summer, while calm is a prevailing condition (49.91%). The prevailing longshore current is flowing from SW to NE.

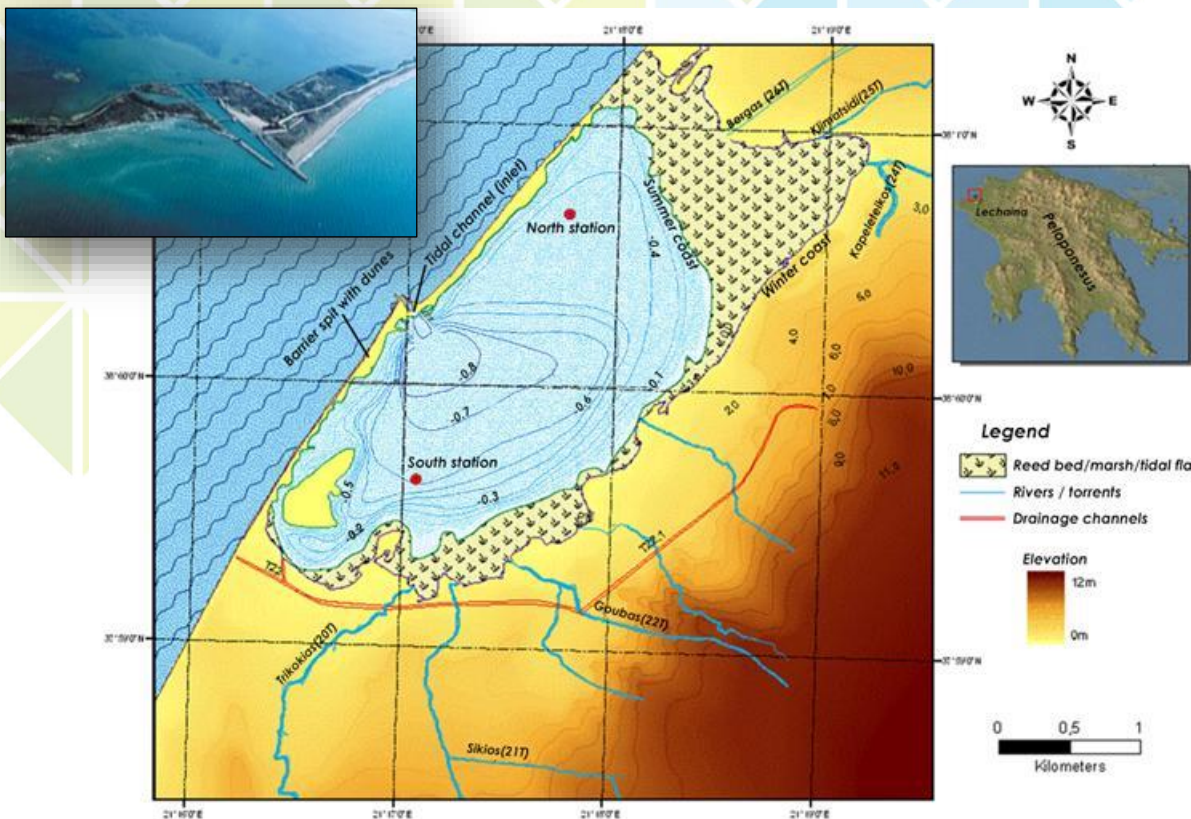


**Figure 3.29:** Map of Kotychi lagoon including: (a) its catchment's main rivers and torrents, (b) its bathymetry, (c) the topography of the surrounding area, (d) the extents of its flooding plane, (e) the location and extent of the barrier spit and tidal channel (inlet). An air photo of the jetty constructed at the inlet is given in the upper left part of the figure.

Kotychi lagoon is a typical Mediterranean Lagoon and is a significant site for the wintering, breeding and migration of water birds, many of which are in dwindling numbers in other regions of the country. The vegetation of the sand dunes is considered very important due to its relative rarity. The endangered species of sea turtle *Caretta caretta* reproduces on the sandy beaches of the area. In addition to the avifauna, Kotychi Lagoon is a significant migration site and habitat for various fish species until the reproductive period commences when they migrate to the sea. It is accordingly a natural vivarium that operates with traditional fish fertilization methods by local cooperatives. The main commercially fished species are mullet, sea bass, eels and bream. Nowadays, Kotychi lagoon is an important supplier of eels to Italy.

Kotychi has been recognized as a Wetland of International Importance in 1975, when it was included in the 10 Wetlands of Greece protected under the Ramsar Convention. Later, it was recognized as Special Protection Areas (SPAs) for Birds and as a Sites of Community Importance (SCIs) while it is included in the European NATURA 2000 Network of protected areas.

#### **3.3.4.2. Anthropogenic interventions, impacts and erosional state**

Unfortunately, Kotychi has been severely degraded and transformed during the past 50 years due to agricultural activities in the surrounding areas and watercourse alteration after the construction of Pinios river dam in the late 60's. It functions as the recipient of several branches of the hydrological network. It is mainly supplied by the streams of Vergas (26T), Klimatsidi (25T), Kapeletaiko (24T), Bratzelaiko, Gouvos (22T), Sykia (21T) and Trikokia (20T). The largest water supply is due to Vergas stream with a flood supply of 278 m<sup>3</sup>/sec and Trikokias with a flood supply of 108 m<sup>3</sup>/sec. As a result, large quantities of transferred sediments, in combination with large quantities of agrochemicals due to the intensive cultivation of the surrounding areas, enter and end up in the lagoon. This resulted in a drastic reduction in the average depth of the lagoon from about 80 cm to 30 cm in low water period, covering the seabed with a thick layer of mud and reducing its total area by about half. The phenomenon of eutrophication and the development of large areas of reeds, especially near the stream tips have been established in recent decades. It is noteworthy that of the total Kotychi's area, which is about 7,100 acres during winter, reeds thrive in 2,000 acres.

Between 1989 and 1991, several engineering works were designed and implemented to improve the situation at the lagoon and ensure the viability of the fish farm infrastructures. The main projects were a couple of peripheral drainage trenches (22T and 22.1T), as well as radial channels that were opened at the bottom of the lagoon to increase the inflow of seawater into it. The peripheral trenches have never been put

Lead Partner

Technical support

Project Partners

into operation, while the radial channels are often covered by sediments and dredging is required. The average depth of the lagoon, before the execution of the works, was about 40 cm, ranging from 10 to 70 cm. After digging the five radial channels, having a total length of 6100 m and an average depth of 1.8 m, and the construction of a flooding basin of an area of 25 acres and a maximum depth of 5 m, there has been a notable increase in the average depth of the lagoon.

Coastal lagoons fronted by barrier spits typically have entrances that migrate over time. Any stabilization effort of the barrier, using hard engineering means, lead to its gradual weakening or destruction. Such engineering interventions in Kotychi were the construction of a coastal road and more importantly a jetty for fixing the inlet of the lagoon. The south part of this jetty has been further elongated recently to prevent sedimentation in the inlet and protect the fish-capturing infrastructures. The average width of the inlet, before the execution of the engineering works of the period 1989-1992, was about 15 m and its average depth about 1.5-2 m. After the completion of the works, the inlet has a minimum of 23 m width and 2 m depth. Prior to the jetty, the southern part of the sand dune appeared to be relatively stable, while the northern part was in a slight state of erosion. It seems that the jetty was an inappropriate solution that led to more extensive erosion of the northern part of the barrier spit, as it transposed the longshore drift, moved it to the deeper and caused a local sediment imbalance both sides the tidal inlet.

Especially after 2011, the barrier spit has been severely eroded several times and regular temporary engineering solutions are being carried out to restrain fish losses. The destruction of the northern part of the barrier spit in 2013 threatened with complete destruction the natural fish farm of the area but also with a general disturbance of the biotic and abiotic parameters of the wetland. Until now there has been no severe effort to undo or improve the anthropogenic interventions in the tidal inlet, but there have been rather a bunch of temporary constructions built wherever a washover has occurred along the barrier spit (Fig. 3.30).

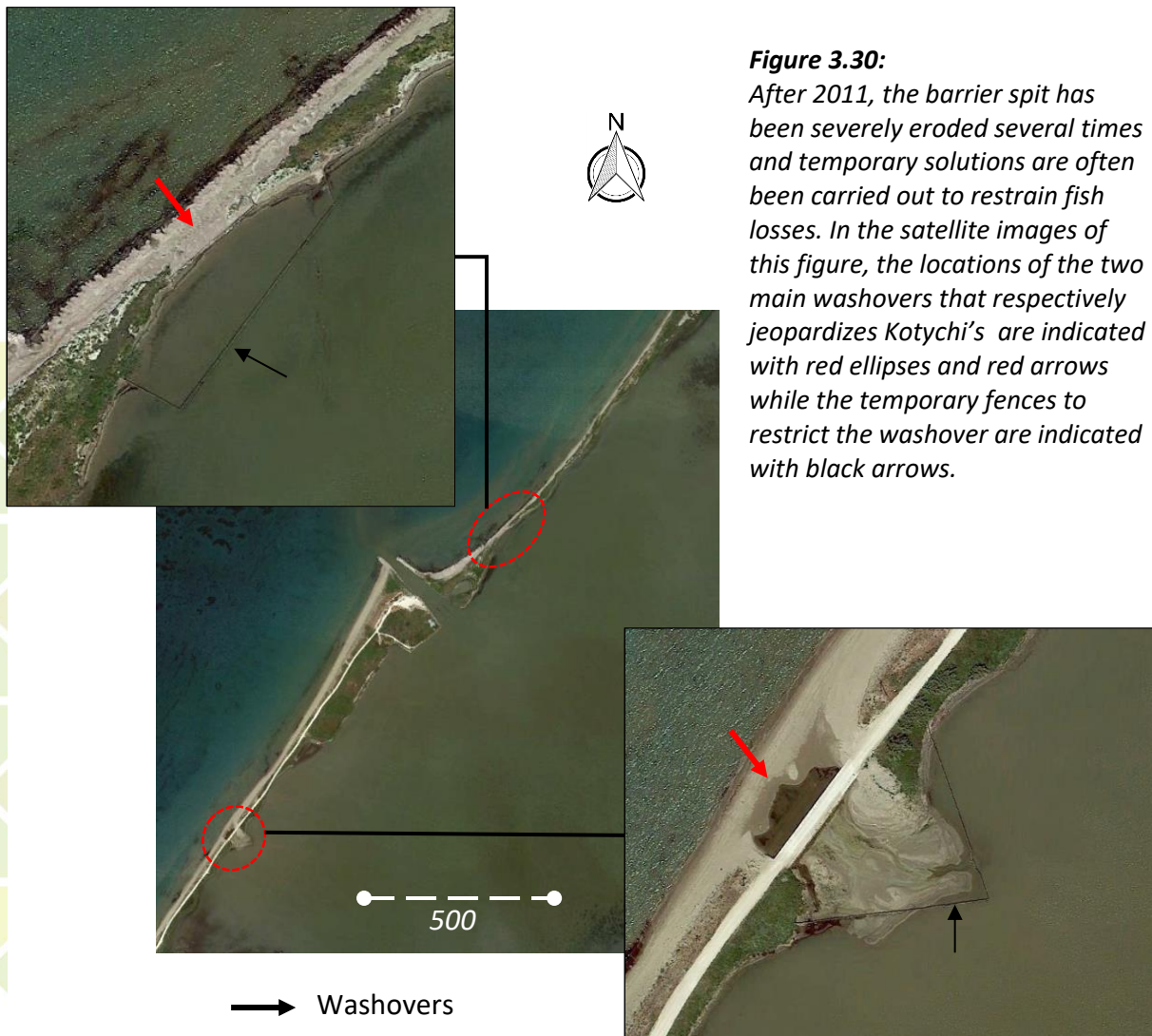


**Figure 3.30:**

After 2011, the barrier spit has been severely eroded several times and temporary solutions are often been carried out to restrain fish losses. In the satellite images of this figure, the locations of the two main washovers that respectively jeopardizes Kotychi's are indicated with red ellipses and red arrows while the temporary fences to restrict the washover are indicated with black arrows.

### 3.3.4.3. Environmental monitoring

The first telemetry stations for monitoring the water quality of Kotychi lagoon, were installed in December 2003, as part of the LIFE-Nature program "Protection and Management of National Park of Strofilia-Kotychi wetlands" (LIFE2002NAT / GR / 8491). There were two stations (Fig 3.29) and data recording lasted from January 1, 2004 to November 30, 2006. Data storing occurred every 15 minutes and the recorded parameters included water level, temperature, conductivity, pH, redox potential, turbidity, dissolved oxygen, and chlorophyll concentration (only at the northern station). In addition, at the southern station of the lagoon a meteorological station offered continuous recording of temperature and relative humidity, speed and direction of the wind, solar radiation, and precipitation. At the end of the LIFE-Nature program, the stations

were granted to the management body and kept recording until April 2009. However, between 2009 and 2011 they were set out of order due to insufficient maintenance. It was at late 2015 that new monitoring stations and a meteorological station replaced the old equipment, which was included in the programme "Protection and Preservation of the Biodiversity of the National Park of Wetlands of Strofylia -Kotychi" under the Operational Program "Development and Environment". The data are still sent every 15 minutes to a data server and are made available on demand through a dedicated web-platform.



Lead Partner



Technical support



Project Partners



### 3.3.5 Numerical study of waves, currents, and sediment transport in the Gulf of Patras

#### 3.3.5.1 Input data

With the use of the geotechnical data mentioned before and the relevant analysis performed in the shoreline' sediments, the dominant coastal erosion processes in the pilot area of the Patras Gulf, was examined. The coastal zone of the pilot area is mainly affected by wind-generated waves of northeastern, northwestern, western, and southwestern direction.

The study was carried out by performing coupled numerical simulations of wave propagation, wave-generated currents, sediment transport and bed morphodynamic evolution in the coastal zone of the pilot area, using the numerical model MIKE 21 (2014) developed by the Danish Hydraulic Institute (DHI). The specific numerical model can simulate wind-induced wave generation, growth, and propagation.

The input data for the MIKE 21 numerical model are the bathymetry of the Patras Gulf, the bathymetry of the Ionian Sea between the Gulf of Patras and the islands of Kefallonia and Zakynthos, the geometry of existing harbor works in the area, the sediment composition in the coastal zone, as well as the significant wave height and wave period of the offshore incoming waves.

For clarity of the presentation of the results and better understanding of the coastal processes, the pilot area was divided into 8 coastal independent subregions, which are presented in **Figure 3.31** and listed in **Table 3.7**.

**Table 3.7:** The 8 subregions of the pilot area of the Gulf of Patras from west to east, as presented in Figure 3.31, and the corresponding values of the mean sediment grain diameter,  $D_{50}$ , in the coastal zone of each subregion

Number	Subregion	Mean Grain Diameter (mm)
1	Papas Lagoon – Karnari	0.173
2	Karnari – Ioniki Akti	0.393
3	Ioniki Akti – Alykes	0.292
4	Alykes – Gialos (Peiros estuary)	0.263
5	Gialos – Western Kaminia	0.102
6	Western Kaminia – Western Vrachneika	0.140
7	Western Vrachneika – Roitika	0.138
8	Roitika – Glafkos	0.150

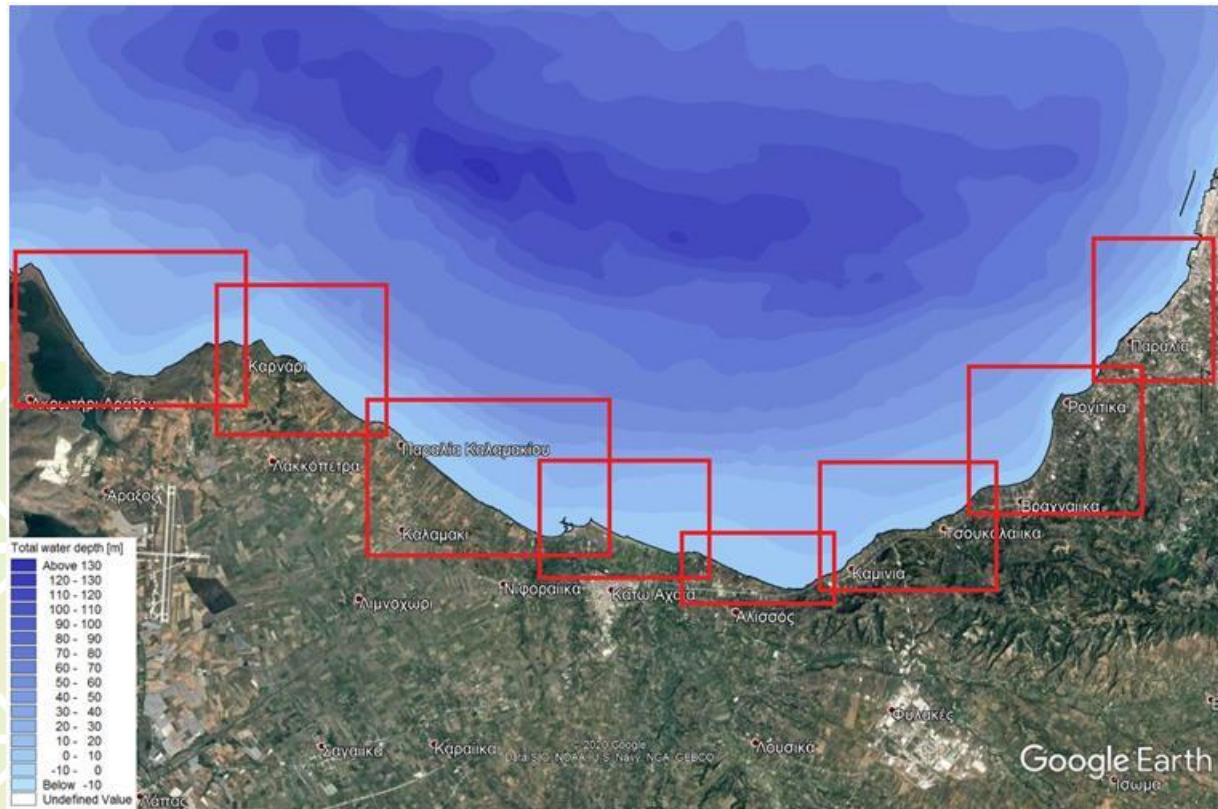


**Figure 3.31:** Satellite image (Google Earth) of the pilot area of the Gulf of Patras showing the 8 coastal independent subregions

The numerical simulations include 4 stages:

1. Determination of the wave climate in the deep waters of the Gulf of Patras due to NE winds in the area east of the Gulf of Patras and NW, W and SW winds in the area west of the Gulf of Patras.
2. Numerical simulation of wave propagation in the Gulf of Patras for wind speed of 1 year return period for each wind direction.
3. Numerical simulation of the magnitude and the direction of the wave-generated currents in the coastal zone of the Gulf of Patras for each one of the wind cases of Stage 2.
4. Numerical simulation of the magnitude and the direction of sediment transport in the coastal zone of the Gulf of Patras for each one of the wind cases of Stage 2.

### 3.3.5.2 Wave Development in the Gulf of Patras

The characteristics of the waves in the deep waters of the coastal zone of the pilot area were calculated using wind data taken from the HNMS meteorological stations at Nafpaktos (from 1/1/1977 to 31/12/2011) and Araxos (from 1/1/1955 to 31/12/2011).

From the mean annual wind data of these two stations, the wind speed,  $U_{10}$ , of 1 year return period was calculated, per each wind direction, as presented in **Table 3.8**. Using the Spectral Waves (SW) module of the MIKE 21 software (DHI, 2014), simulations of wind-induced wave generation, growth and propagation were performed in the Gulf of Patras and the Ionian Sea between the islands of Kefallonia and Zakynthos and the Gulf of Patras.

The SW module solves numerically the wave action equation in a computational mesh of the bathymetry of the specific region. The bathymetry data are derived from the digital database C-MAP of DHI (2014), which includes measurements of the Hellenic Navy's Hydrographic Service, and from bathymetric measurements performed in the framework of the TRITON research project. In the present work, the computational field, shown in **Figure 3.32**, was discretized with 181,406 triangular cells in an unstructured computational mesh with resolution from 100 m in shallow waters to 300 m in deep waters. The input data for the module SW are the computational mesh and the wind characteristics with 1 year return period (**Table 3.8**). The module SW was set to compute the steady state of the wave propagation.

Typical results of wave height, direction and velocity distribution for the northeastern wind, are shown in **Figure 3.33**. From the results of all wind directions, the wave height and direction in deep waters offshore of the coastal zone of the pilot area of the Gulf of Patras and deep waters (**Figure 3.31**) were found and they are given in **Table 3.8**. These data were used as input data in the numerical simulations of wave propagation, wave-generated currents, sediment transport and bed morphodynamic evolution in the specific coastal zone.

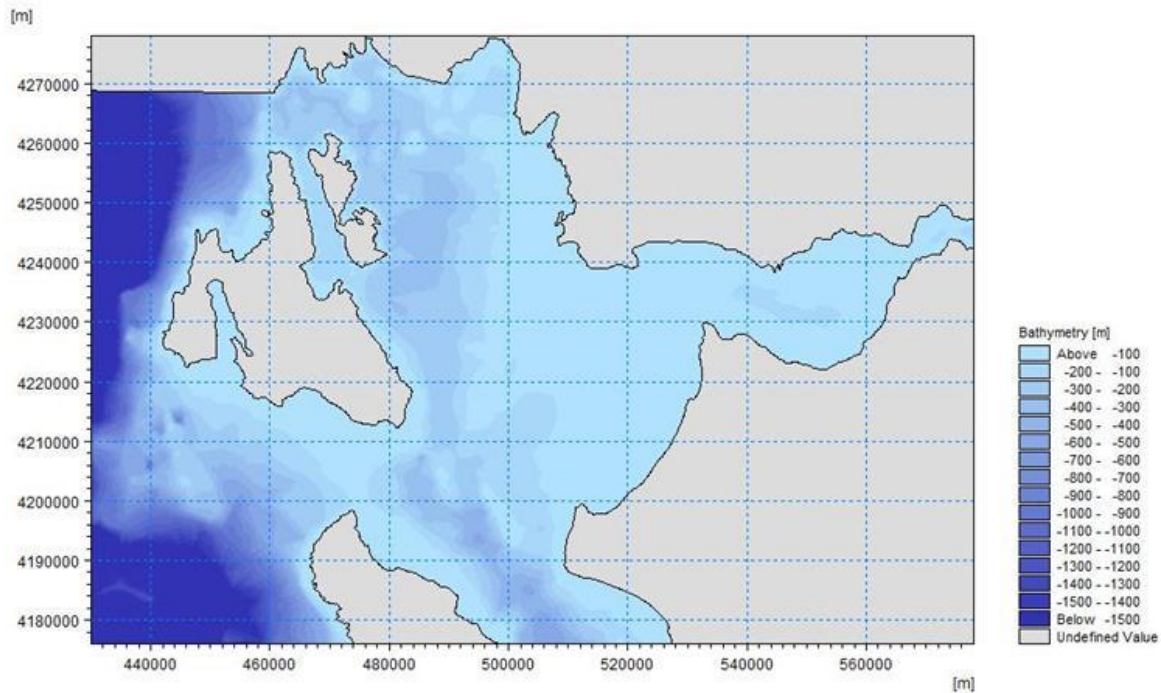


**Figure 3.32:** The bathymetric computational mesh of the Ionian Sea west of the Gulf of Patras, which was used the numerical in simulations of wind-induced wave generation, growth and propagation.

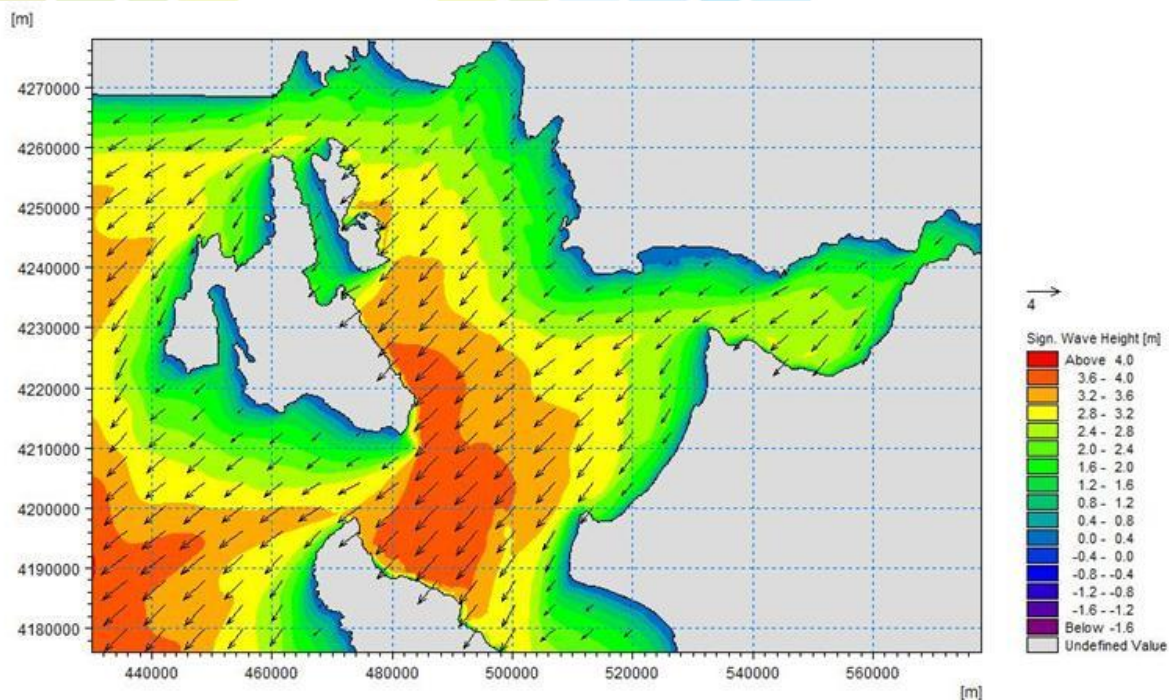


**Figure 3.33:** Wave height, velocity and direction distribution in the area of the Ionian Sea west of the Gulf of Patras due to the action of northeastern winds (Table 3.8).

**Table 3.8:** Wind and wave data with a return period of 1 year, per wind direction, in deep waters offshore of the coastal zone of the pilot area of the Gulf of Patras.

HNMS Station		Nafpaktos		Araxos		
Wind Direction		NE	E	NW	W	SW
Wind Speed, $U_{10}$	m/s	18.9	10.3	9.3	13.0	11.6
Wind Intensity	Beaufort	8	5	5	6	6
Significant Wave Height, $H_{S-1yr}$	m	2.7	0.6	0.6	1.8	1.5
Wave Spectrum Peak Period, $T_{P-1yr}$	s	8	4.4	5	8	6.8
Wave Direction with respect to the North	°	45	60	315	270	235

### 3.3.5.3 Coastal Erosion Vulnerability Assessment

Typical results of waves, currents, sediment transport and bed morphology are presented for the case of the NE wind direction and for subregion 1 of the pilot area of the Gulf of Patras.

The action of NE winds induces large values of significant wave height in the area of the Papas lagoon (Figure 3.34), as well as intense wave-generated currents and noticeable wave setup (Figure 3.35). Furthermore, intense coastal erosion is observed throughout the subregion (Figure 3.36). Therefore, the action of NE winds obviously creates favorable erosion conditions in the specific subregion of the coastal zone of the pilot area.

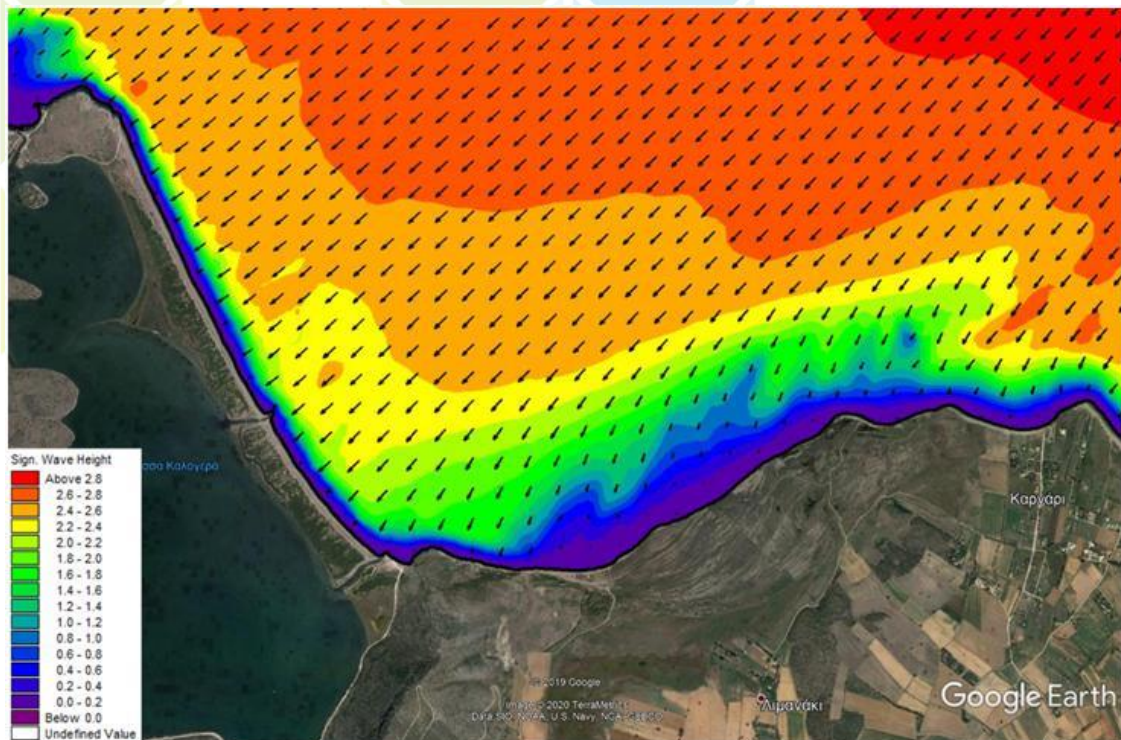


**Figure 3.34:** Significant wave height and velocity (vectors) distribution due to northeastern waves (Table 3.8) in the coastal zone of subregion 1.

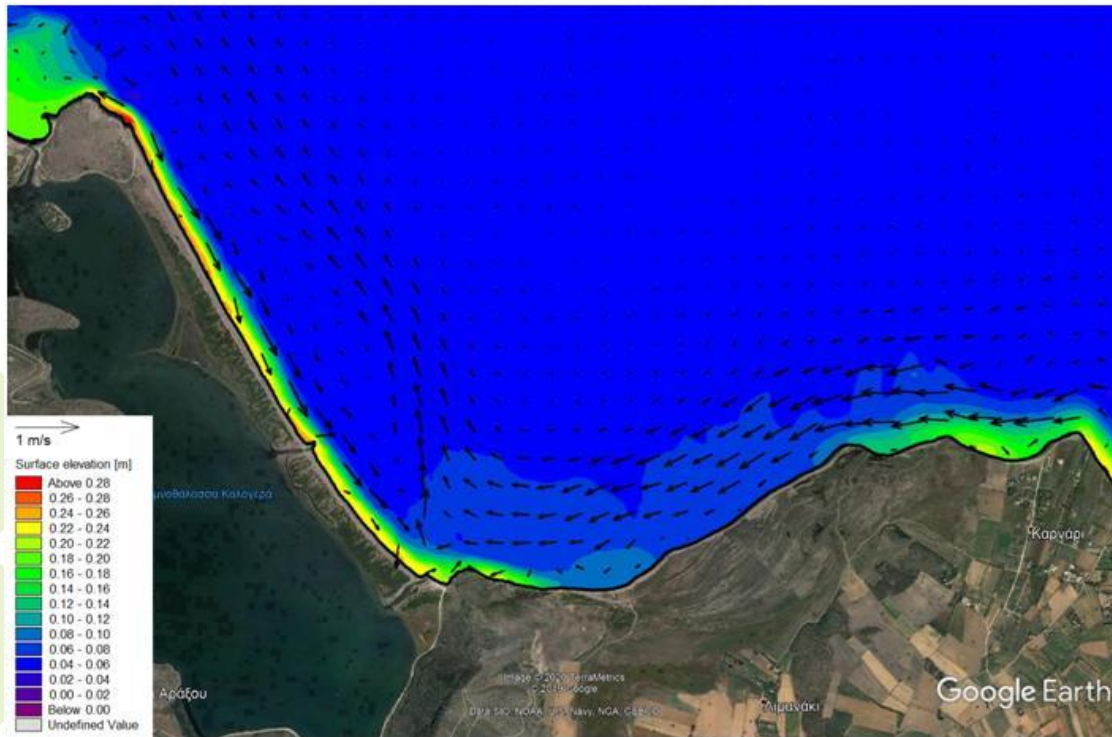


**Figure 3.35:** Wave-generated currents (vectors) and wave setup due to northeastern waves (Table 3.8) in the coastal zone of subregion 1.

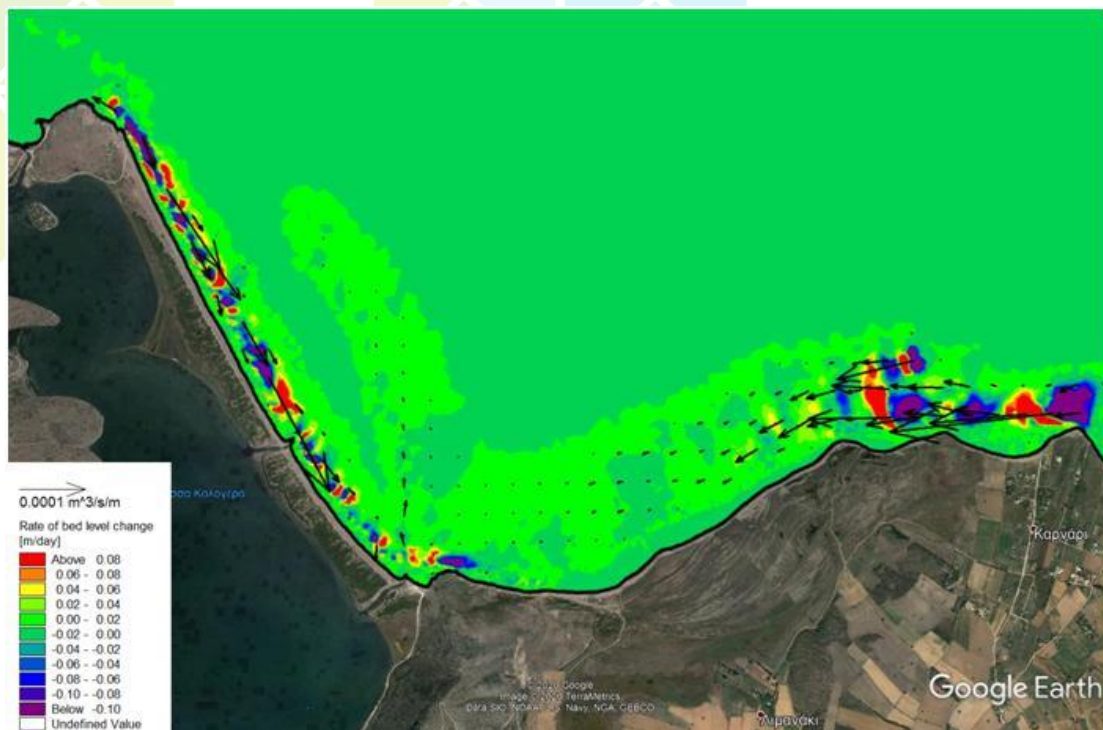


**Figure 3.36:** Bed level change due to northeastern waves (Table 3.8) in the coastal zone of subregion 1.

### 3.3.5.4 Conclusions

In the present section, the combined effect of waves and wave-generated currents on the permanent removal of sediments to deep waters and coastal erosion in the pilot area of the Gulf of Patras was examined in the framework of the TRITON research program.

The main conclusions are:

- Wind-generated northeastern waves have a strong impact on coastal erosion in the pilot area. Strong wave-generated currents are created as well as sediment transport along the coastline, which is generally directed from east to west, but locally it is reversed creating more intense erosion conditions. This impact applies to the entire coastal zone of the pilot area, except for the eastern part of the area, and specifically from Anemomylos to the Glafkos river estuary.
- Wind-generated northwestern waves have also a significant impact on coastal erosion of the pilot area. Quite interesting is the creation of cross-shore sediment transport conditions towards the deep waters through rip currents in the eastern part of the area, and specifically from Anemomylos to the Glafkos river estuary.
- The effect of wind-generated western and southwestern waves is generally weak throughout the coastal zone of the pilot area. Erosion conditions occur only in the eastern part of the area, and specifically from Roitika to the Glafkos river estuary.

Therefore, based on the results of the numerical simulations of the present work, the characterization of erosion intensity, as zero, low, moderate or high, in the 8 subregions of the pilot area of the Gulf of Patras, per wind direction, is summarized in **Table 3.9**.

**Table 3.9:** Characterization of the erosion intensity in the 8 subregions of the pilot area of the Gulf of Patras, for each wind direction, according to the numerical results of the present work.

#	Subregion	NE	NW	W	SW
1	Papas Lagoon – Karnari	High	Low	Zero	Zero
2	Karnari – Ioniki Akti	High	Low	Zero	Zero
3	Ioniki Akti – Alykes	Moderate	Low	Zero	Zero
4	Alykes – Gialos (Peiros estuary)	High	Low	Zero	Zero
5	Gialos – Western Kaminia	Moderate	Moderate	Low	Zero
6	Western Kaminia – Western Vrachneika	Moderate	High	Moderate	Zero
7	Western Vrachneika – Roitika	Low	High	High	Low
8	Roitika – Glafkos	Zero	High	High	Low

#### 4 Development and application of the risk-based joint tool across the TRITON pilot cases

Climate change is causing severe threats on natural and human systems worldwide. Climate-related impacts will be especially relevant in coastal areas, where a dense interaction between terrestrial and marine systems occurs. According to the IPCC scenarios, coastal areas, and related ecosystems, will be increasingly exposed to erosion, as a direct consequence of rising sea level and changing patterns of extreme events (e.g. storms and floods) (IPCC, 2014). Located at the land-sea interface, coastal areas are dynamic environments where natural (e.g. waves, tides, storms, tectonic and physical hazards, and sediment transport) and anthropogenic pressures (e.g. land-use changes and touristic activities) interact at diverse temporal and spatial scales, modifying their geomorphological, physical and biological features. As a consequence, the assessment and management of coastal erosion risks represent a complex task due to the high number of environmental and socio-economic factors at stake, as well as the variety and complexity of interactions that may occur among natural and human-induced pressures acting on the same area.

As described in the Deliverable 3.5, several tools and methods supporting policy and decision makers in the implementation of European recommendations and directives for coastal zone management have been developed in recent years by the research community (UNEP, 2008; EC, 2013). They represent valuable support for the assessment of coastal vulnerability and risks against future climate change scenarios (e.g. rising sea level, coastal erosion, increase in extreme events such as storm surge flooding) and different socio-economic conditions (e.g. increase of population, land-use changes) (Ramieri et al., 2011). When focusing on coastal erosion processes, more or less sophisticated tools, ranging from indicators and index-based methods (e.g. Coastal Vulnerability Index – CVI) to more complex Systems methods and machine-learning (ML) based approaches (Gornitz et al., 1994; McLaughlin and Cooper, 2010; Torresan et al., 2016; Zanuttigh et al., 2014) can be applied for understanding and modelling processes underpinning coastal erosion phenomena. Among these, remote sensing techniques (as a part of ML methods) represent an efficient approach for the detection of shoreline evolution over time, since allowing for an accurate mapping of coastlines in both time and space over large areas (Dai et al., 2019). Their integration with GIS-tools can provide an overall picture of physical coastal dynamics underpinning erosion risks, thus representing a valuable support for adaptive ICZM.

This chapter describes the methodological approaches and tools applied for the shoreline detection and extraction from satellite images as well as the evaluation of its evolution overtime through GIS-based

methods (section 4.1), also providing main results from the Ugento, Messolonghi and the gulf of Patras TRITON pilot cases (sections 4.2, 4.3 and 4.4, respectively).

#### 4.1 Methodological approach of shoreline extraction from satellite images

In order to analyze the shoreline evolution trend and identify coastal erosion ‘hotspots’ along the investigated coastal zones, a two-stage approach was implemented including the:

- i) coastline detection and extraction from medium resolution open-source historical satellite images, aerial photographs and high resolution purchased satellite images with the use of remote sensing techniques, and
- ii) evaluation of the shoreline evolution trend in term of annual rate (expressed in meters) of advancing and retreating coasts by means of GIS-based methods.

As far as the first stage is concerned, the methodology employed in the frame of the TRITON project entails the application of a semi-automatic procedure for shoreline delineation, using a semi-automatic image classification technique. Against this method, historic satellite images are analyzed and their shorelines is extracted by applying a semi-automatic classification process, allowing the identification of materials in an image according to their spectral signature (Braud and Feng, 1998).. Within this study, only the Near Infrared Band of the satellite images was used for the classification process. Specifically, the image was processed by applying the Semi-Automatic Classification Plugin (SCP) for QGIS (Congedo, 2018) supporting an easy classification of the image based on the presence/absence of water surfaces (land/sea classification and detection). The shoreline can be then extracted by vectorizing the classified raster image, and by applying a Gaussian filtering algorithm allowing to smooth the polyline and receive a better fit to the coast. The same procedure can be applied to all the historical satellite images collected for the investigated sites, thus allowing a multi-temporal detection of shoreline evolution over the analyzed timeframe. The overall process underpinning coastline extraction is explained in Figure 4.1, also providing simple examples of resulting output from each sub-phase.

Lead Partner

Technical support

Project Partners

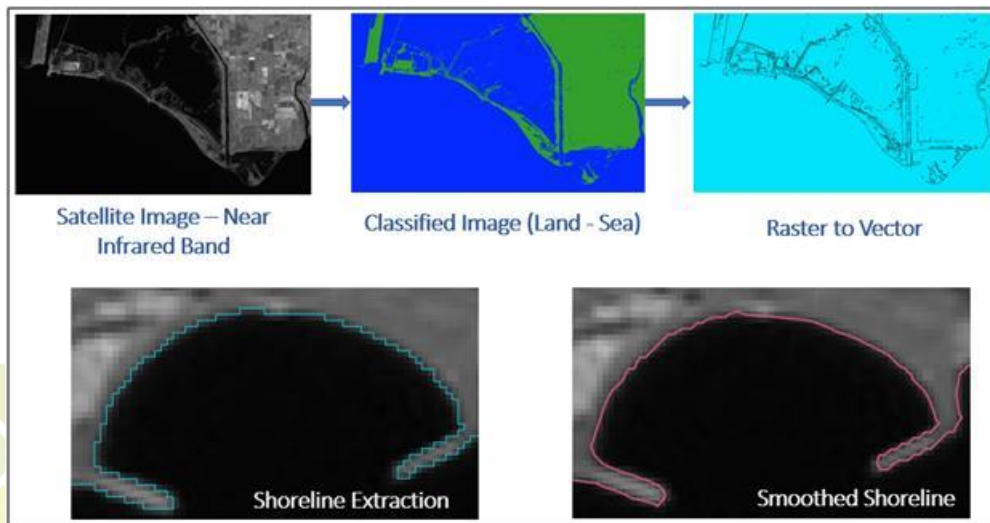


**Figure 4.1:** Coastline extraction methodology in steps.

Then, once the shorelines are extracted across different years, the second stage of the proposed joint approach concerns the analysis of the shoreline evolution trend, carried out by applying the Digital Shoreline Analysis System tool (DSAS) tool, provided by the United States Geological Survey (USGS) as an open-source extension of the ArcGIS Software (Thieler et al., 2009). The DSAS tool is an add-in to Esri ArcGIS desktop enabling potential end-users to calculate rate-of-change statistics from multiple historical shoreline positions. It provides an automated method for establishing measurement locations, performs rate calculations, while providing statistical data required to assess the robustness of the rates. Specifically, the DSAS tool allows developing transects positioned along the investigated shoreline, located in a mutual distance defined by the user according to the possibility to capturing coastal spatial variability across time. Moreover, it supports the development of a set of statistics allowing to summarize the main findings of the analysis. These statistics include: the net shoreline movement (NSM) for reporting the distance between the oldest and the earliest shorelines for each set transect; the End Point Rate (EPR, expressed in m/y) calculated by dividing the distance of the Net Shoreline Movement by the time elapsed between the oldest and the most recent shoreline; the Weighted Linear Regression (WLR, expressed in m/y), in which the weight  $W$  is a function of the variance of the measured uncertainty (Genz et al., 2007).

#### 4.2 Results from the pilot study area of the Ugento shoreline - Apulia region

Following the methodological approach presented in the Section 4.1, in order to analyze coastal evolution trend and identify erosion “hotspots” along the shoreline of the municipality of Ugento (Apulia region – Italy), five historical RapidEye satellite images were retrieved from the Planet Explorer Beta website

([www.planet.com/explorer/](http://www.planet.com/explorer/)). The advantage of using RapidEye satellite images to analyze shoreline evolution, relies on their spatio-temporal coverage and the enhancement of the spatial resolution. RapidEye provides free images with 5m resolution, a better resolution compared to other open source satellite imagery (e.g. Landsat 4-5 TM with 30 meters resolution). Based on the correction (e.g. cloud cover) and geo-referencing of each image, as well as the same range of sea water level (as analyzed through Copernicus CMEMS data), the images were selected on the following dates 07/05/2009, 24/08/2012, 28/10/2013, 06/08/2015 and 20/07/2018. As specified in Table 4.1, they present a spatial resolution of 5m, and together they allow covering the 2009 to 2018 timeframe.

**Table 4.1.** Metadata of the satellite images used in the frame of the Ugento pilot case

Data Products	Resolution	Year of Image Acquisition	Source
RapidEye	5 m	07/05/2009	Planet Explorer Beta <a href="http://www.planet.com/explorer">www.planet.com/explorer</a>
		24/08/2012	
		28/10/2013	
		06/08/2015	
		20/07/2018	

By applying the semi-automatic classification process discussed in the previous section and with the use of the Semi-Automatic Classification Plugin (SCP) for QGIS (Congedo, 2018), the Ugento coastline was detected and extracted against the considered timeframe (Figure 4.2).



**Figure 4.2:** Shoreline evolution in the coastal area of the Municipality of Ugento (Apulia region) under the 2009-2018 timeframe

Based on these vector layers, representing the Ugento shoreline across the investigated timeframe (2009-2018), the analysis of the shoreline evolution trend was carried out by applying the Digital Shoreline Analysis System tool (DSAS), provided by the USGS (Thieler et al., 2009). As explained in Section 4.1, the DSAS tool uses transects positioned along the shoreline at the distance defined by the user to evaluate the net shoreline movement (NSM), reporting the distance between the oldest and the earliest shorelines for each set transect. The distance among transects was set, for the Ugento case study, equal to 10m to capture the high spatial variability of input data and to have a smoother visualization of the final outputs.

As represented in Figure 4.3 and by reporting the NSM across the overall Municipality of Ugento for the 2009-2018 timeframe, different trends can be detected across 4 selected sites: i) a stable shoreline around the Regional park of Ugento (represented with the white colour); ii) an overall shoreline accretion of about 32 meters in the coastal area of Fontanelle against the analyzed 10 years' timeframe (represented with shade of blue); iii) coastal erosion of about 61 meters as a whole in the marina of Torre Mozza, under the investigated period (represented with shade of red); iv) a mixed zone (erosion and accretion; red and blue shades) around the shoreline of Lido Marini.

Shoreline evolution trends across these four specific locations are deeply analyzed and discussed in the following paragraphs.

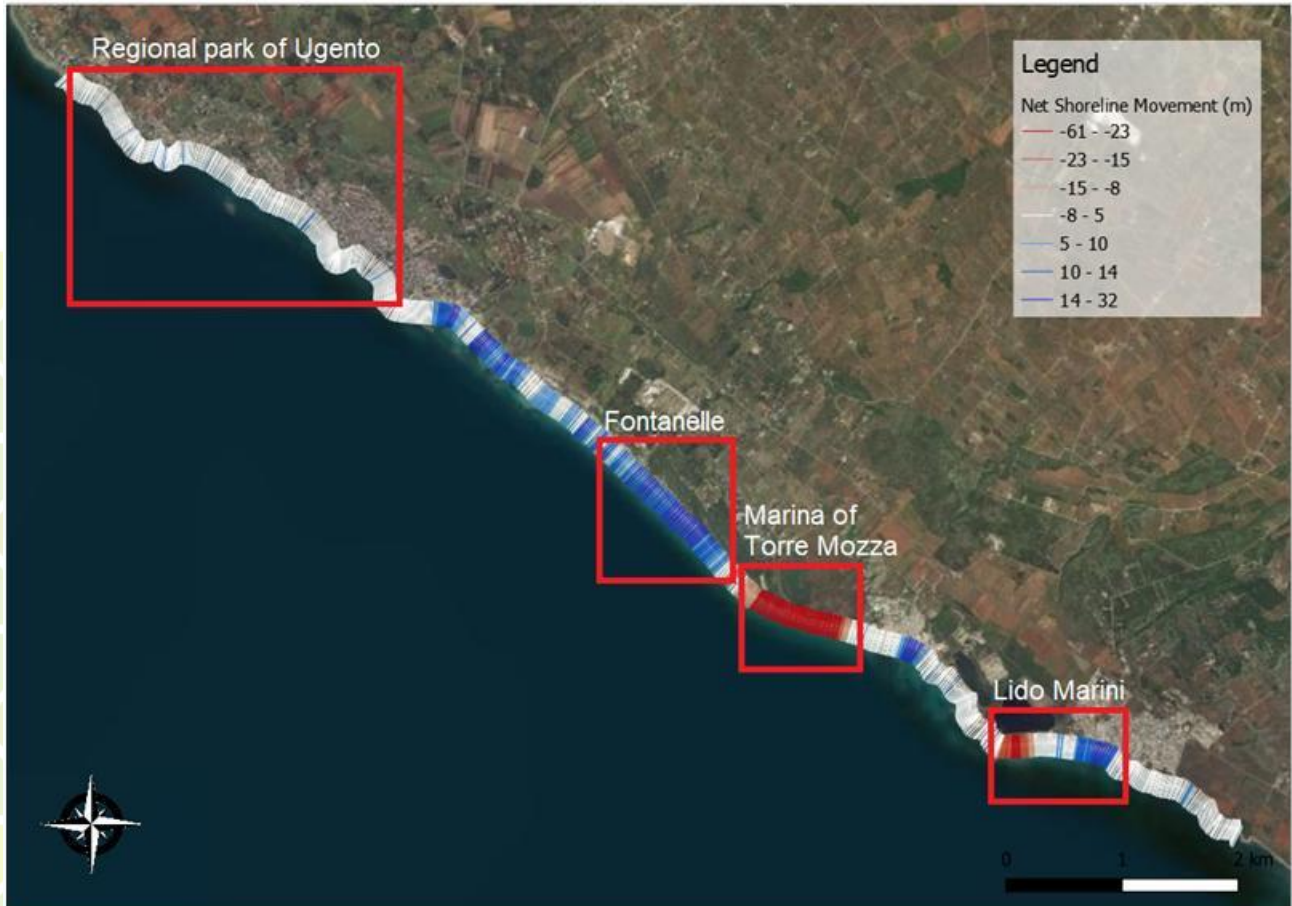


**Figure 4.3:** Net Shoreline Movement (NSM) in coastal zone of the Municipality of Ugento (Apulia region) for the 2009-2018 timeframe

#### 4.2.1 Regional park of Ugento

In the northern part of the municipality of Ugento, where the Regional park is located, the shoreline appears stable since the area is mostly featured by a rocky coast. In fact, in this area was quite stable we observed a NSM in the range of (-0.5 – 1.7 m) (see Figure 4.4b) with an average change rate of about 0.01m over the investigated period (2009-2018) (see Figure 4.4c). Moreover, we observed a fluctuate trend among segments (i.e. change from erosion to accretion) with the change rate of about  $\pm 0.5\text{m}$  per year (see Figure 4.4d).

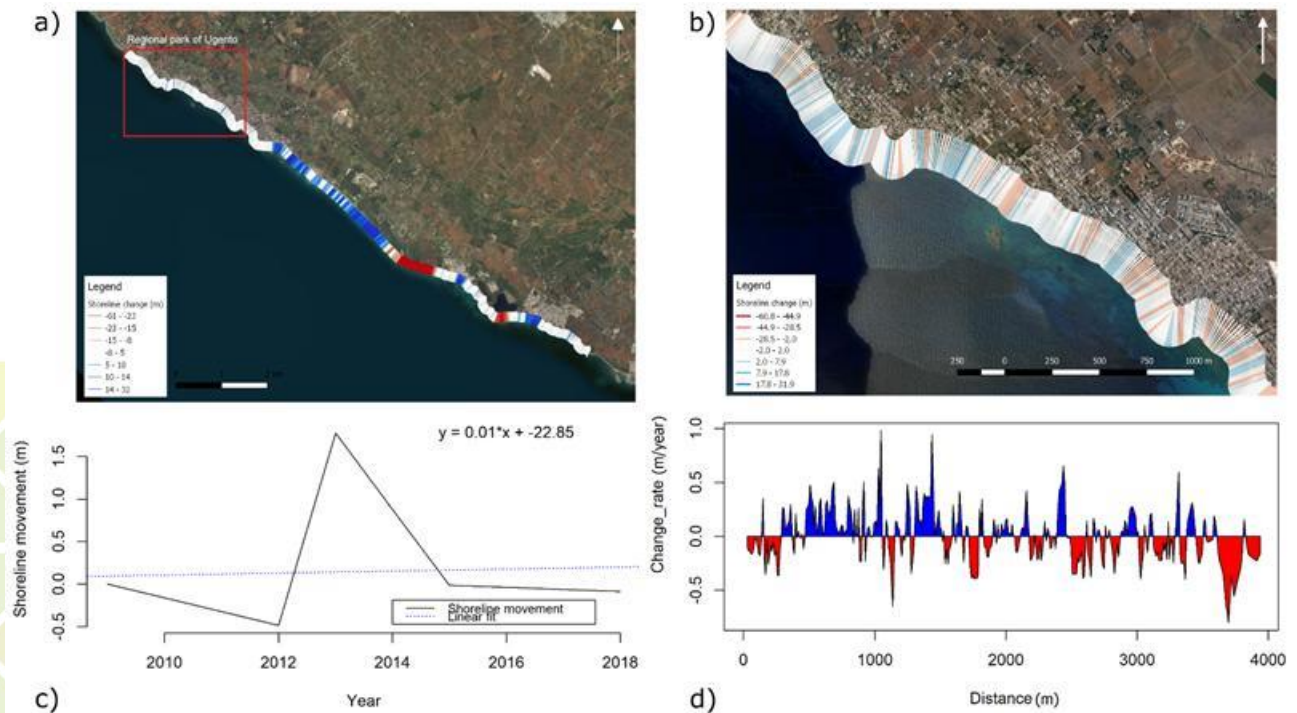


**Figure 4.4:** a) Shoreline changes across the Ugento case study as evaluated through the DSAS tool (high accretion – blue; high erosion – red); b) shoreline changes within the Regional park of Ugento (moderate accretion – light blue; moderate erosion – orange); c) Temporal variability of shoreline movement within the Regional park of Ugento over the 2009–2018 timeframe; d) erosion/accretion rate along the coastal zone of Regional park of Ugento.

#### 4.2.2 Fontanelle area

Moving downward from the stable area the Regional park of Ugento to the Fontanelle area, we can observe a high rate of shoreline accretion in this coastal zone. This area is completely in high advancing trend since we observed positive values of NSM in all transects, with the maximum value of about 15.5 meters under the study period (2009 – 2018) (see Figure 4.5). Additionally, the average change rate over this period was about 2.5m (see Figure 4.5c) and the the maximum yearly change of about 3.2 m per year (see Figure 4.5**Σφάλμα! Το αρχείο προέλευσης της αναφοράς δεν βρέθηκε.**). This phenomenon is mainly due to the presence of a system of groins and breakwaters located in correspondence to the lower part of the marina, built in 2001 to stem the strongly advancing shoreline.

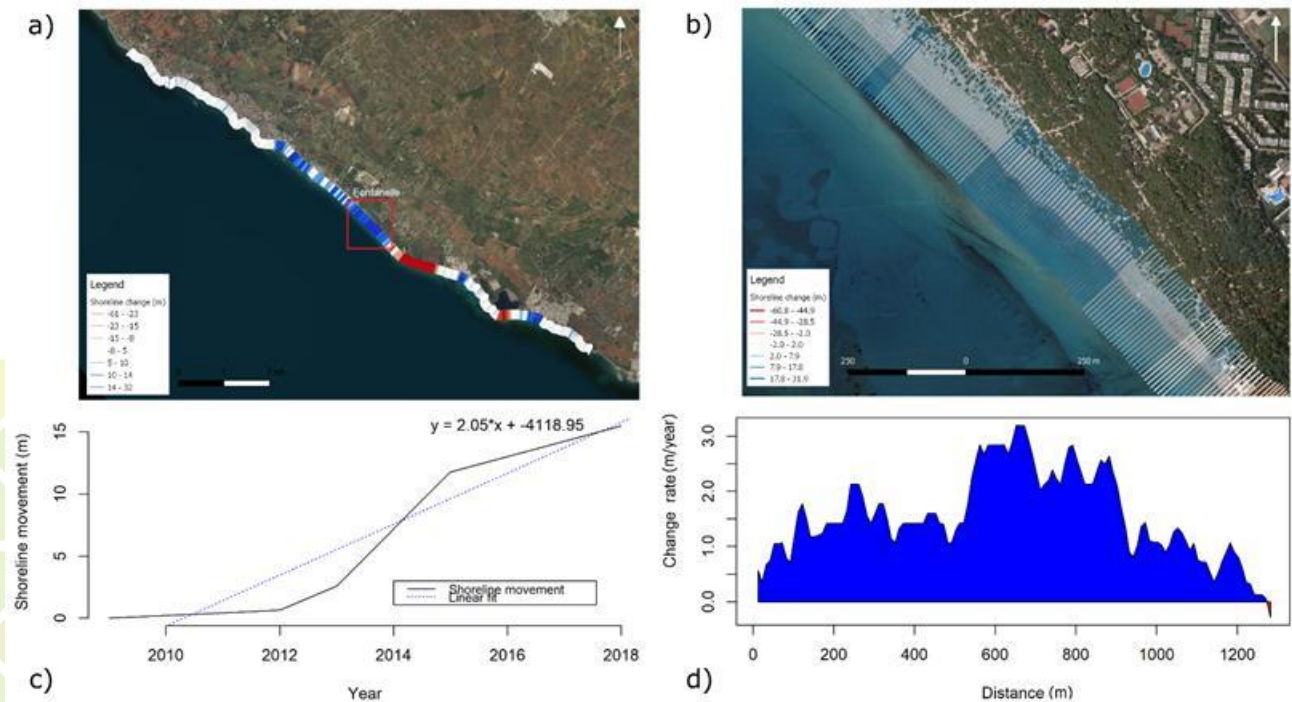


**Figure 4.5:** a) Shoreline changes across the Ugento case study as evaluated through the DSAS tool (high accretion –blue; high erosion – red); b) shoreline changes within the Fontanelle area (moderate accretion – light blue; high accretion – blue); c) Temporal variability of shoreline movement within the Fontanelle area over the 2009-2018 timeframe; d) erosion/accretion rate along the coastal zone of Fontanelle.

### 4.2.3 Marina of Torre Mozza

Moving south just about 1.2 km from the accretion area of Fontanelle, we observed a contrast situation in the sandy beach of Torre Mozza, where a high erosion rate was detected across the investigated timeframe. Specifically, we observed negative values of NSM with the maximum value of about 61 meters (see Figure 4.6: a) Shoreline changes across the Ugento case study as evaluated through the DSAS tool (high accretion – blue; high erosion – red); b) Shoreline changes within the marina of Torre Mozza (moderate erosion – light red; high erosion – red); c) Temporal variability of shoreline movement of the Torre Mozza area over the 2009-2018 timeframe; d) erosion/accretion rate along the coastal zone of Torre Mozza. b) and the average change rate of about -3.9m over the time period 2009-2018 (see Figure 4.6: a) Shoreline changes across the Ugento case study as evaluated through the DSAS tool (high accretion –blue; high erosion – red); b) Shoreline changes within the marina of Torre Mozza (moderate erosion – light red; high erosion – red); c) Temporal variability of shoreline movement of the Torre Mozza area over the 2009-2018 timeframe; d) erosion/accretion rate along the coastal zone of Torre Mozza.c). Moreover, the maximum yearly change rate was about -6.2 m per year

(see Figure 4.6: a) Shoreline changes across the Ugento case study as evaluated through the DSAS tool (high accretion –blue; high erosion – red); b) Shoreline changes within te marina of Torre Mozza (moderate erosion – light red; high erosion – red); c) Temporal variability of shoreline movement of the Torre Mozza area over the 2009-2018 timeframe; d) erosion/accretion rate along the coastal zone of Torre Mozza. d) positioning the marina of Torre Mozza as Torre Mozza as the most eroded marina of the municipality. This pattern is mainly due to storm surges events which are becoming even more frequent and severe on this area, as well as the transport of unbalanced sediments. The latter is the result of the port and pier built in Torre San Giovanni during the 1981-2003 timeframe, contributing to the sediment imbalance in the southern part of the municipality.

Several management strategies have been put in place by the local municipality including beach nourishment and dune restoration measures in order to face rising erosion risk. Specifically, as far as dune restoration is concerned, Posidonia Oceanica leaves were collected in two different areas of Ugento (i.e. river mouths around Torre San Giovanni and Fontanelle) and then replaced in five hot-spot risk areas experiencing high damages on the dune system and the coastal area itself, including the marina of Torre Mozza and Lido Marini.

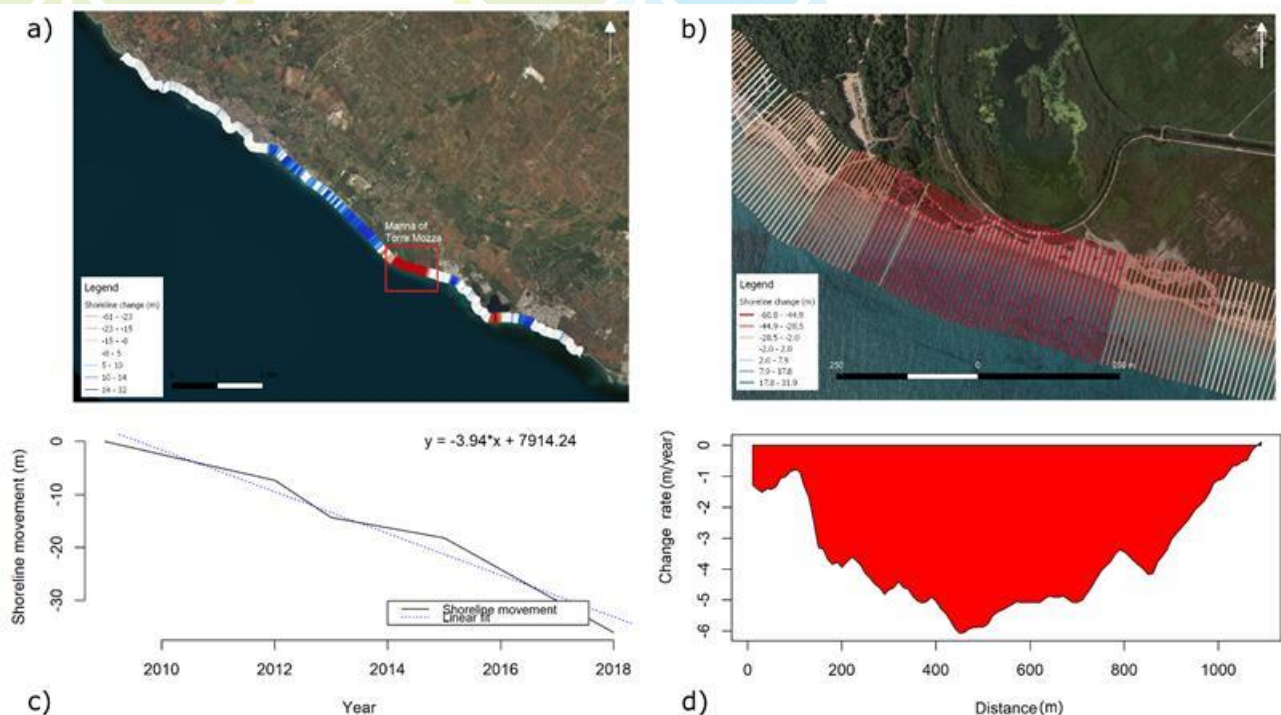


**Figure 4.6:** a) Shoreline changes across the Ugento case study as evaluated through the DSAS tool (high accretion –blue; high erosion – red); b) Shoreline changes within te marina of Torre Mozza (moderate erosion – light red; high erosion – red); c) Temporal variability of shoreline movement of the Torre Mozza area over the 2009-2018 timeframe; d) erosion/accretion rate along the coastal zone of Torre Mozza.

#### 4.2.4 Lido Marini

Differently from the previous cases, when looking at the shoreline of Lido Marini it can be observed as the first part of this coastal area is retreating, while the other one is advancing. Specifically, this area experienced a maximum erosion of about 26m in the western part while the highest accretion of about 21 m in the east side (see Figure 4.7: *a) Shoreline changes across the Ugento case study as evaluated through the DSAS tool (high accretion –blue; high erosion – red); b) Shoreline changes within Lido Marini (moderate accretion – light blue; moderate erosion – orange); c) Temporal variability of shoreline movement of the Lido Marini area over the 2009-2018 timeframe; d) erosion/accretion rate along the coastal zone of Lido Marini.*) under the analyzed timeframe. Overall, the rate of change for the whole investigated period (2009-2018) is about -0.18m for the whole area (see Figure 4.7: *a) Shoreline changes across the Ugento case study as evaluated through the DSAS tool (high accretion –blue; high erosion – red); b) Shoreline changes within Lido Marini (moderate accretion – light blue; moderate erosion – orange); c) Temporal variability of shoreline movement of the Lido Marini area over the 2009-2018 timeframe; d) erosion/accretion rate along the coastal zone of Lido Marini.*). Moreover, the maximum yearly change rate was about  $\pm 2$  m per year (see Figure 4.7: *a) Shoreline changes across the Ugento case study as evaluated through the DSAS tool (high accretion –blue; high erosion – red); b) Shoreline changes within Lido Marini (moderate accretion – light blue; moderate erosion – orange); c) Temporal variability of shoreline movement of the Lido Marini area over the 2009-2018 timeframe; d) erosion/accretion rate along the coastal zone of Lido Marini.*). This strange phenomenon of a mixed erosion-accretion pattern can be associated to the geomorphological pattern of this coast, where the presence of both rocky and sandy coasts deeply influence the erosion processes on the area. Finally, it is interesting to observe as the shoreline evolution turned from erosion to accretion since 2012, as the reconstruction of the dunes implemented under the Ugento coastal plan were completed in that year.

Lead Partner

Technical support

Project Partners

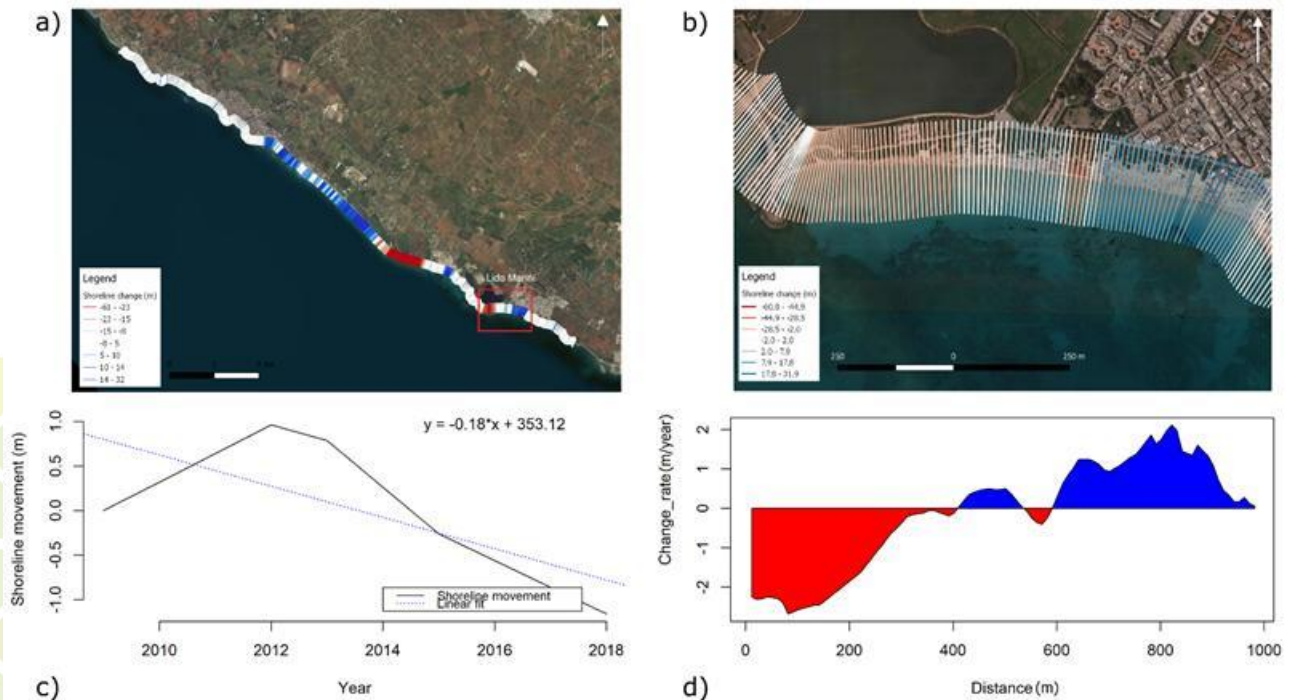


**Figure 4.7:** a) Shoreline changes across the Ugento case study as evaluated through the DSAS tool (high accretion – blue; high erosion – red); b) Shoreline changes within Lido Marini (moderate accretion – light blue; moderate erosion – orange); c) Temporal variability of shoreline movement of the Lido Marini area over the 2009-2018 timeframe; d) erosion/accretion rate along the coastal zone of Lido Marini.

### 4.3 Results on Coastal Erosion Analysis from the pilot study area of the Messolonghi shoreline in the northern part of the gulf of Patras– Region of Western Greece

Following the methodological approach presented in the Section 4.1, with the main aim of analyzing coastal evolution trend along the shoreline of the municipality of Messolonghi (region of Western Greece), two different time periods i.e. 1986 – 2009 and 2009 – 2019 were considered, based on the availability of high spatial resolution satellite images for the investigated area. Specifically, as reported in the Table 4.2 (a) satellite images from Landsat 4-5 TM, with lower spatial resolution (pixel size of 30 m), retrieved from the Earth Explorer database of the United States Geological Survey Global Visualizer, were used to analyse shoreline changes across the 1986-2009 timeframe; and (b) satellite images from RapidEye and PlanetScope retrieved from Planet Explorer Beta, with higher spatial resolution of 5 m and 3.1 m respectively, for the 2009-2019 timeframe.

The historical satellite image selection was mainly based on the correct geo-reference of each image, the clarity from cloud cover and the seasonality. Accordingly, all images were retrieved during summer months

(May to September) and in the same tide phase (ebb tide phase), in order to reduce the impact of seasonality and tidal effects. The monochromatic Near Infrared Band was selected for the image analysis and historic shoreline extraction.

**Table 4.2.** Metadata of the satellite images used in the frame of the Messolonghi pilot case

Data Products	Resolution (meters)	Year of Image Acquisition	Source
Landsat 4-5 TM	30	20-04-1986	Earth Explorer, USGS
		29-07-1999	
		08-04-2005	
		15-08-2009	
RapidEye	5	23-06-2009	Planet Explorer Beta
		12-07-2012	
		18-07-2015	
PlanetScope	3.1		

Using data produced through the DSAS transects tool, a statistical analysis of the shoreline evolution along the study years was applied and various statistical parameters were calculated and analysed. The results were verified by applying two methodologies for outlier removal: The Interquartile Range (IQR) method and the method of extreme values removal (based on quantile distribution – 1%) to “clip” the data and remove the outliers. Both methods were applied in combination with an optical and empirical detection.

Messolonghi coastal zone is a vulnerable and dynamic environment with significant variation in erosion and accretion activity. Investigation of the shoreline status from 1985 to 2019 reveals that several erosion and accretion hotspots are identified along the coastal area of the Municipality Ieras Poleos Messolonghiou. The entire study area is characterized by moderate values of erosion and accretion rates, mainly affected by sea waves, low river discharge, extreme storm surges and sea level rise.

As explained above, the study was carried out into two steps: a) the shoreline movement analysis for the periods 1985 to 2009 and 2009 to 2019, highlighting on the erosion and accretion hotspots, and b) a more detailed investigation of shoreline change rates for the period 2009 to 2018, using images with a higher spatial resolution (Figure 4.8). The results of this analysis in the total study area and in four sub-areas of the Municipality of Ieras Poleos Messolonghiou coastline (Louros beach, Lournisides, Alikes and Tournida beach as well as at the Evinos river estuaries) are presented below.

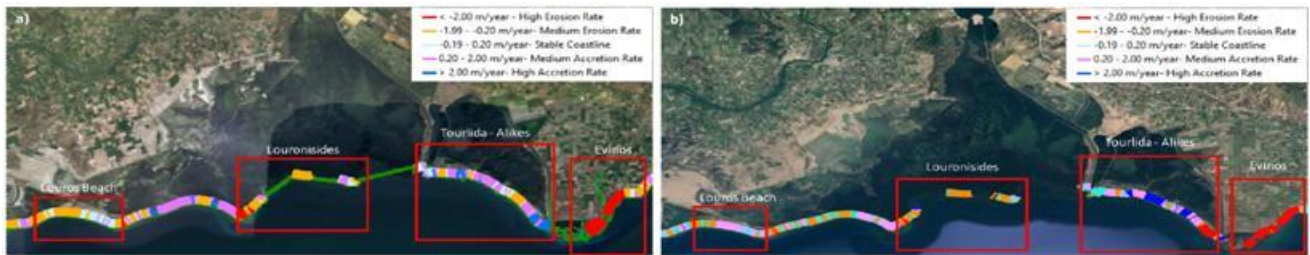


**Figure 4.8:** Shoreline movement results in coastal zone of the Municipality of Ieras Poleos Messolonghiou; a) for the time period 1985 to 2009 and b) for the time period 2009 to 2019.

### 4.3.1 Louros Study site

Louros beach is located in the Eastern part of the study site, covering a coastal area of around 5 km long.

**1985-2009:** For the time period 1985 to 2009 the average shoreline retreat of  $-0.25$  m/y is observed. The western site of Louros beach is the most eroded area with maximum erosion rates up to  $1.04$  m/y. On the other hand, at the eastern site of the beach, accretion rates with maximum rate of  $+0.28$  m/y are observed.

**2009-2019:** The average shoreline change rate of the total shoreline was estimated around  $+0.02$  m/year for the time period 2009 to 2019 (Figure 4.9). More precisely, in the west part of Louros beach, high erosion activity is observed (up to  $-0.65$  m/year). The western shoreline of Louros Beach retreated around  $3.5$  m during the last decade (2009 – 2019). Several hotspots of erosion and accretion are observed along the western coastal zone for the time period 2009-2019, with average erosion rate of  $+0.02$  m/y. High erosion rates are observed in the western area of Louros coastline (about  $-0.35$  m/y), where the estimated shoreline movement was about  $-6.8$  m. On the other hand, the higher accretion rates are observed in the east side of Louros beach, with maximum shoreline movement of  $+9$  m and average accretion rate of around  $+0.45$  m/y.

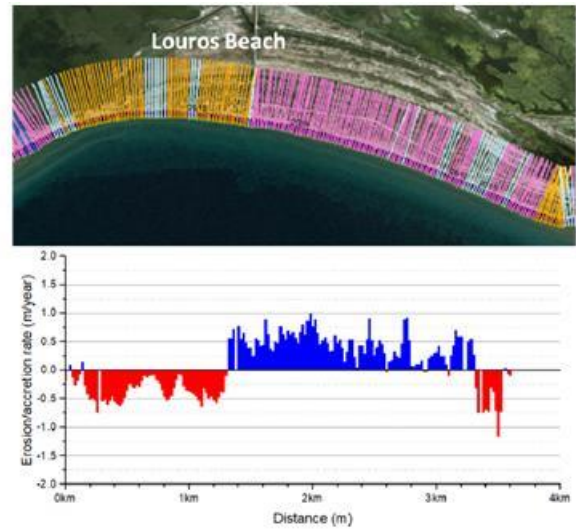
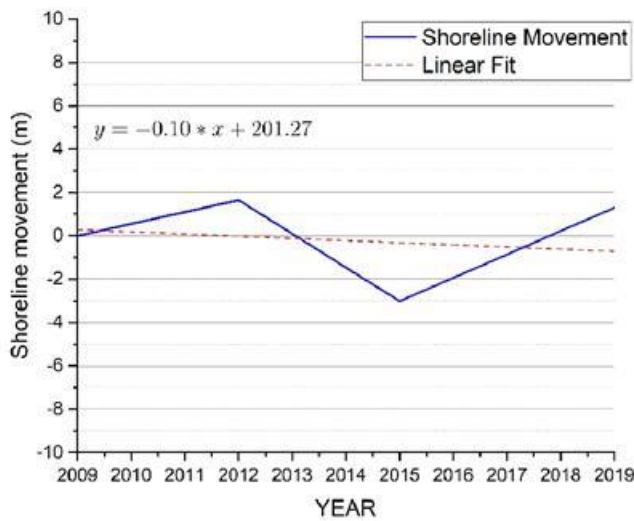


**Figure 4.9:** a) Temporal variability of shoreline movement over the period 2009-2019, b) illustration of erosion and accretion on coastal zone of Louros beach (moderate accretion- purple and moderate erosion- orange) and c) erosion/accretion rate along coastal zone of Louros beach.

### 4.3.2 Louronisides Study site

Louronisides are long sandy islands in the entrance of the Messolonghi lagoon. The coastline of Louronisides study area consists by three sites Prokopanistos (around 2.5 km), Schinias (around 1.5 km) and Komma (around 1.7 km).

**1985-2009:** The erosion activity in Louronisides study site is significantly higher compared to the Louros coastline. More precisely, for the time period 1985 to 2009 average shoreline retreat (-0.92 m/y) is observed. The higher erosion activity is recorded in Prokopanistos site (-3 m/y). Moreover, erosion activity was observed in Schinias (-0.9 m/y) and in the western and eastern part of Komma island (-0.20m/y). Although, the higher erosion action was recorded in Prokopanistos site, some parts are accreting with maximum accretion rate of +1.00 m/y.

**2009-2019:** The shoreline in Louronisides retreated gradually from 2009 to 2019 and the total retreat was estimated around 5 m, with average rate of the total shoreline change about -0.53 m/y, maximum erosion rate of -4.2 m/y and maximum accretion rate of +4.5 m/y (Figure 4.10). In Prokopanistos site high average shoreline retreat through the decade is observed (-10 m). Although, in the north-east part of the shoreline, high accretion rate (-1.8 m/y) is occurred. As well, the action of erosion appears consistently in Schinias and Komma sites during the last decade. The average shoreline retreat is estimated around -1 m/y in Schinias site and -0.5 m/y in Komma site, with the maximum erosion rate to be observed in the western site of Schinias

coastline (-2 m/y) and the higher accretion rate to be occurred in the eastern part of Komma coastline (+1.1 m/y).

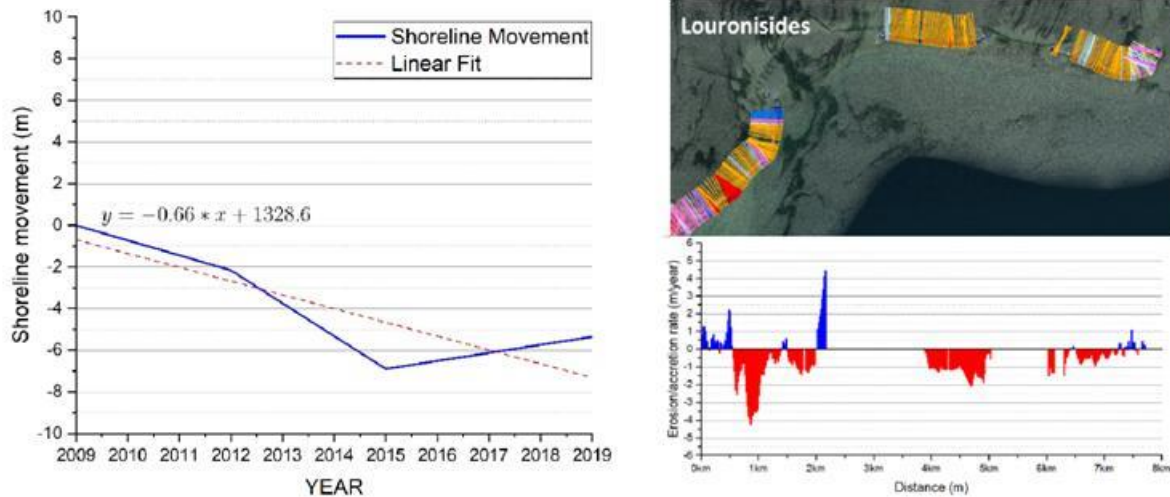


**Figure 4.10:** a) Temporal variability of shoreline movement over the period 1009-2019, b) illustration of erosion and accretion on coastal zone of Louronisides (high erosion-red and high accretion- blue) and c) erosion/accretion rate along coastal zone of Louronisides.

### 4.3.3 Alikes and Toulrida Beach Study site

Alikes study site is a long coastal zone with length of around 7.6 km, from Toulrida beach to Babakoulia channel. In that study site is also included the artificial Toulrida beach, which is the most significant touristic beach of the Municipality Ieras Poleos Messolonghiou coastline.

**1985-2009:** In Alikes study site significant accretion activity (+1.20 m/y) through the years 1985 to 2009 was observed. Maximum accretion rates are recorded in the south-eastern part of the study site (up to +7 m/y), where sediment accumulated in the western site of Babakoulia channel. Slight erosion activity (up to -1.20 m/y) was recorded through that time period.

**2009-2019:** Along the coastline significant accretion is observed with average accretion rates of +1 m/y from 2009 to 2019 (Figure 4.11). Although, in the southern-east coastline, close to the Babakoulia channel, very high erosion rates (up to +15.3 m/y) are recorded, the sediment moves towards the south, and accumulates to the channel dike. Furthermore, the shoreline of Toulrida beach retreated up to -5 m in the last decade with average erosion rate of around -0.15 m/y.

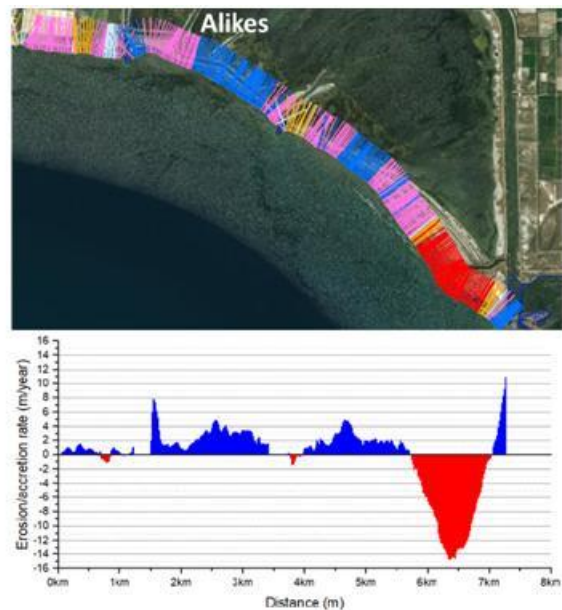
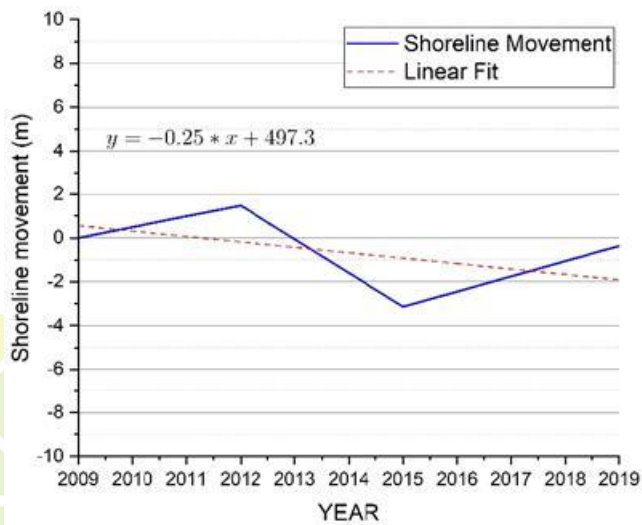


**Figure 4.11:** a) Temporal variability of shoreline movement over the period 2009-2019, b) illustration of erosion and accretion on coastal zone of Alikes and Tourlida study site and c) erosion/accretion rate along coastal zone of Alikes and Tourlida study site.

#### 4.3.4 Evinos Estuary Study site

Evinos river discharge has been significantly reduced throughout the latest decade and the impact of that is shown in the coastal zone of Evinos estuaries.

**1985-2009:** From 1985 to 2009 high erosion activity was recorded with average erosion rate of around -10.70 m/y and maximum erosion rate up to -30.14 m/y.

**2009-2019:** These enormous erosion rates are mostly observed during the recent time period (2009 to 2019), with average shoreline retreat of -125 m and erosion rates up to -33 m/y (Figure 4.12). A straight of land located in Babakoulia area has moved from east to west by almost 350 m through the years 2009 – 2019. Moreover, there are high average erosion rates estimated (~ -14 m/y) in the areas located on both sides of Evinos estuary and the shoreline retreated up to -120 m.

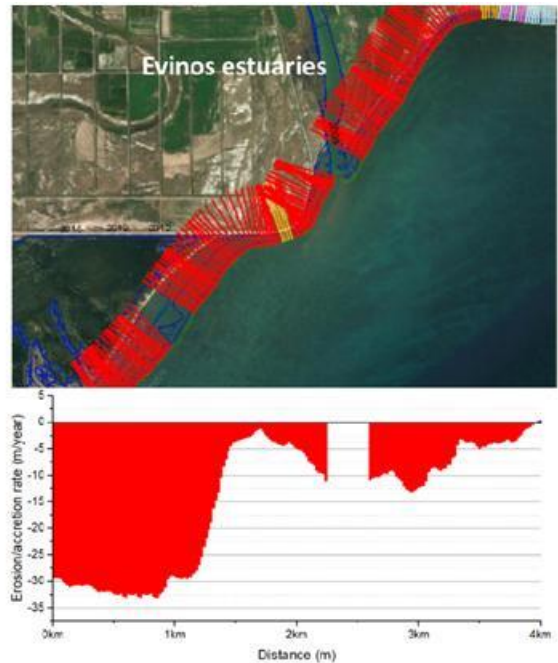
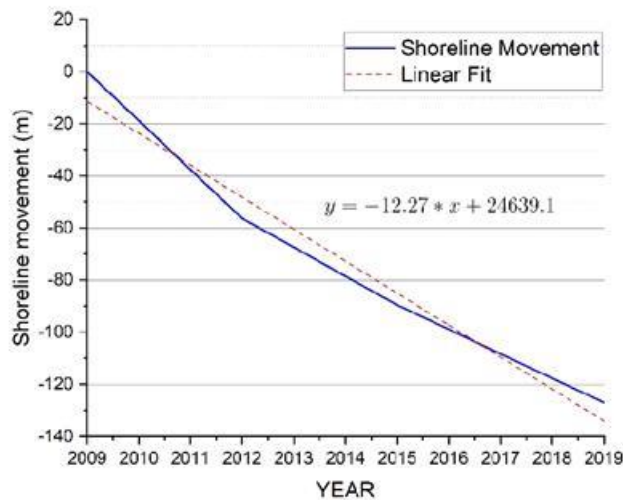


**Figure 4.12:** a) Temporal variability of shoreline movement over the period 1009-2019, b) illustration of erosion and accretion on coastal zone of Evinos estuary and c) erosion/accretion rate along coastal zone of Evinos estuary.

#### 4.4 Results on Coastal Erosion Analysis from the pilot study area of the southern part of the gulf of Patras - Region of Western Greece

Aiming to map with very high accuracy the coastal evolution trend along the shoreline of the southern part of the gulf of Patras (region of Western Greece), a time period from 1945 up to 2018 was considered, based on the availability of (a) air photos and (b) high spatial resolution satellite images for the investigated area. Specifically, as reported in the Table 4.3 (a) air photos with a spatial resolution of 1m and (b) very high resolution satellite images (Worldview-2) with a spatial resolution of 0.5 were used to analyse shoreline changes across the 1945-2018 timeframe; and (c) medium resolution satellite images (Landsat and Sentinel) were also assessed for their accuracy in coastline evolution.

The remote sensing image selection was mainly based on the availability of historical images and the potentiality for accurate orthorectification. Furthermore, cloud cover and seasonality were also taken into consideration. Accordingly, all images were retrieved during summer months (May to September) and in the same tide phase (ebb tide phase), to reduce the impact of seasonality and tidal effects. All the airphotos and high-resolution satellite images were photogrammetrically processed in Leica Photogrammetry Suite and orthophotos with minimum Root Mean Square Error were developed.

**Table 4.3.** Metadata of the satellite images used in the frame of the southern part of the gulf of Patras

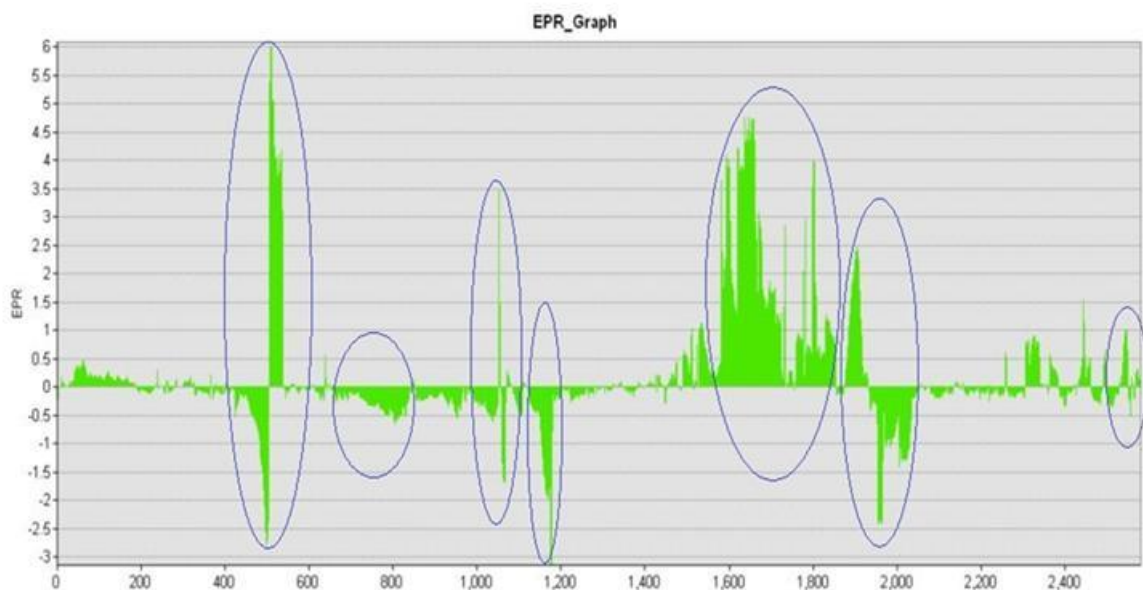
Data Products	Resolution (meters)	Year of Image Acquisition	Source
Airphoto	1	1945	Hellenic Military Geographical Service
		1996	
Declassified satellite imagery	2	1973	USGS
Worldview-2	0.5	2018	Digital Globe

Using data produced through the DSAS transects tool, a statistical analysis of the shoreline evolution along the study years was applied and various statistical parameters were calculated and analysed.

The coastal zone of the gulf of Patras is a vulnerable and dynamic environment with significant variation in erosion and accretion activity. Investigation of the shoreline status from 1945-2018 reveals that seven erosion and accretion hotspots are identified along the coastal area of the gulf of Patras. The entire study area is characterized by moderate values of erosion and accretion rates, mainly affected by sea waves, low river discharge, extreme storm surges and sea level rise.

The results of this analysis in the study area in seven sub-areas concluded that seven (7) areas are suffering from erosion or accretion higher than 30m during the period 1945-2018.

Figure 4.13 presents the mean annual rate from 1945 until 2018 of the spotted seven (7) areas, which show a tendency of high erosion or accretion, more than 30m during the referred period.



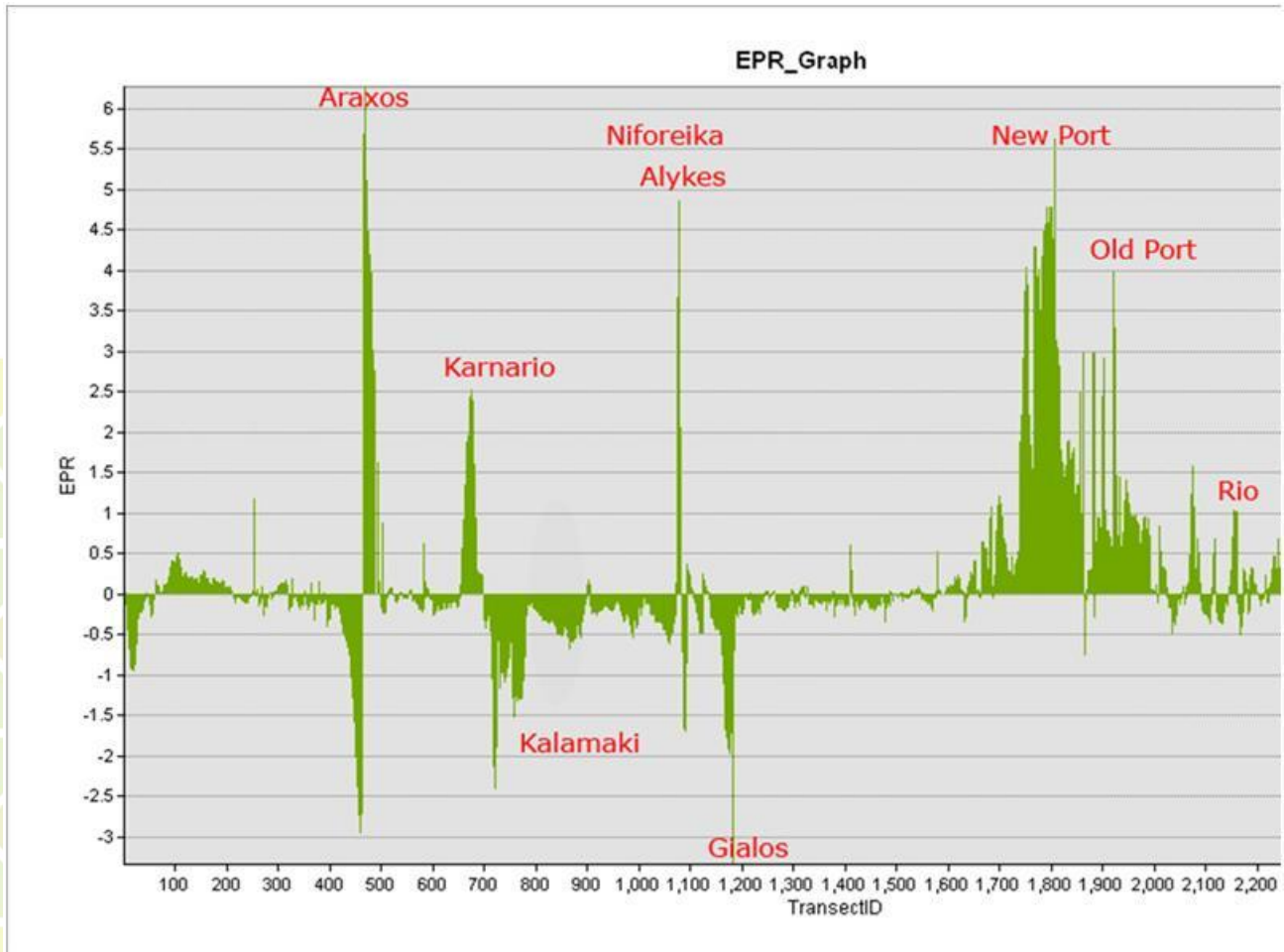


**Figure 4.13:** Diagram of the mean annual rate of erosion or deposition along the area of study. The circled areas correspond to the areas with an erosion or accretion more than 30m. Transects numbering starts from Kotychi Lagoon (no1) and reaches Rio at Transect (no2150)

#### 4.4.1 Carnario study area

In Figures 4.14 and 4.15 a characteristic example of the shoreline displacement during the 73-year period (1945-2018) in the Karnario study area is presented. The specific area is a characteristic example of the complexity of the phenomenon. In the same area there is an alternation of intense erosion and deposition. Intense erosion was found in the eastern part of the area, equal to shoreline displacement inland of 78.74 m and a rate of -1.07 m/year. Sedimentation was located in the western part equal to 113 m and 1.56 m/year.

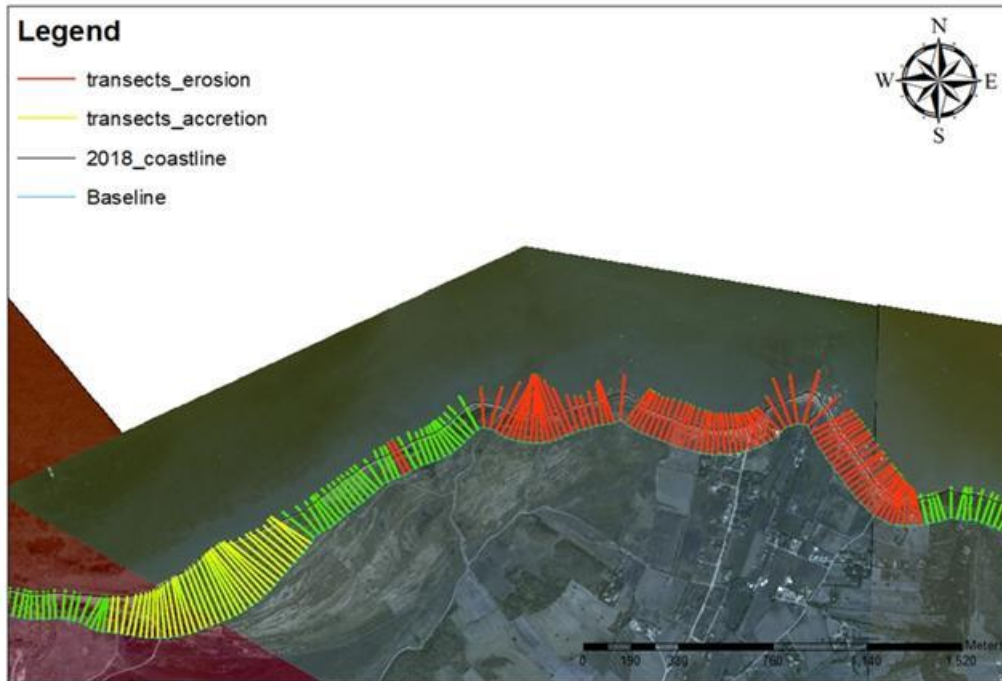


**Figure 4.14:** Map of the shoreline displacement from 1945 to 2018 in Karnario area. Red color represents areas with intense erosion while yellow color marks areas where the deposition is high. Areas where the shoreline displacement is lower than 30m during the 1945-2018 period are presented with green color.



**Figure 4.15:** Map of the shoreline displacement from 1945 to 2018 in Karnario area. Different colors represent the shoreline position at different dates.

#### 4.4.2 Gialos study area

This area is the estuary of the river Peiros one of the three rivers that flow into the Gulf of Patras. High erosion rates are measured for the period 1945-2018 (Figure 4.16). The mean erosion rate overpassed 1.15m/year and the coastline has retreated for almost 80m (average value) during the specific period. A dam was recently built in Peiros stream and so the erosion is expected to be higher in the forthcoming years.

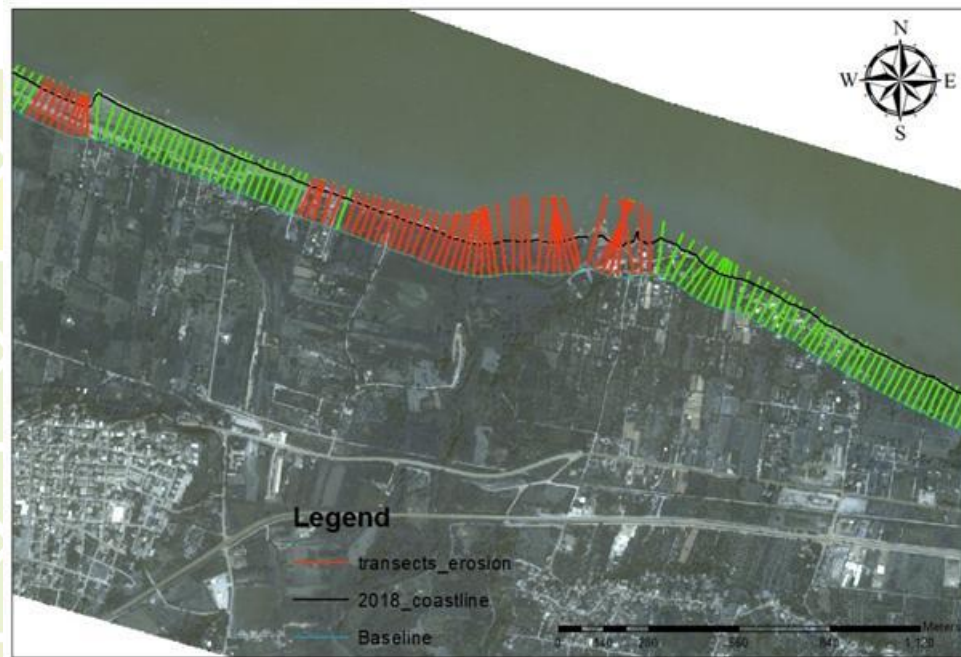


**Figure 4.16:** Map of the shoreline displacement from 1945 to 2018 in Gialos area. Red color represents areas with intense erosion.

#### 4.4.3 Patras New Port

The specific area is a characteristic example of the human intervention in the coastal environment. The construction of the Patras new Port provoked the accretion of the land over the sea. Due to the construction of the port facilities, an artificial increase of the (more than 226m) and an accretion rate equal to 3.12m/year are observed (Figure 4.17).

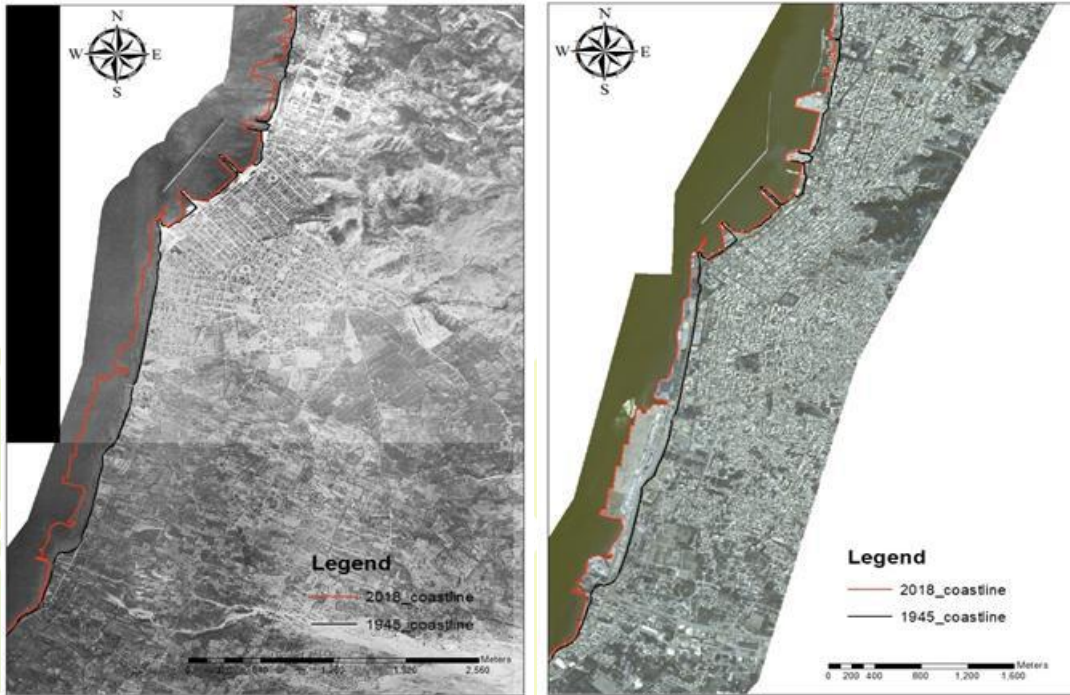


**Figure 4.17:** The area of the new port of Patras. At the left an airphoto of 1945 and at the right a Worldview image of 2018

Lead Partner



Technical support



Project Partners



## 5 Discussion

This Deliverable presents the TRITON risk-based joint tool blending remote sensing and GIS-based techniques for the multi-temporal detection and analysis of shoreline evolution across the TRITON pilot cases. Specifically, the proposed joint tool is applied across the Messolonghi (Greece), the gulf of Patras (Greece) and the Ugento (Italy) shorelines, identifying hotspots risk areas requiring urgent intervention in terms on management and adaptation measures, including nature-based solutions (NBSs). In addition, a pilot erosion observatory is established in the gulf of Patras and the Kotychi lagoon comprising appropriate instrumentation for real-time data collection in both sites, as well as development of accurate geotechnical, bathymetric, and coastal engineering plans in the pilot area of the gulf of Patras.

From a methodological point of view, the joint tool blending remote sensing and GIS-based techniques represents a flexible tool for interdisciplinary studies, in which satellite images are exploited to assess coastal erosion risks and provide science-based knowledge to put into practice cross-border ICZM initiatives. The flexibility of the proposed tool also lies on the possibility to update the analysis with new satellite images with higher spatial resolution as they become available, increasing the reliability of the resulting output for the assessment and management of local-scale erosion processes. Thanks to its graphically-based output (building on GIS vector layers), the proposed tool provides a simplified representation of the spatio-temporal dynamics of coastal erosion processes, as well as the identification of hotspots risk areas, thus facilitating an easy and transparent communication of the outcomes of the assessment to potential end-users committed in coastal protection and adaption planning (e.g. coastal planners and decision-makers, coastal engineers).

However, even though the implementation of TRITON risk-based joint tool has produced useful results to put into practice ICZM initiatives across the project pilot cases, this approach encounters some limitations mainly related to the input data. Specifically, it has to be highlighted that the open-source satellite images used in the analysis (i.e. data products from Landsat 4-5 TM, RapidEye, PlanetScope) have significantly constrained the assessment due to their coarse spatial resolution (from 30 to 3.1m). On the other hand, if airphotos or very-high resolution satellite images are used, like the Worldview-2 images that have been used in the pilot area of the gulf of Patras, the final orthomosaic provides a spatial resolution of 0.5m which is more efficient for the identification of hotspot risk areas and coastal engineering applications.

The processing of airphotos and satellites images in the frame of TRITON project proved that remote sensing data provide an accurate and reliable solution for the diachronic monitoring of the coastal zone. It is shown

Lead Partner



Technical support



Project Partners



that shorelines derived from high-resolution datasets can be used for shoreline mapping, with great accuracy and only one limitation. The high spatial resolution of the data must be accomplished with the lowest possible temporal resolution in order to produce results that are more reliable. A full coverage of the coastal zone with remote sensing data acquired every three to five years is a prerequisite for an accurate forecast of the shoreline evolution. The low-resolution data are feasible for low-scale studies, where accuracy is not a prerequisite, or low-budget studies, where the free availability of data is the main demand.

Building on this fact, a future challenging improvement of the designed risk-based joint tool should consider satellite images with higher spatial resolution, similar to those that were used in the pilot case of the gulf of Patras, allowing to better capturing local-scale erosion dynamics. Moreover, with the advances in computer science, numerical modelling or more complex machine-learning based algorithm for data clustering could be exploited, thus leveraging the potential of numerical modelling or advanced machine learning methods for a better classification of shoreline evolution.

Another important join-tool that has been developed in the frame of the TRITON project is the new WebGIS observatory platform, especially designed to cover the coastal zone of the Municipality of Ieras Poleos Messolonghiou and the southern part of the gulf of Patras, in Western Greece. This WebGIS tool is tailored for decision-making, risk assessment and emergency preparation and response in coastal areas and collects environmental, meteorological, oceanographic, hydrographic, hydrological dynamic spatio-temporally-varying data, combined with static data on land-use, geology, topography, erosion/accretion rates, seagrass abundance, etc. All datasets are retrieved from external platforms and data providers like NOAA, Copernicus Marine Environmental Service, Corine, etc as well as from the real-time monitoring stations that have been installed in the pilot areas.

The tool is designed to combine sophisticated forecast modelling systems from multi-scale analysis of water bodies (rivers, open and coastal sea), including waves, hydrodynamics and wave energy prediction, with real-time monitoring networks for forcing and continuous validation purposes. Tailor-made visualization and analysis products, conceptualized for multiple uses through a service-oriented framework, provide an easy and interactive access to both data and operational forecasts. Thus, the TRITON's WebGIS is a website for interactive visualization of the spatial data collected in the Project and organized in a common spatial infrastructure in Greek language and is available to the public through the Municipality of Ieras Poleos Messolonghiou official website. Details on the development of this WebGIS tool are presented in WP5.

Lead Partner



Technical support



Project Partners



## Bibliography

- Anfuso, G., Pranzini, E., & Vitale, G. (2011). An integrated approach to coastal erosion problems in northern Tuscany (Italy): Littoral morphological evolution and cell distribution. *Geomorphology*, 129(3-4), 204-214.
- Arheimer, B., Lindström, G., & Olsson, J. (2011). A systematic review of sensitivities in the Swedish flood-forecasting system. *Atmospheric Research*, 100(2-3), 275-284.
- Braud, D.H., Feng, W., 1998. Semi-automated construction of the Louisiana coastline digital land/water boundary using Landsat Thematic Mapper satellite imagery. Louisiana Appl. Oil Spill Res. Dev. Program, OS2 RAPD Tech. Rep. Ser. 97.
- Congedo, L. (2016). Semi-automatic classification plugin documentation. *Release*, 4(0.1), 29.
- Dai, C., Howat, I.M., Larour, E., Husby, E., 2019. Coastline extraction from repeat high resolution satellite imagery. *Remote Sens. Environ.* 229, 260–270.
- DHI Water & Environment, 2014. MIKE 21 Wave Modelling, User Guide
- Dolan, D. M., Yui, A. K., & Geist, R. D. (1981). Evaluation of river load estimation methods for total phosphorus. *Journal of Great Lakes Research*, 7(3), 207-214.
- EC, 2013. Proposal for a directive of the European Parliament and the Council establishing a framework for maritime spatial planning and integrated coastal management 0074.
- Genz, A. S., Fletcher, C. H., Dunn, R. A., Frazer, L. N., & Rooney, J. J. (2007). The predictive accuracy of shoreline change rate methods and alongshore beach variation on Maui, Hawaii. *Journal of Coastal Research*, 87-105.
- Gornitz, V.M., Daniels, R.C., White, T.W., Birdwell, K.R., 1994. The development of a coastal risk assessment database: vulnerability to sea-level rise in the US Southeast. *J. Coast. Res.* 327–338.
- Gianni, A., & Zacharias, I. (2012). Modeling the hydrodynamic interactions of deep anoxic lagoons with their source basins. *Estuarine, Coastal and Shelf Science*, 110, 157-167. doi:<https://doi.org/10.1016/j.ecss.2012.04.030>
- IPCC, 2014. Climate Change 2014 Synthesis Report. IPCC Fifth Assess. Rep. 80.
- Kourmoulis, N. (1984). Inventory of karsic springs of Greece. V. Western Central Greece Abstract in English.
- Koutsogiannis, D., Marinos, P., & M., M. (1995). Hydrological framework of Acheloos River deviation (in Greek). *Pirforos*(21), 29-33.
- Lagkadinou, M. (2005). Special environmental-residential study of the complex of the lagoons Messolonghi – Aetoliko using GIS (in Greek).
- Leonardos, I., & Sinis, A. (1998). Reproductive strategy of *Aphanius fasciatus* Nardo, 1827 (Pisces: Cyprinodontidae) in the Mesolongi and Etolikon lagoons (W. Greece). *Fisheries Research*, 35(3), 171-181. doi:[https://doi.org/10.1016/S0165-7836\(98\)00082-4](https://doi.org/10.1016/S0165-7836(98)00082-4)
- Lindström, G., Pers, C., Rosberg, J., Strömquist, J., & Arheimer, B. (2010). Development and testing of the HYPE (Hydrological Predictions for the Environment) water quality model for different spatial scales. *Hydrology research*, 41(3-4), 295-319.
- McLaughlin, S., Cooper, J.A.G., 2010. A multi-scale coastal vulnerability index: A tool for coastal managers? *Environ. Hazards* 9, 233–248.
- Mills, J. P., Buckley, S. J., Mitchell, H. L., Clarke, P. J., & Edwards, S. J. (2005). A geomatics data integration technique for coastal change monitoring. *Earth Surface Processes and Landforms: The Journal of the British Geomorphological Research Group*, 30(6), 651-664.
- Ministry of Environment and Public Works. (1995). *Consultancy services for the adaptation of environmental impacts produced from the deviation of Acheloos River to Thessaly, Annex D, Study of aquatic systems (in Greek)*.

- Papaspyropoulos, C. (1981). Calculations of annual water use from the Monastiraki waters (in Greek). *Hydrologic and Hydrogeologic Research*, 38.
- Ramieri, E., Hartley, A., Barbanti, A., Santos, F.D., Gomes, A., Hilden, M., Laihonon, P., Marinova, N., Santini, M., 2011. Methods for assessing coastal vulnerability to climate change. ETC CCA Tech. Pap. 1, 1–93.
- Rasuly, A., Naghdifar, R., & Rasoli, M. (2010). MonitorinCaspian Sean sea coastline changes using object-oriented techniques. *Procedia Environmental Sciences*, 2, 416-426.
- Thieler, E. R., Himmelstoss, E. A., Zichichi, J. L., & Ergul, A. (2009). *The Digital Shoreline Analysis System (DSAS) version 4.0-an ArcGIS extension for calculating shoreline change (2331-1258)*. Retrieved from US Army Corps of Engineers. (2008). Coastal engineering manual.
- Torresan, S., Critto, A., Rizzi, J., Zabeo, A., Furlan, E., Marcomini, A., 2016. DESYCO: A decision support system for the regional risk assessment of climate change impacts in coastal zones. *Ocean Coast. Manag.* 120, 49–63. <https://doi.org/https://doi.org/10.1016/j.ocecoaman.2015.11.003>
- UNEP/MAP/PAP, 2008. Mediterranean Protocol. *Protoc. Integr. Coast. Zo. Manag. Mediterr.* <https://doi.org/10.1017/CBO9781107415324.004>
- Van Rijn, L. C. (1993). *Principles of sediment transport in rivers, estuaries and coastal seas* (Vol. 1006): Aqua publications Amsterdam.
- Zanuttigh, B., Simcic, D., Bagli, S., Bozzeda, F., Pietrantoni, L., Zagonari, F., Hoggart, S., Nicholls, R.J., 2014. THESEUS decision support system for coastal risk management. *Coast. Eng.* 87, 218–239. <https://doi.org/10.1016/j.coastaleng.2013.11.013>

Lead Partner



Technical support



Project Partners



[www.greece-italy.eu](http://www.greece-italy.eu)



*Interreg V-A Greece-Italy Programme is a European Territorial Cooperation Programme that aims to help public institutions and local stakeholders to develop cross-border projects and pilot actions and to create new policy, products and services, with the final goal to improve the citizens' quality of life. Strategically, the programme will enhance innovation in a number of fields such as blue growth, tourism and culture, agro food and cultural and creative industries. Interreg V-A Greece-Italy Programme aims to get maximum return from EUR 123 million financed per 85% by European Regional Development Fund (ERDF) and per 15% by the 2 member states through a national co-financing.*

Lead Partner



Technical support



Project Partners

